# A ROBUST DIGITAL FLIGHT CONTROL SYSTEM FOR AN UNMANNED RESEARCH VEHICLE USING DISCRETE QUANTITATIVE FEEDBACK THEORY

THESIS

Donald Jerry Lacey Jr.
Captain, USAF

AFIT/GE/ENG/91D-33

# REPORT DOCUMENTATION PAGE

Form Approved
OMB No. 0704-0188



| 1. AGENCY USE ONLY *(Leave blank)* | 2. REPORT DATE | 3. REPORT TYPE AND DATES COVERED |
|---|---|---|
| | December 1991 | Master's Thesis |

**4. TITLE AND SUBTITLE**
A ROBUST DIGITAL FLIGHT CONTROL SYSTEM FOR AN UNMANNED RESEARCH VEHICLE USING DISCRETE QUANTITATIVE FEEDBACK THEORY

**5. FUNDING NUMBERS**

**6. AUTHOR(S)**
Donald Jerry Lacey Jr.
Captain, USAF

**7. PERFORMING ORGANIZATION NAME(S) AND ADDRESS(ES)**
Air Force Institute of Technology
WPAFB OH 45433-6583

**8. PERFORMING ORGANIZATION REPORT NUMBER**
AFIT/GE/ENG/91D-33

**9. SPONSORING/MONITORING AGENCY NAME(S) AND ADDRESS(ES)**
Capt Stuart N. Sheldon
Control Systems Development Branch
Wright Laboratory
Wright-Patterson AFB, OH 45433

**10. SPONSORING/MONITORING AGENCY REPORT NUMBER**

**11. SUPPLEMENTARY NOTES**

**12a. DISTRIBUTION/AVAILABILITY STATEMENT**
Approved for Public Release; Distribution Unlimited.

**12b. DISTRIBUTION CODE**

**13. ABSTRACT** *(Maximum 200 words)*

This thesis describes application of digital multiple-input multiple-output (MIMO) Quantitative Feedback Theory (QFT) technique to the design of a three axis rate controller for the Lambda Unmanned Research Vehicle. The resulting robust controller performs well throughout the flight envelope without gain scheduling. It results from research done at the Air Force Institute of Technology. The Lambda URV was designed by the Control Systems Development Branch of the Wright Laboratory at Wright-Patterson AFB, OH for flight testing aircraft control hardware and software. The flight control system is built using a small perturbation linear model developed from flight test data. The actuators, also modelled from aircraft test data, are second order in roll and pitch and first order in yaw. Nineteen separate plants are used to represent the flight envelope of the aircraft resulting from variations in speed, altitude, center of gravity location, and weight. The sample rate is 50 Hertz. The pitch channel is decoupled from the lateral-directional channel resulting in a single-input single-output (SISO) system for the pitch channel and a two-by-two MIMO system for the lateral-directional channel. The design employs the Nichols Chart and is accomplished in the w′-domain.

| 14. SUBJECT TERMS | 15. NUMBER OF PAGES |
|---|---|
| QFT, Quantitative Feedback Theory, UAV, Unmanned Aerial Vehicle, URV, Unmanned Research Vehicle, Flight Control System, Discrete QFT, Lambda, Nichols Chart | 176 |
| | 16. PRICE CODE |

| 17. SECURITY CLASSIFICATION OF REPORT | 18. SECURITY CLASSIFICATION OF THIS PAGE | 19. SECURITY CLASSIFICATION OF ABSTRACT | 20. LIMITATION OF ABSTRACT |
|---|---|---|---|
| Unclassified | Unclassified | Unclassified | UL |

## GENERAL INSTRUCTIONS FOR COMPLETING SF 298

The Report Documentation Page (RDP) is used in announcing and cataloging reports. It is important that this information be consistent with the rest of the report, particularly the cover and title page. Instructions for filling in each block of the form follow. It is important to ***stay within the lines*** to meet ***optical scanning requirements***.

**Block 1.** Agency Use Only *(Leave blank)*.

**Block 2.** Report Date. Full publication date including day, month, and year, if available (e g 1 Jan 88). Must cite at least the year.

**Block 3.** Type of Report and Dates Covered. State whether report is interim, final, etc If applicable, enter inclusive report dates (e.g. 10 Jun 87 - 30 Jun 88).

**Block 4.** Title and Subtitle A title is taken from the part of the report that provides the most meaningful and complete information. When a report is prepared in more than one volume, repeat the primary title, add volume number, and include subtitle for the specific volume On classified documents enter the title classification in parentheses.

**Block 5.** Funding Numbers. To include contract and grant numbers; may include program element number(s), project number(s), task number(s), and work unit number(s). Use the following labels:

| | | | |
|---|---|---|---|
| **C** | - Contract | **PR** | - Project |
| **G** | - Grant | **TA** | - Task |
| **PE** | - Program Element | **WU** | - Work Unit Accession No |

**Block 6.** Author(s). Name(s) of person(s) responsible for writing the report, performing the research, or credited with the content of the report. If editor or compiler, this should follow the name(s)

**Block 7.** Performing Organization Name(s) and Address(es). Self-explanatory.

**Block 8.** Performing Organization Report Number. Enter the unique alphanumeric report number(s) assigned by the organization performing the report

**Block 9.** Sponsoring/Monitoring Agency Name(s) and Address(es) Self-explanatory.

**Block 10.** Sponsoring/Monitoring Agency Report Number *(If known)*

**Block 11.** Supplementary Notes Enter information not included elsewhere such as: Prepared in cooperation with ; Trans. of ; To be published in When a report is revised, include a statement whether the new report supersedes or supplements the older report

**Block 12a.** Distribution/Availability Statement. Denotes public availability or limitations. Cite any availability to the public. Enter additional limitations or special markings in all capitals (e.g NOFORN, REL, ITAR).

- **DOD** - See DoDD 5230.24, "Distribution Statements on Technical Documents."
- **DOE** - See authorities.
- **NASA** - See Handbook NHB 2200 2.
- **NTIS** - Leave blank.

**Block 12b.** Distribution Code.

- **DOD** - Leave blank.
- **DOE** - Enter DOE distribution categories from the Standard Distribution for Unclassified Scientific and Technical Reports.
- **NASA** - Leave blank.
- **NTIS** - Leave blank.

**Block 13.** Abstract. Include a brief *(Maximum 200 words)* factual summary of the most significant information contained in the report.

**Block 14.** Subject Terms. Keywords or phrases identifying major subjects in the report.

**Block 15.** Number of Pages. Enter the total number of pages.

**Block 16.** Price Code Enter appropriate price code *(NTIS only)*

**Blocks 17. - 19.** Security Classifications. Self-explanatory Enter U.S. Security Classification in accordance with U.S. Security Regulations (i.e., UNCLASSIFIED) If form contains classified information, stamp classification on the top and bottom of the page

**Block 20.** Limitation of Abstract. This block must be completed to assign a limitation to the abstract. Enter either UL (unlimited) or SAR (same as report) An entry in this block is necessary if the abstract is to be limited If blank, the abstract is assumed to be unlimited

AFIT/GE/ENG/91D-33

# A ROBUST DIGITAL FLIGHT CONTROL SYSTEM FOR AN UNMANNED RESEARCH VEHICLE USING DISCRETE QUANTITATIVE FEEDBACK THEORY

THESIS



Presented to the Faculty of the School of Engineering
of the Air Force Institute of Technology
Air University
In Partial Fulfillment of the
Requirements for the Degree of
Master of Science in Electrical Engineering



Donald Jerry Lacey Jr., B.S.E.E.
Captain, USAF

December, 1991

## *Preface*

The purpose of this study was to build a robust flight control system for Lambda, an unmanned research vehicle. My interest in unmanned aerial vehicles led me to choose this topic and I am thankful to have had the opportunity. Although many controllers have been synthesized for Lambda, this is the first design applying Quantitative Feedback Theory to a mathematical model developed from Lambda's flght test data and based on Lambda's entire flight envelope. Simulations show encouraging performance and I hope to see my controller implemented on Lambda in the near future.

My sincere thanks go to the many people who helped me during the research. First, I'd like to thank my fellow classmates in the Guidance and Control Section for their help, advice and support. I've learned and benefited from every one of them and wish them all the best of luck in their Air Force careers. I'd also like to thank those students who worked on the project previously and had a great impact on this effort. In particular, I'd like to thank Capt David Wheaton for proving the concepts and sharing his results with me, and First Lieutenant Gerald Swift for developing the mathematical model from flight test data. My thanks also to the Control Systems Development Branch of the Wright Laboratory and especially to Capt Stuart Sheldon for providing the thesis topic and giving welcome advice and direction. It has been a pleasure working with Professor Constantine Houpis and I've enjoyed the unique opportunity to work with Professor Isaac Horowitz employing his Quantitative Feedback Theory. Finally, I'd like to thank my wife, Nancy and my son for their understanding and patience. I couldn't have done it without them.

Donald Jerry Lacey Jr.

*Table of Contents*

## *List of Figures*

## *List of Tables*

## *List of Symbols*

*Abstract*

This thesis describes the application of the digital multiple-input multiple-output (MIMO) Quantitative Feedback Theory (QFT) technique to the design of a three axis rate controller for the Lambda Unmanned Research Vehicle. The resulting robust controller performs well throughout the flight envelope without gain scheduling. It results from research done at the Air Force Institute of Technology . The Lambda URV was designed by the Control Systems Development Branch of the Wright Laboratory at Wright-Patterson AFB, OH for flight testing aircraft control hardware and software. The flight control system is built using a small perturbation linear model developed from flight test data. The actuators, also modelled from aircraft test data, are second order in roll and pitch and first order in yaw. Nineteen separate plants are used to represent the flight envelope of the aircraft resulting from variations in speed, altitude, center of gravity location, and weight. The sample rate is 50 Hertz. The pitch channel is decoupled from the lateral-directional channel resulting in a single-input single-output (SISO) system for the pitch channel and a two-by-two MIMO system for the lateral-directional channel. The design employs the Nichols Chart and is accomplished in the w′-domain.

# A ROBUST DIGITAL FLIGHT CONTROL SYSTEM FOR AN UNMANNED RESEARCH VEHICLE USING DISCRETE QUANTITATIVE FEEDBACK THEORY

## *I.* Introduction

### *1.1* Background

The Control Systems Development Branch of the Wright Laboratory at Wright-Patterson AFB, OH (WL/FIGL) developed the Lambda unmanned research vehicle (URV) for in-flight testing of aircraft control hardware and software. The Wright Laboratory, at the request of Congress, is using Lambda to develop and test the common core avionics package destined to be used on all unmanned aerial vehicles (UAVs) in the Department of Defense [25]. In order to provide the necessary test data, Lambda requires a stable, robust flight control system which performs well throughout the entire flight envelope. Capt David Wheaton, in his masters thesis, designed a flight control system for Lambda using digital Quantitative Feedback Theory [26]. The Wright Laboratory is pleased with the design; however, it is based on an earlier mathematical model of Lambda derived solely from the physical dimensions of the aircraft design. Flight test data indicates that the aircraft behaves much differently than the physically derived predictions. A new, more representative model, derived from flight test data, was created by Lt Gerald Swift [24] and is used for this design. A new flight control system providing the robustness of Wheaton's design but using an updated model is needed. The Wright Laboratory is sponsoring

this thesis because they require a robust controller for Lambda. Using Quantitative Feedback Theory in the design will provide the robustness required.

Quantitative Feedback Theory (QFT) was developed by Dr Horowitz in 1979. It is an extension of his work, which began in 1958 [10], concerning the control of plants with uncertain parameters. QFT is a frequency design technique incorporating plant uncertainty early in the design process resulting in a robust controller [8]. Robust automatic flight control systems in a URV, and UAVs in general, reduce pilot work load, increase safety, and aid in the recovery of the vehicle. The automatic flight control system gives the ground-based pilot the ability to hold a desired flight condition. Additionally, functions normally provided by an on-board pilot, such as turn coordination, can be performed by the automatic flight control system.

## *1.2* Problem

The challenge is to produce a robust digital flight control system for Lambda using QFT and deliver a set of controller difference equations to the sponsor. The sponsor, the Wright Laboratory, is responsible for installing and testing the system on Lambda. The system must uncouple the roll, pitch and yaw responses. For example, a command to roll the airplane should not produce a yaw or pitch response. The system must meet all performance specifications throughout the flight envelope. The flight envelope includes speeds from 45 to 110 knots, center of gravity locations between 21.8 and 32.4% Mean Aerodynamic Cord (MAC), vehicle weights from 181 to 215 pounds, and altitudes up to 5000 feet. Speed will vary between 76 and 185 feet-per-second. The system must perform several autopilot functions including: attitude hold, altitude hold, heading hold, and out-of-sight maneuvering.

## *1.3* Summary of Current Knowledge

Quantitative Feedback Theory is a design technique aimed at meeting both stability and performance specifications [20] and guarantees system performance over a

wide range of uncertainties in the plant and environment [26]. In 1963, Dr Horowitz first proposed a Nichols chart design technique that accounted for uncertainties "up front," early in the design. In 1979, after years of work, he refined the technique and coined the name Quantitative Feedback Theory or QFT [26], which later became known as Method One. From the beginning, QFT was criticized for its tendency for overdesign and less than optimum realization. However, Dr Horowitz never claimed his technique produced optimum designs. He simply claimed, "The technique guarantees a satisfactory design . . . by a comparatively straightforward systematic procedure [8]." In fact, QFT is one of the very few methods claiming a straightforward approach that addresses robust performance [20]. In 1982, Dr Horowitz developed the QFT Improved Method, called Method Two, which reduced the overdesign [9]. According to Horowitz [10], plant and disturbance uncertainties are the reasons for feedback in the system. This philosophy is fundamental to QFT [8]. Quantitative Feedback Theory, a development of conventional control theory, is growing in acceptance in spite of criticism from modern control theorists. Modern control theory, or optimal control theory, completely ignored plant uncertainties until recently [27]. Additionally, history has shown QFT designs to succeed where other techniques have failed. Specifically, QFT designers working on the F-4B were able to produce a flight control system with excellent stability margins using a single fixed gain compensator. The original compensator used a gain scheduling technique to handle variations in the plant and environment but did not work well due to its additional complexity and inherent computational lag [27]. Successful QFT controllers have been synthesized for the YF16CCV, C135, AFTI-F16, STOL, and F4B aircraft. "There is a great lack of similar design examples by other modern robustness method[s]. . .But where quantitative comparison was possible, QFT design was much more economical in loop compensation gain and bandwidth [27]." Air Force Institute of Technology (AFIT) students have been designing flight control systems using QFT since 1982. The following is a partial list of theses using QFT:

- J. M. Adams — *Digital QFT Design for the AFTI/F- 16* [1] (1988)
- P. B. Arnold — *FCS Reconfiguration Using QFT* [2] (1894)
- B. T. Clough — *Reconfiguration for a STOL Aircraft Using QFT* [4] (1985)
- J. S. Coucouies — *Effects of Discretizing QFT Designs* [5] (1985)
- S. W. Hamilton — *Digital QFT Design for an Unmanned Research Vehicle* [6] (1987)
- B. S. Migyanko — *Integrated Flight/Propulsion Control for a STOL Aircraft Using QFT* [15] (1986)
- K. N. Neumann — *Digital QFT Design for the Control Reconfigurable Combat Aircraft* [19] (1988)
- P. T. Ott — *URV Reconfiguration using Digital QFT* [21] (1988)
- H. H. Russell — *Analog QFT Design for the KC-135* [22] (1984)
- D. L. Schneider — *AFTI/F-16 FCS Design Using Digital QFT* [23] (1986)
- D. G. Wheaton — *AFCS Design for a URV Using Discrete QFT* [26] (1990)

## *1.4* Assumptions

This thesis uses a linear time-invariant (LTI) model of Lambda which is known to be a nonlinear system. Further, the equations of motion and the aircraft dynamics are Laplace transformable. In addition, the following conditions are assumed:

- Small-angle perturbation models are valid.
- Aircraft mass is constant.
- The aircraft is rigid: that is, no bending or flutter modes.
- The earth is an inertial reference frame.
- The atmosphere is fixed in relation to the earth.
- The commanded inputs and the commanded outputs are measurable.

- Three-axis rate signals—pitch rate ($q$), roll rate ($p$) and yaw rate($r$)—and the Euler angles— pitch angle ($\theta$), roll angle ($\phi$), and yaw angle ($\psi$)—are available on the Lambda URV.
- A digital sampling rate of 50 Hz is used.

## *1.5* Scope

The design is limited to the development of the set of controller difference equations needed to control Lambda throughout the expected flight envelope. The Wright Laboratory will implement the design on Lambda. Although the success of the design will be proven when the automatic flight control system is installed and flown on Lambda, this design ends with a successful computer simulation.

## *1.6* Standards

The controller is required to have a 45° phase margin throughout the flight envelope in all three axes—pitch, roll, and yaw. In addition, the aircraft is required to meet figures-of-merit including specific rise time and overshoot requirements. See Table (1.1). The performance requirements are the same as in the previous work done by Wheaton [26]. Frequency response tracking bounds for pitch, roll, yaw are included in Figure (1.1). Time response tracking bounds are included in Figure (1.2)

## *1.7* Approach/Methodology

This design begins with a mathematical description of the airplane, followed by definition of the flight envelope and flight conditions. Individual flight conditions include variations in flight speed, center of gravity location, vehicle weight, and altitude. Analysis of the model reveals the lateral–directional dynamics can be separated from the longitudinal dynamics. Since separation is possible, the design reduces to a single–input single–output (SISO) QFT system design and a two–by–two multiple–input multiple–output (MIMO) QFT system design. Analysis of the system indicates

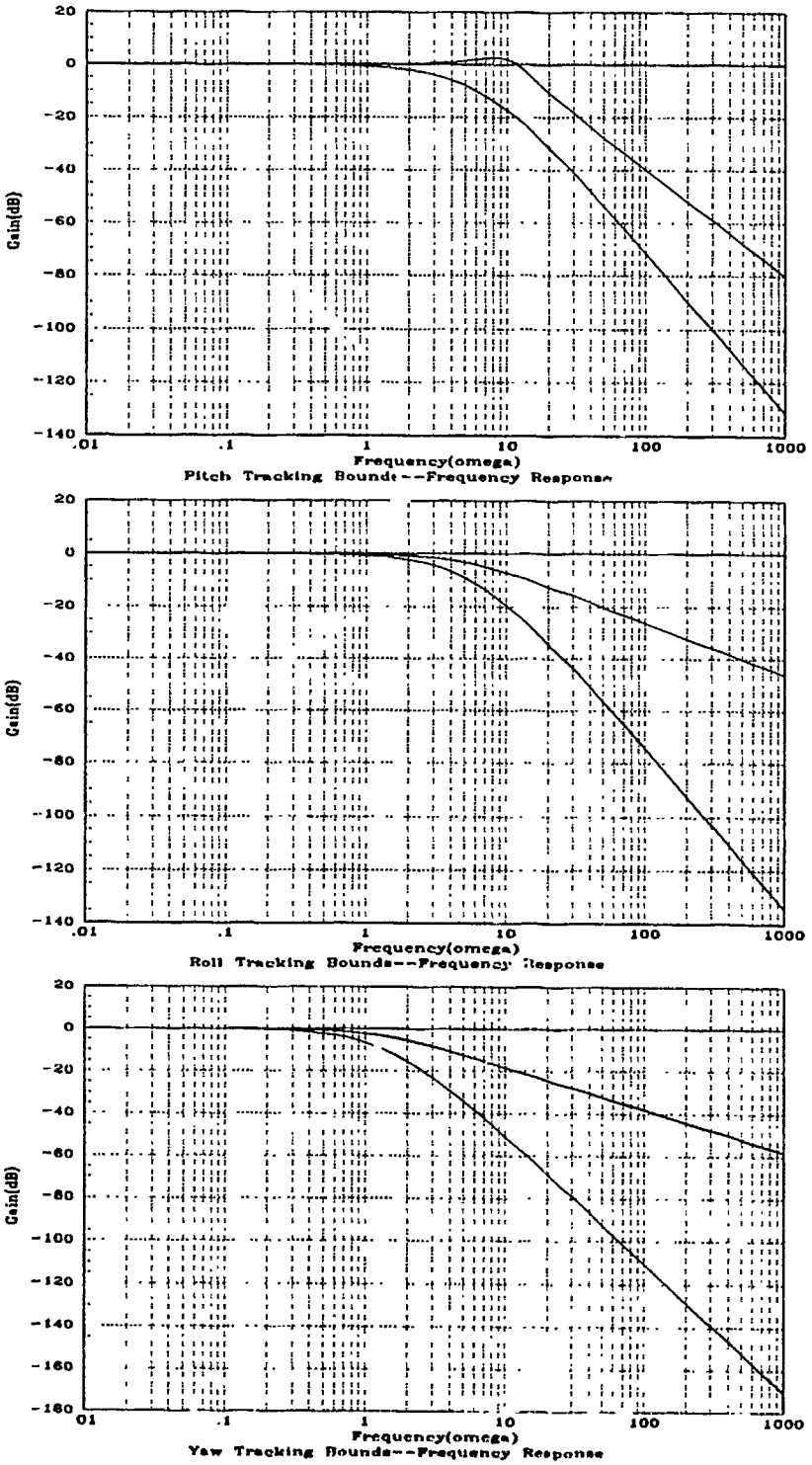


Figure 1.1. Pitch, Roll, and Yaw Frequency Response Tracking Bounds

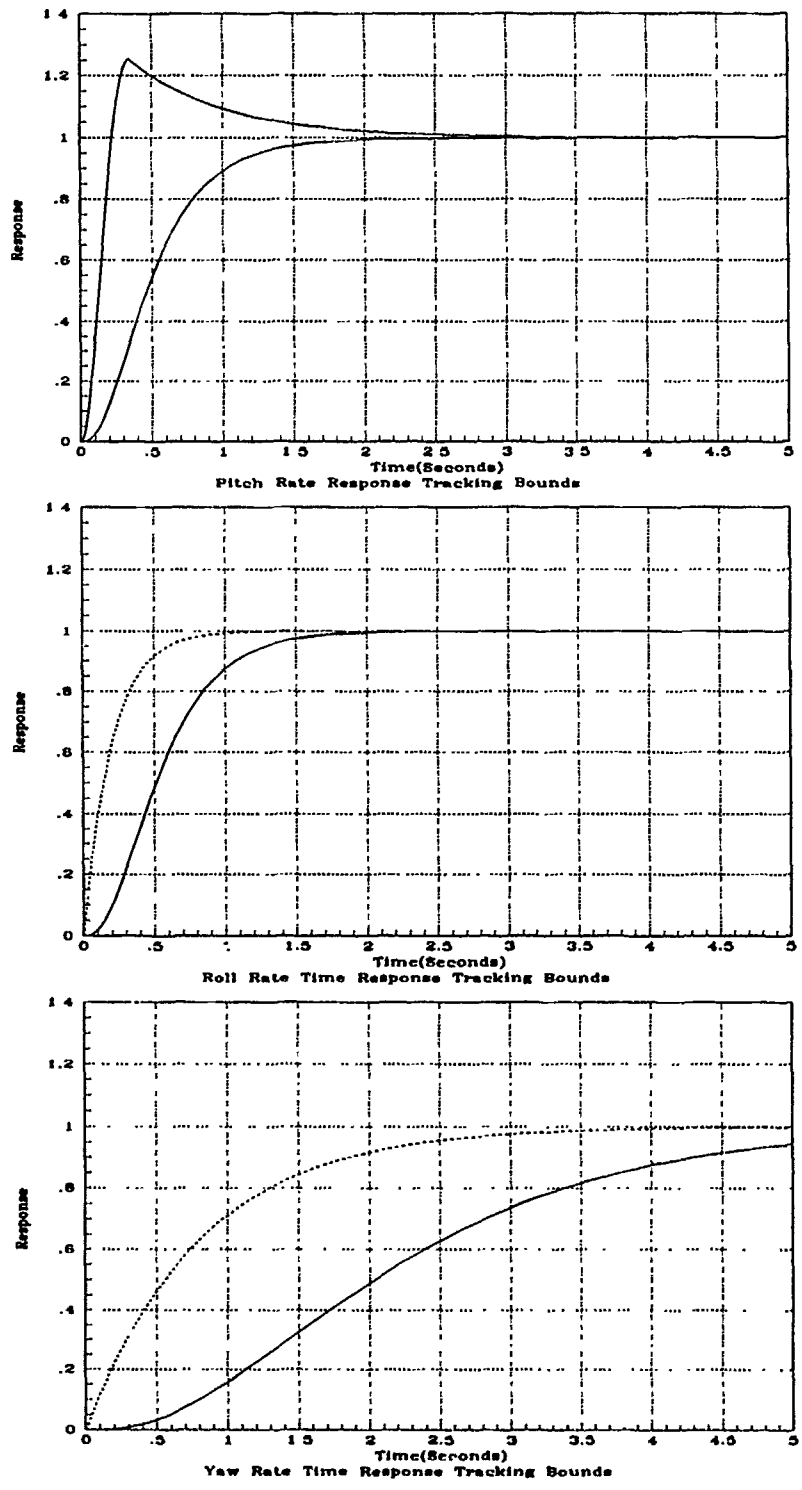


Figure 1.2. Pitch, Roll, and Yaw Time Response Tracking Bounds

Table 1.1. Figures-of-Merit for the QFT Response Models

| Model | $T_r$ (sec) | $T_s$ (sec) | $M_p$ $(\frac{rad}{sec})$ |
|---|---|---|---|
| $\frac{q_{LB}(s)}{q_{cmd_{LB}}(s)}$ | 0.84 | 1.56 | 1.0 |
| $\frac{q_{UB}(s)}{q_{cmd_{UB}}(s)}$ | 0.15 | 2.05 | 1.25 |
| $\frac{p_{LB}(s)}{p_{cmd_{LB}}(s)}$ | 0.87 | 1.56 | 1.0 |
| $\frac{p_{UB}(s)}{p_{cmd_{UB}}(s)}$ | 0.44 | 0.78 | 1.0 |
| $\frac{r_{LB}(s)}{r_{cmd_{LB}}(s)}$ | 3.48 | 6.22 | 1.0 |
| $\frac{r_{UB}(s)}{r_{cmd_{UB}}(s)}$ | 1.76 | 3.13 | 1.0 |

that unstable and nonminimum phase conditions exist. In contrast with Wheaton's work, a weighting matrix to blend the multiple inputs into three effective inputs [26] is already included in the mathematical model. Since inversion of the plant matrix is necessary [8], the plants must be square, (the same number of outputs as inputs) in this case, three–by–three. Flight data, used for the mathematical model, produced square plants.

A three–by–three MIMO system QFT design requires the synthesis of three separate transmission loops; a two–by–two plant requires two loops. Design starts with the loop with the smallest bandwidth. Once obtained, the first loop is used in developing the second and third loops. The technique of designing loops using elements of previously designed loops is part of Dr Horowitz's improved method (Method Two). It reduces the inherent overdesign, a characteristic of the QFT method [9]. Once the three loops are shaped, the design is simulated on the computer to validate the performance expectations. In designing the controller for the SISO system, the steps used for application of the discrete QFT technique are:

- Choose the Flight Conditions
- Determine the Plant Transfer Functions, $P_i(s)$
- Transform $P_i(s)$ to the w′ Domain, $P_i(w')$

- Determine the Frequency Response Data
- Extract the Template Data from the Frequency Response Data
- Plot the Templates
- Choose a Nominal Plant, $P_o$
- Use the Templates to form the Stability and Performance Bounds
- Shape the Nominal Loop, $L_o(w')$
- Extract the Compensator, $G(w')$, from $L_o(w')$
- Synthesize the Prefilter, $F(w')$
- Verify Loop Shaping in the w'-Plane
- Transform $F(w')$ to $F(z)$ and $G(w')$ to $G(z)$
- Simulate using $G(z)$, $F(z)$, and $P_i(s)$

A slightly modified procedure must be followed when designing the controller for the MIMO system using the discrete QFT technique. The steps are:

- Choose the Flight Conditions
- Determine the Plant Transfer Function Matrix, $\mathbf{P}(s)$
- Invert $\mathbf{P}(s)$

$$\mathbf{P}^{-1}(s) = \begin{bmatrix} p_{11}^*(s) & p_{12}^*(s) \\ p_{12}^*(s) & p_{22}^*(s) \end{bmatrix} \tag{1.1}$$

- Calculate the $\mathbf{Q}(s)$ Matrix

$$\mathbf{Q}(s) = \begin{bmatrix} \frac{1}{p_{11}^*(s)} & \frac{1}{p_{12}^*(s)} \\ \frac{1}{p_{12}^*(s)} & \frac{1}{p_{22}^*(s)} \end{bmatrix} = \begin{bmatrix} q_{11} & q_{12} \\ q_{21} & q_{22} \end{bmatrix} \tag{1.2}$$

- Transform **Q**(s) to the w′ Domain, **Q**(w′) which includes the necessary zero order hold (ZOH).
- Determine the Frequency Response Data
- Extract the Template Data from the Frequency Response Data
- Plot the Templates for One Input–Output Pair
- Choose a Nominal Plant
- Use the Templates to Form the Stability and Performance Bounds
- Shape the Nominal Loop, $L_o(w')$
- Extract the Compensator, G(w′), from $L_o(w')$
- Synthesize the Prefilter, F(w′)
- Shape the Remaining Loops
- Form the Remaining G(w′)s and F(w′)s
- Verify Loop Shaping in the w′-Plane
- Transform the F(w′)s to F(z)s and the G(w′)s to G(z)s
- Simulate using the G(z)s, F(z)s, and **P**(s)s

The next step adds the automatic flight control modes. The first mode is turn coordination. There are at least four methods of turn coordination [3]. One is chosen based on the sensors available and the desires of the Wright Laboratory. Wheaton added and tested a wings leveler to his design [26]. This effort extends the design by allowing the pilot to set a bank angle. Auto speed and altitude hold modes are the final modes added to Lambda. Finally, the system is simulated on MATRIX$_X$.

## *1.8* Materials and Equipment

The design and analysis is performed using MATRIX$_X$ on the SPARC station 2 computers available at the Air Force Institute of Technology and at the Wright

Laboratory. MATRIX$_X$ is a matrix calculator with graphics and a system build capability which can be used to simulate the complete system [14].

## *1.9* Other Support

The Wright Laboratory, owners of Lambda and sponsor of the thesis, provided performance specifications and aircraft dynamics models. The thesis committee, consisting of Dr Houpis, Dr Horowitz, Dr Ewing, and Capt Sheldon, provided direction, advice, and constructive feedback during and after the design effort.

# *II.* The Aircraft Model

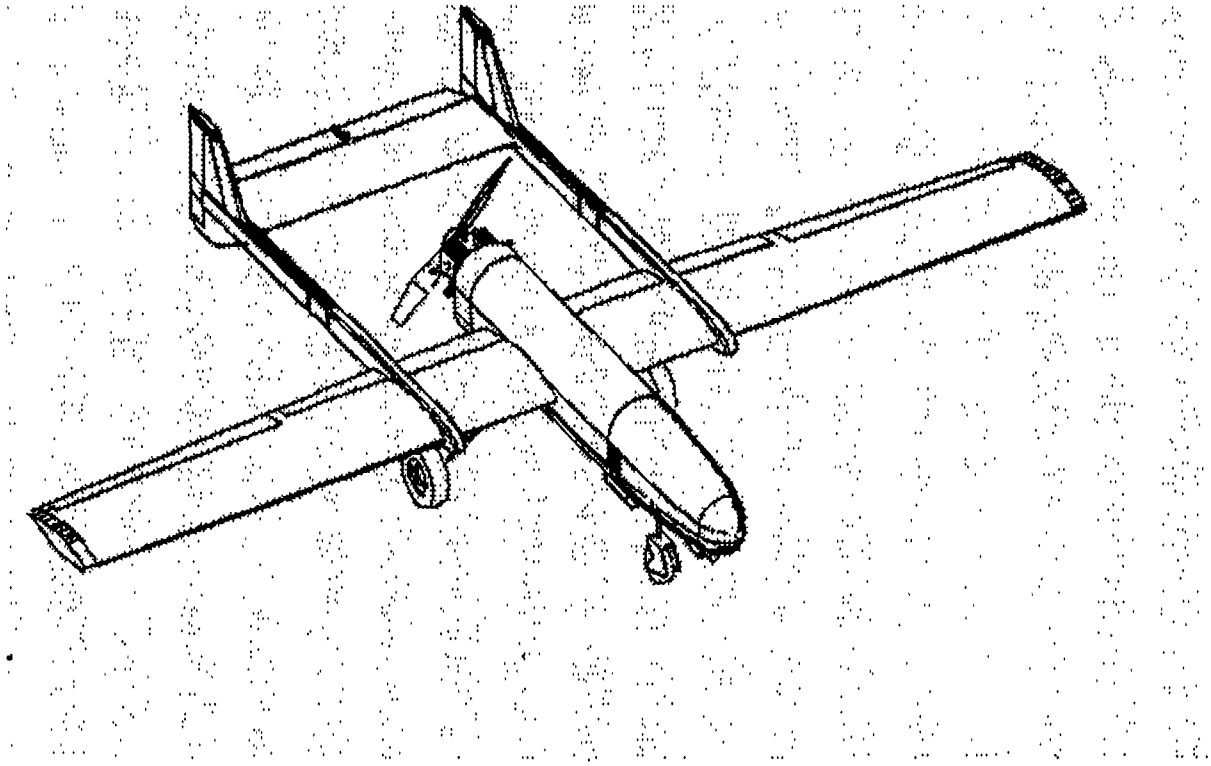

Figure 2.1. Lambda URV

This chapter discusses the Lambda aircraft and the model used in the design of the QFT rate controller.

## *2.1* The Aircraft

Lambda, shown in Figure 2.1, is a small remotely–piloted airplane with a 14 foot wing span and weight of approximately 200 pounds. See Table 2.1 for Lambda's characteristics. It uses a pusher propeller behind the fuselage and in front of a conventional aft tail. The horizontal tail consists of a horizontal stabilizer and a split elevator. A vertical tail is located on either end of the horizontal tail, and consists of a vertical stabilizer and rudder. The wings are slightly tapered; each has three trailing, moveable control surfaces. Lambda closely resembles the Pioneer

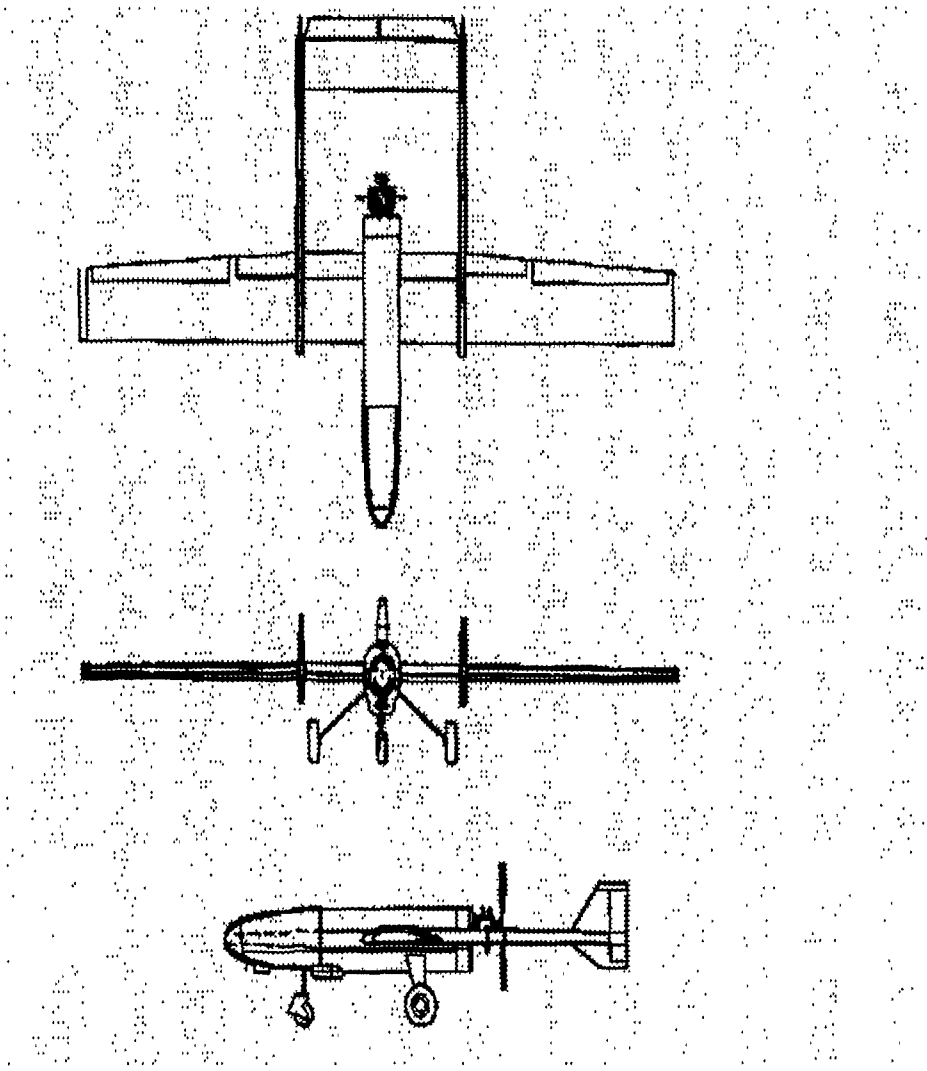

Figure 2.2. Three Views of the Lambda URV

UAV successfully employed by the United States Navy in the Persian Gulf War. The Pioneers are slightly larger and twice as heavy but share the configuration of an aft tail, center mounted engine, and pusher propeller. Lambda has ten separate control surfaces. They are:

- Left Elevator
- Right Elevator
- Left Rudder

Table 2.1. Lambda Descriptive Data

| | | |
|---|---|---|
| **Dimensions** | Wing Span ..... | 14 ft |
| | Wing Area ..... | 19 sq ft |
| | Length ..... | 9.6 ft |
| | Height With Landing Gear ..... | 3 ft |
| | Propeller Diameter ..... | 2.3 ft |
| **Weights** | Maximum Fuel ..... | 14 lb |
| | Maximum Payload ..... | 15 lb |
| | Maximum Flight Weight ..... | 200 lb |
| **Performance** | Maximum Level Speed at Sea Level | 115 mph (100 knots) |
| | Stall Speed ..... | 63 mph (55 knots) |
| | Stall Speed With Flaps ..... | 52 mph (45 knots) |
| **Engine** | Power ..... | 18 hp |
| | Type ..... | 2 cycle, 2 cylinder |
| **Control Limits** | Elevator Deflection Limit ..... | $\pm$ 15° |
| | Rudder Deflection Limit ..... | $\pm$ 25° |
| | Flap Deflection Limit ..... | 20° down |
| | Aileron Deflection Limit ..... | $\pm$ 15° |

- Right Rudder
- Left Aileron
- Right Aileron
- Left Outer Flap
- Right Outer Flap
- Left Inner Flap
- Right Inner Flap

Even though each control surface can be operated independently, the flight data, used to create the mathematical model upon which this design is based, were obtained using the control surfaces together. All four of the flap control surfaces were operated together as were the two rudders. The split elevators were deflected together while the ailerons were operated differentially. Much of the flexibility built into Lambda was discarded by employing the surfaces in this manner. Future projects should

consider implementing control schemes that rely on independent control surface deflections. Since the mathematical model does not include flap actuator dynamics, the flaps are not used as a control surface. Again, a future design might incorporate the flaps as an active part of the flight control system once the flap actuator dynamics are known and included in the model.

This control system is based on the design specifications of Lambda. It is expected that Lambda will gain weight. Indeed, today's model of Lambda is heavier than it was when first built, which was heavier than specified. The weight increase results from adding equipment, such as video cameras and additional sensors. For this reason, this design includes weights up to 215 pounds. Additionally, since Lambda is designed to fly at speeds up to 100 knots, speeds up to 110 knots are included to encompass all of the expected plant variation. The heavier weights are very demanding of the technique and contribute greater plant variation compared with the higher speeds which contribute little variation.

## *2.2* The Model

Lt Gerald Swift developed the small perturbation model based on a series of test flights conducted by the Wright Laboratory [24]. His model incorporates the traditional stability derivatives into a state space representation of the aircraft. Lt Swift provided a MATLAB macro file which creates the state space representation along with the stability derivatives when given a set of flight conditions (see Appendix A). The aircraft, excluding actuator and sensor dynamics, can be described using nine states. They are: q, p, r, $\theta$, $\phi$ ,$\psi$, $\alpha$, u, $\beta$. Of these, q, $\theta$, $\alpha$, and u are used to describe the longitudinal channel, while the states p, r, $\phi$, $\psi$, and $\beta$ describe the lateral-directional dynamics. The aircraft model state space representation is:

$$\dot{\mathbf{x}}(t) = \mathbf{A}(t)\mathbf{x}(t) + \mathbf{B}(t)\mathbf{u}(t) \tag{2.1}$$

$$\mathbf{y}(t) = \mathbf{C}\mathbf{x}(t) \tag{2.2}$$

Assuming zero initial conditions ($\mathbf{x}_0 = \mathbf{0}$) and a trim condition ($\dot{\mathbf{x}}_0 = \mathbf{0}$), the Laplace transform of the plant is the perturbation model:

$$\dot{\mathbf{X}}(s) = \mathbf{A}(s)\mathbf{X}(s) + \mathbf{B}(s)\mathbf{U}(s) \tag{2.3}$$

$$\mathbf{Y}(s) = \mathbf{C}(s)\mathbf{X}(s) \tag{2.4}$$

where:

$$\mathbf{A}(s) = \begin{bmatrix} \mathbf{A}(s)_{long} & \mathbf{0} \\ \mathbf{0} & \mathbf{A}(s)_{lat} \end{bmatrix} \quad \mathbf{B}(s) = \begin{bmatrix} \mathbf{B}(s)_{long} \\ \mathbf{B}(s)_{lat} \end{bmatrix} \tag{2.5}$$

$$\mathbf{C}(s) = \begin{bmatrix} \mathbf{C}(s)_{long} & \mathbf{C}(s)_{lat} \end{bmatrix} \tag{2.6}$$

The Lambda longitudinal and lateral-directional dynamics are modelled as decoupled. In other words, pitch motion doesn't induce a roll or yaw response and a yaw or roll does not induce a pitch response. While the model has decoupled dynamics, actually , there is some unmodelled coupling. However, this design uses the best model available for Lambda.

## *2.3* Actuators and Sensors

The actuators used in the mathematical model of Lambda are second-order in the pitch and roll channels and first-order in the yaw channel. The model used for the pitch channel actuator is:

$$\frac{87}{s^2 + 18s + 120} \tag{2.7}$$

The model used for the roll channel is:

$$\frac{84}{s^2 + 18s + 120} \tag{2.8}$$

The model used for the yaw channel is:

$$\frac{5.58}{s+3.2} \tag{2.9}$$

The sensors used to measure the rates are identical gyroscopes with transfer functions modelled as:

$$\frac{50}{s+50} \tag{2.10}$$

## *2.4* Center of Gravity

Lt Swift also provided the formula for calculating the center of gravity (cg) location:

$$cg_{\%MAC} = 100(\frac{X_{cg} - 41.875}{18.12}) \tag{2.11}$$

where $X_{cg}$ is the location of the center of gravity in inches from the nose of the aircraft.

## *2.5* Flight Envelope

The Wright Laboratory built Lambda to fly within the flight envelope:

- Speeds from 45 to 100 Knots
- Maximum Flight Weight 200 Pounds
- Altitude up to 5000 Feet

# *III.* Longitudinal SISO Design

This chapter covers the design of the longitudinal channel of Lambda using QFT. The design steps are outlined in Section 1.7 of Chapter 1.

## *3.1* Flight Conditions

The flight conditions are selected from the design flight envelope of Lambda with considerations given to the growth of the program and expected changes. There are four variables considered in the selection of flight conditions. They are:

- Center of Gravity Location
- Flight Speed
- Altitude
- Aircraft Weight

The minimum and maximum values of each variable create a set of sixteen flight conditions. The sixteen flight conditions produce two widely spaced plant groupings. The difference in speed contributes the most to the wide plant variation, with the other variables contributing smaller variations. Three additional speeds are added to fill in the gap between the lower and higher speeds. A weight of 200 pounds, a center of gravity location in the center of the range, along with the lowest altitude, are chosen for the additional conditions. A total of nineteen separate plants are used. See Table 3.1 for the conditions used in the design.

Table 3.1. The Aircraft Flight Conditions

| Plant # | cg (% MAC) | Speed (kts) | $Q_\infty$ (lbs/ft$^2$) | Weight (lbs) |
|---|---|---|---|---|
| 1 | 21.8 | 110 | 35.05 | 181 |
| 2 | 21.8 | 110 | 35.05 | 215 |
| 3 | 21.8 | 110 | 40.08 | 181 |
| 4 | 21.8 | 110 | 40.08 | 215 |
| 5 | 32.4 | 110 | 35.05 | 181 |
| 6 | 32.4 | 110 | 35.05 | 215 |
| 7 | 32.4 | 110 | 40.08 | 181 |
| 8 | 32.4 | 110 | 40.08 | 215 |
| 9 | 27.1 | 61 | 12.61 | 200 |
| 10 | 27.1 | 77 | 20.08 | 200 |
| 11 | 27.1 | 93 | 29.90 | 200 |
| 12 | 32.4 | 45 | 5.915 | 181 |
| 13 | 32.4 | 45 | 5.915 | 215 |
| 14 | 32.4 | 45 | 6.765 | 181 |
| 15 | 32.4 | 45 | 6.765 | 215 |
| 16 | 21.8 | 45 | 5.915 | 181 |
| 17 | 21.8 | 45 | 5.915 | 215 |
| 18 | 21.8 | 45 | 6.765 | 181 |
| 19 | 21.8 | 45 | 6.765 | 215 |

## *3.2* s–Plane Transfer Fu. ctions

The longitudinal plant transfer functions are developed from MATRIX$_X$ using the MATRIX$_X$ System Build capability. Each condition is used as an input into the MATLAB macro file provided to the Wright Laboratory by Lt Swift (see Appendix A). The outputs include **A** and **B** matrices for the longitudinal and lateral-directional dynamics of Lambda. The **A** and **B** matrices for the longitudinal

channel are of the form:

$$\mathbf{A}_{long} = \begin{bmatrix} X_u & X_\alpha & 0 & -32.174\cos(\theta) \\ \frac{Z_u}{u-Z_{\dot{\alpha}}} & \frac{Z_\alpha}{u-Z_{\dot{\alpha}}} & \frac{u+Z_q}{u-Z_{\dot{\alpha}}} & -32.174\sin\theta \\ \frac{M_u+M_{\dot{\alpha}}Z_u}{u-Z_{\dot{\alpha}}} & \frac{M_\alpha+M_{\dot{\alpha}}Z_\alpha}{u-Z_{\dot{\alpha}}} & \frac{M_q+M_\alpha u+Z_q}{u-Z_{\dot{\alpha}}} & -32.174M_{\dot{\alpha}}\sin\theta \\ 0 & 0 & 1 & 0 \end{bmatrix} \tag{3.1}$$

$$\mathbf{B}_{long} = \begin{bmatrix} X_{\delta_{elev}} & X\delta_{flap} \\ \frac{Z_{\delta_{elev}}}{u-Z_{\dot{\alpha}}} & \frac{Z_{\delta_{flap}}}{u-Z_{\dot{\alpha}}} \\ \frac{M_{\delta_{elev}}+M_{\dot{\alpha}}Z_{\delta_{elev}}}{u-Z_\alpha} & \frac{M_{\delta_{flap}}+M_{\dot{\alpha}}}{u-Z_{\dot{\alpha}}} \\ 0 & 0 \end{bmatrix} \tag{3.2}$$

Since the flaps are not used as a control input, the second column of $\mathbf{B}_{long}$ is discarded which results in:

$$\mathbf{B}_{long} = \begin{bmatrix} X_{\delta_{elev}} \\ \frac{Z_{\delta_{elev}}}{u-Z_{\dot{\alpha}}} \\ \frac{M_{\delta_{elev}}+M_{\dot{\alpha}}Z_{\delta_{elev}}}{u-Z_{\dot{\alpha}}} \\ 0 \end{bmatrix} \tag{3.3}$$

The longitudinal matrices, **A**,**B**,**C**, and **D** are then assembled into a state space representation:

$$\begin{bmatrix} \mathbf{A} & \vdots & \mathbf{B} \\ \cdots & \cdots & \cdots \\ \mathbf{C} & \vdots & \mathbf{D} \end{bmatrix} \tag{3.4}$$

The state space representation is used in a MATRIX$_X$ System Build simulation to produce a linearized state space model which includes the actuators and sensors. The resulting state space representation is then transformed to a transfer function which relates the output to the input. The transfer functions are used in the design of the QFT controller which includes a compensator as well as a prefilter (see Figure 3.1). The following transfer function represents the longitudinal channel at the nominal

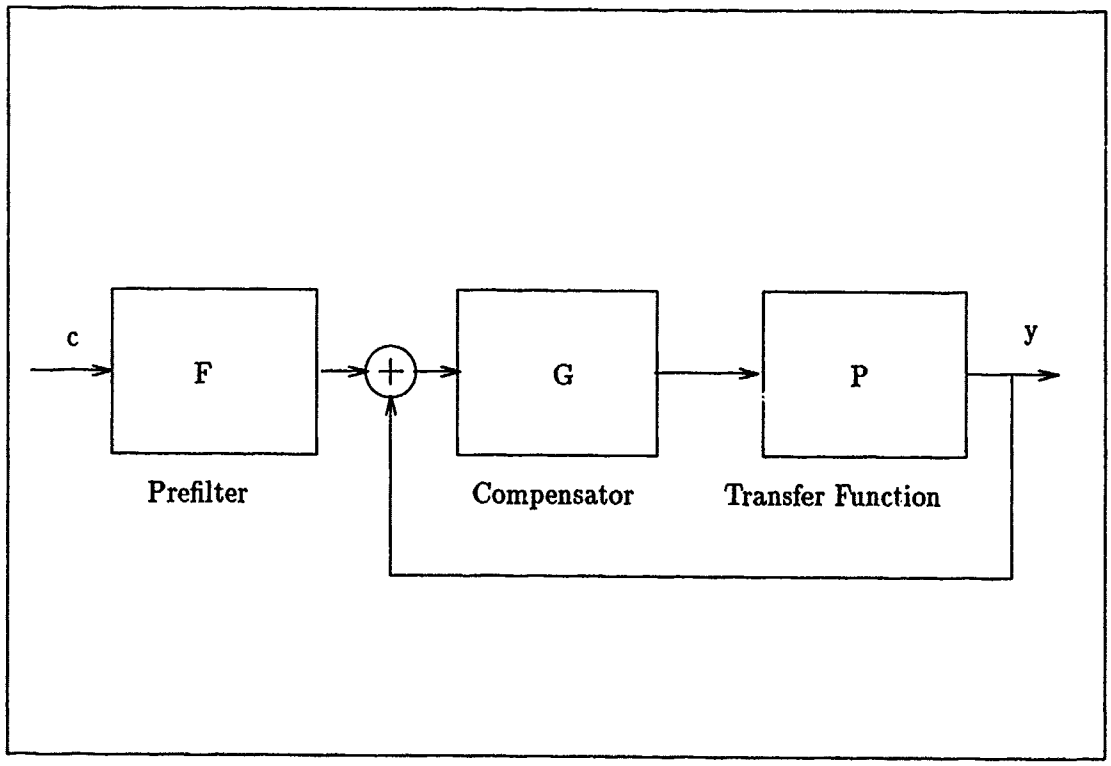


Figure 3.1. QFT Controller Block Diagram

conditions:

$$\frac{q(s)}{\delta_{elev}(s)} = \frac{1.5774 \times 10^5 (s)(s+0.054837)(s+3.7340)}{(s+0.0017819 \pm j0.22985)(s+3.2050 \pm j8.0129)(s+9 \pm j6.2450)(s+50.000)} \quad (3.5)$$

A complete set of transfer functions used in the design is included in Appendix B.

### *3.3* w′ Plant Transfer Functions

Lambda uses digital flight control hardware requiring a digital (discrete) flight control system design. Although an additional transform is necessary, the w′–plane is used in this design because it allows use of s–plane design tools, such as the Nichols Chart in the design of a discrete controller. Other options include designing in the z–domain or designing in the s–domain and then discretizing the results. Designing directly in the z–domain is tedious and very sensitive to small numerical errors because the entire left half of the s–plane is compressed into a unit circle. Designing

either in the w′–plane or the s–plane, the psuedo–continuous approach (PCT), involves the property of warping when transforming the s or w′–plane controller into the z–domain. The degree of "warping" decreases as the sampling time decreases as shown in Chapter VI of reference [13]. A good degree of correlation between the w′– and z–domain is maintained for a longer sample time than for the s– to z–domain correlation. Thus, for these reasons, the w′–plane is an excellent compromise. The w′–plane representation is normally obtained by transforming the s–plane plant, with a zero order hold (ZOH), into the z–plane then performing the bilinear transformation:

$$\mathrm{w}' = \frac{2}{\mathrm{T}}\left[\frac{z-1}{z+1}\right] \tag{3.6}$$

$$z = \frac{2+\mathrm{w}'\mathrm{T}}{2-\mathrm{w}'\mathrm{T}} \tag{3.7}$$

where T is equal to the sampling interval. The sampling interval is obtained from:

$$\mathrm{T} = \frac{1}{\text{Sampling Frequency}} \tag{3.8}$$

Lambda has a sampling frequency of 50 Hz which is equivalent to a sampling interval of 0.02 seconds.

As a review, the following relationships between $s$, z, and the w′–plane are presented [13]:

$$s = \sigma_{s-plane} + j\omega_{s-plane} = \sigma + j\omega \tag{3.9}$$

$$\mathrm{w}' = \sigma_{\mathrm{w}'\,plane} + j\omega_{\mathrm{w}'\,plane} = u + jv = \frac{2}{\mathrm{T}}\left[\frac{z-1}{z+1}\right] \tag{3.10}$$

$$z = \left[\frac{\mathrm{T}\mathrm{w}'+2}{-\mathrm{T}\mathrm{w}'+2}\right] \tag{3.11}$$

$$v = \left[\frac{2}{\mathrm{T}}\right]\tan\left[\frac{\omega\mathrm{T}}{2}\right] \tag{3.12}$$

$$z = \epsilon^{s\mathrm{T}} = \epsilon^{\sigma\mathrm{T}}\angle\omega\mathrm{T} = \mid z \mid \angle\omega\mathrm{T} \tag{3.13}$$

If:

$$\left[\frac{\sigma_{s-plane}T}{2}\right]^2 \ll 2 \tag{3.14}$$

and:

$$\frac{\omega_{s-plane}T}{2} \leq 0.297 \tag{3.15}$$

are satisfied then:

$$s \approx \mathrm{w}' \tag{3.16}$$

where:

$$s = \sigma_{s-plane} \pm j\omega_{s-plane} \tag{3.17}$$

and $\sigma_{s-plane}$ and $\omega_{s-plane}$ are the components of the fastest pole or zero in the plant. The fastest pole in the longitudinal plants is the pole associated with the sensor located at $-50$. The highest frequency in Equation (3.5) is associated with the complex pole pair at $(s + 3.205 \pm j8.013)$. Using $\sigma_{s-plane} = -50$ and T=0.02 Equation (3.14) becomes:

$$\left[\frac{\sigma_{s-plane}T}{2}\right]^2 = \left[\frac{(-50)(0.02)}{2}\right]^2 = 0.25 < 2 \tag{3.18}$$

Using $\omega_{s-plane} = 8.01$ and T=0.02 Equation (3.15) becomes:

$$\frac{\omega_{s-plane}T}{2} = \frac{(8.01)(0.02)}{2} = 0.0801 \leq 0.297 \tag{3.19}$$

Therefore the condition of Equation (3.15) is definitely satisfied. In Equation (3.14), the "much less" requirement may not be met. The ratio of 2 to $\left[\frac{\sigma_{s-plane}T}{2}\right]^2 = \left[\frac{(-50)(0.02)}{2}\right]^2$ is 8:1 which is sufficient providing the next highest real pole is sufficiently small. In this case, the next highest real pole is located at s= $-9$. Using Equation (3.14):

$$\left[\frac{\sigma_{s-plane}T}{2}\right]^2 = \left[\frac{(-9)(0.02)}{2}\right]^2 = 0.0081 \ll 2 \tag{3.20}$$

which meets the requirement by a wide margin. Therefore, even though some warping occurs due to the pole at $-50$ there is little warping due to the remaining poles and $s \approx w'$ is assumed. This indicates that the warping in going from the w'-plane to the s-plane should be minimal.

*3.3.1 The Hofmann Algorithm* In this design, the w'-plane representation of the plants are found using the Hofmann algorithm [7]. The Hofmann algorithm allows conversion of the s-domain representation through the z-plane and into the w'-plane without the normal numerical difficulties [26]. An important feature of Hofmann's algorithm is the automatic inclusion of the zero order hold. A ZOH is assumed to exist between the controller and the aircraft. A block diagram of the sampled-data system is included (see Figure 3.2). The Hofmann algorithm allows

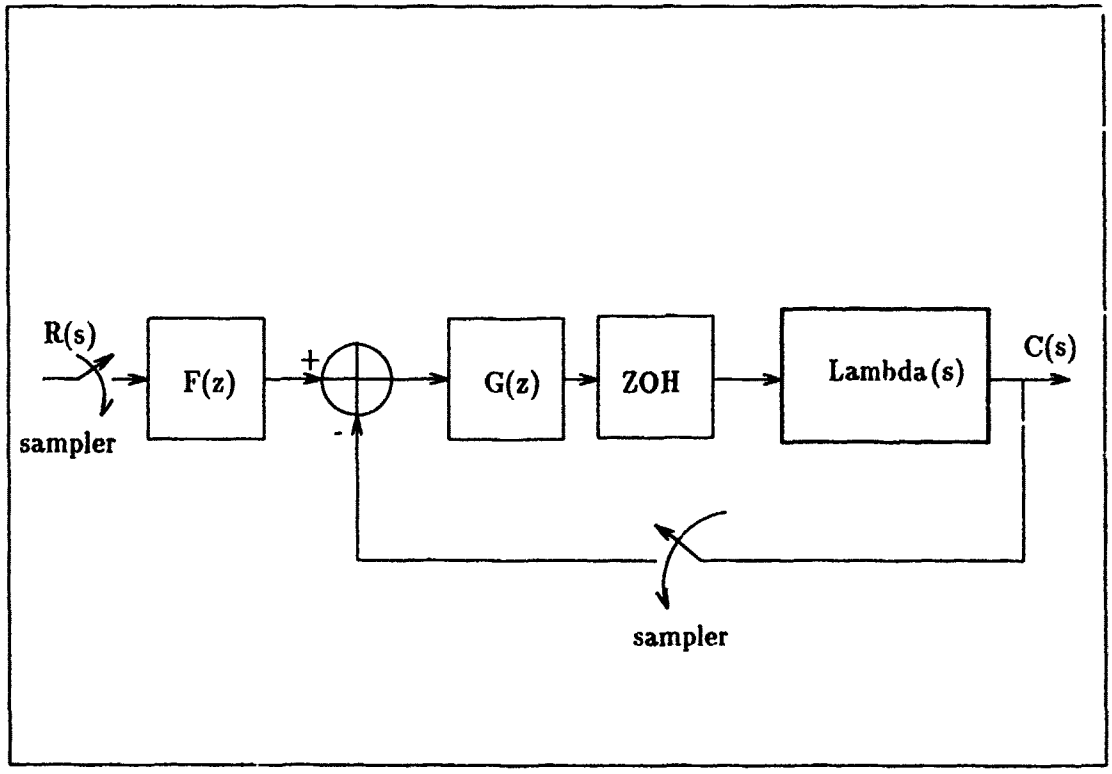


Figure 3.2. Sampled Data System

conversion of:

$$s\mathbf{X}(s) = \mathbf{A}\mathbf{X}(s) + \mathbf{B}\mathbf{U}(s) \tag{3.21}$$

and:

$$\mathbf{Y}(\mathbf{s}) = \mathbf{C}\mathbf{X}(s) + \mathbf{D}\mathbf{U}(s) \tag{3.22}$$

to:

$$\mathrm{w}'\mathbf{X}(\mathrm{w}') = \mathbf{A}^*\mathbf{X}(\mathrm{w}') + \left[1 - \frac{\mathrm{w}'T}{2}\right]\mathbf{B}^*\mathbf{U}(\mathrm{w}') \tag{3 23}$$

and:

$$\mathbf{Y}(\mathrm{w}') = \mathbf{C}\mathbf{X}(\mathrm{w}') + \mathbf{D}\mathbf{U}(\mathrm{w}') \tag{3.24}$$

where:

$$\mathbf{A}^* = \mathbf{A}\left[\frac{\mathbf{A}T}{2}\right]^{-1}\tanh\left(\frac{\mathbf{A}t}{2}\right) = \mathbf{A}^*\mathbf{A}_\epsilon \tag{3.25}$$

$$\mathbf{B}^* = \left[\frac{\mathbf{A}T}{2}\right]^{-1}\tanh\left(\frac{\mathbf{A}t}{2}\right)\mathbf{B} = \mathbf{A}_\epsilon\mathbf{B} \tag{3.26}$$

The six term Taylor series approximation of $\mathbf{A}_\epsilon$ used in this design is:

$$\mathbf{A}_\epsilon \approx \mathbf{I} - \frac{1}{3}\left[\frac{\mathbf{A}T}{2}\right]^2 + \frac{2}{15}\left[\frac{\mathbf{A}T}{2}\right]^4 - \frac{17}{315}\left[\frac{\mathbf{A}T}{2}\right]^6 + \frac{62}{2835}\left[\frac{\mathbf{A}T}{2}\right]^8 - \frac{1382}{155925}\left[\frac{\mathbf{A}T}{2}\right]^{10} \tag{3.27}$$

A MATRIX$_X$ executable file is used to perform the calculation and is included below:[1]

```
//Hofmann.cmd
t=1/50;  //sample rate of Lambda
[a,b,c,d]=split(s,ns);
ae=[eye-1/3*(a*t/2)**2+2/15*(a*t/2)**4...
-17/315*(a*t/2)**6...
+62/2835*(a*t/2)**8...
-1382/155925*(a*t/2)**10];
aw=a*ae;
be=ae*b;
bw=be-t/2*aw*be;
cw=c;
```

[1]This MATRIX$_X$ executable file differs from the one included in Capt Wheaton's Thesis [26]. The executable file included in Wheaton's thesis contains typographical errors.

```
dw=d-t/2*c*be;
sw=[aw,bw;cw,dw];
```

Since there are nineteen plants included in this design, the Hofmann algorithm is performed nineteen times. This is accomplished by using the programming capability of MATRIX$_X$ and placing the above code in an iterative loop. The following is a w′-plane representation of the transfer function at the nominal conditions:

$$\frac{q(\mathrm{w}')}{\delta_{elev}} = \frac{K\mathrm{w}'(\mathrm{w}'+0.005484)(\mathrm{w}'+3.732)(\mathrm{w}'-100)(\mathrm{w}'+116.2)(\mathrm{w}'-130.3)(\mathrm{w}'+718.7)}{(\mathrm{w}'+0.001782\pm j0.2299)(\mathrm{w}'+3.225\pm j8.022)(\mathrm{w}'+9.010\pm j6.203)(\mathrm{w}'+46.21)} \tag{3.28}$$

$$(K = 1.3414\times 10^{-4})$$

The above equation contains non-minimum phase (NMP) zeros at 100 and 130. They result from the w′ transformation, which always produces a transfer function with the same number of zeros as poles. The NMP zero at 100 is due to the sampling rate. The NMP zero at 130 is due to the excess number of poles over zeros in the s domain transfer function. According to Horowitz [10], if the number of poles exceeding the number of zeros is two, there will be two additional zeros created and one will be NMP. A complete set of w′-plane transfer functions is included in Appendix B.

## *3.4* Frequency Response Data

The QFT technique uses templates that represent the plant parameter uncertainty, at the specified design frequencies. The plant uncertainty for this thesis is represented by the nineteen LTI plants. For this reason, the frequency response information for all of the plants at the design frequencies is necessary. While obtaining the frequency response data, a problem was discovered in the way MATRIX$_X$ handles phase information. See Appendix E for a discussion of the problem. The frequency response data of the nineteen longitudinal plants are summarized in Figure 3.3.

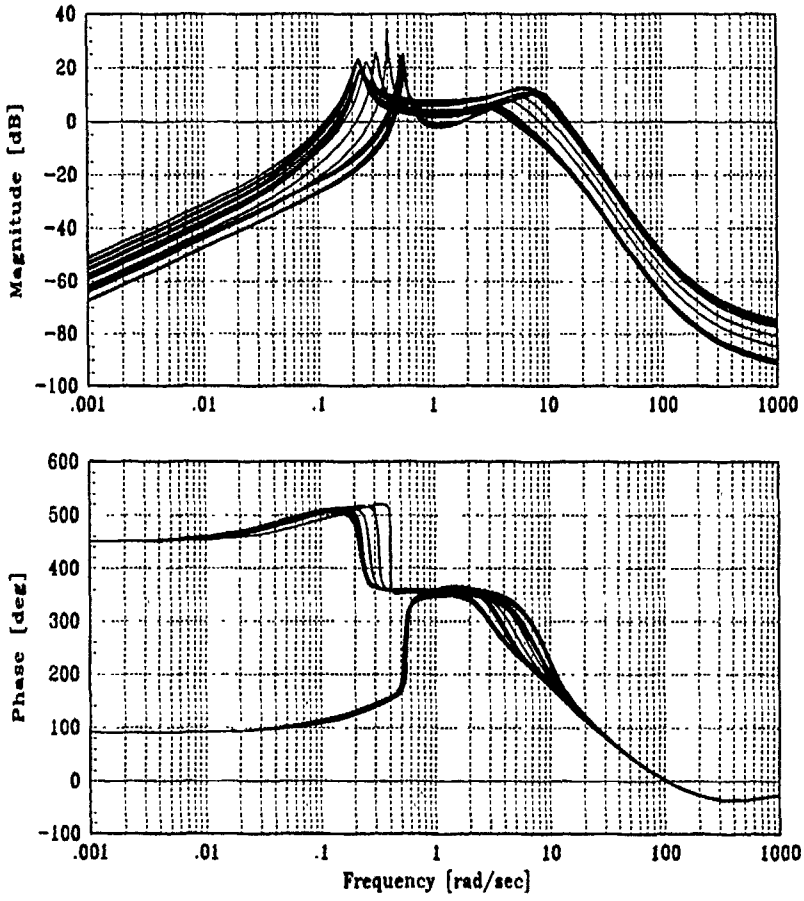


Figure 3.3. Frequency Response of the Nineteen Longitudinal Plants

## *3.5* Plant Templates

Plant templates are developed from the frequency response data. First the template frequencies are chosen on the basis of plant variation. Where the plants vary significantly, the template frequencies must be closely spaced. Where the plants are closely spaced, the frequencies can be more widely spaced.

For this design the frequencies $v$= 0.001, 0.005, 0.01, 0.05, 0.1, 0.2, 0.3, 0.4, 0.5, 0.6, 0.7, 1, 2, 3, 4, 5, 6, 8, 10, 20, 50, 100 (rad/sec) are used; where $v$ is the w′ analog of $\omega$ in the s-plane, and is given by Equation 3.12.

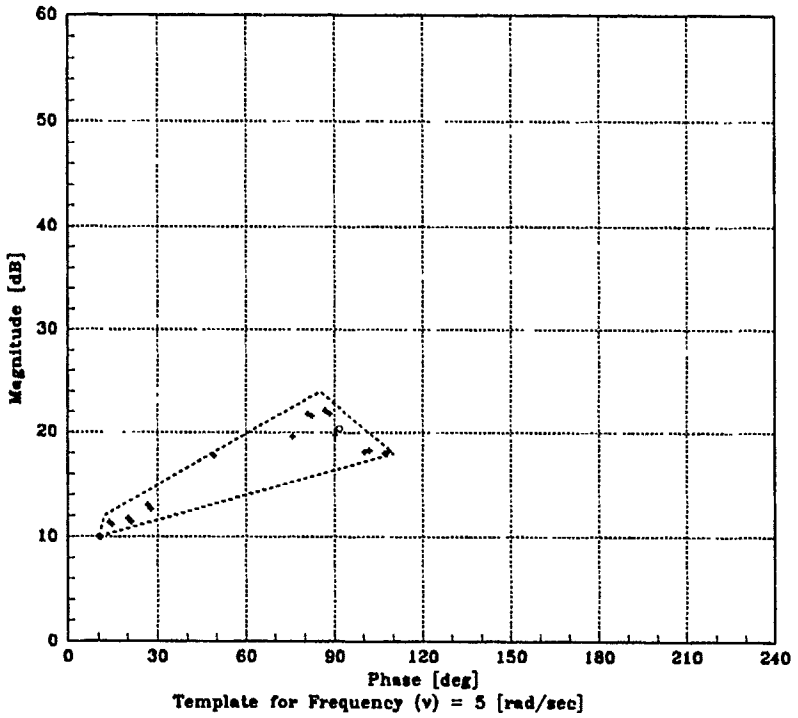


Figure 3.4. Example of Template Used in Longitudinal SISO Design

Next, the template data are "stripped out" of the frequency response data. Twenty two sets of template data are formed, a set for each template frequency. Each set contains magnitude and phase information for the nineteen plants at the template frequency. Only the magnitude and phase differences are important to the QFT technique. In plotting the templates, the data is normalized by subtracting the smallest phase from the phase data and the smallest magnitude from the magnitude data. The templates are then plotted for use in determining the stability bounds. An example template is shown in Figure 3.4 for $v = 5$. The template is defined by a set of points, each representing a plant. The spread of the points is due to the plant variation at the template frequency. In the example template, the lowest point is not located at the origin because a small magnitude and phase is added to the template data to distinguish all points from the plot axes. The circle represents the nominal plant. Choosing the nominal plant is discussed in the next section. The data used to plot the twenty–two templates are included in Appendix D.

## *3.6* Nominal Plant

Any one of the plants can be chosen as the nominal plant; however, choosing the plant with the least number of right–half–plane (RHP) poles and zeros may make the loop shaping easier [10]. The location of the nominal plant on each of the templates is needed before the bounds—tracking, disturbance, and stability—can be plotted on the Nichols Chart (NC). Plotting the bounds on the NC is key to the QFT technique. Because the plant uncertainty is captured in the templates and the templates are used to form the bounds, the single transmission loop shape meeting or exceeding the plotted NC bounds guarantees each plant considered will meet or exceed the tracking, disturbance, and stability performance specifications. The nominal plant chosen for the longitudinal SISO design is flight condition one. Additionally, the same flight condition is used in the lateral–directional MIMO system design discussed in Chapter IV.

## *3.7* Stability Bounds

A benefit to the designer using a predetermined (fixed) sampling rate is the need to consider only the stability bounds during the transmission loop shaping [10]. The maximum gain in the loop is primarily constrained by the NMP zeros. Therefore, the objective is to "pack in" as much transmission loop gain as possible. If the tracking and performance specifications are not met, a change in the sampling rate must be made to allow higher loop transmission gain. The military standard requirement, from MIL-STD-1797A [16], specifies a phase margin $\gamma = 45°$ to be used to form the NC stability contour $M_L$. The $\gamma = 45°$ requirement corresponds to a 3 dB $M_L$ contour on the NC. Figure 3.5 is an example of a NC with the 3 dB contour highlighted.

*3.7.1 The All–Pass–Filter Technique.* The all–pass–filter (apf) technique is used throughout this design [12] to remove the NMP elements from the design while

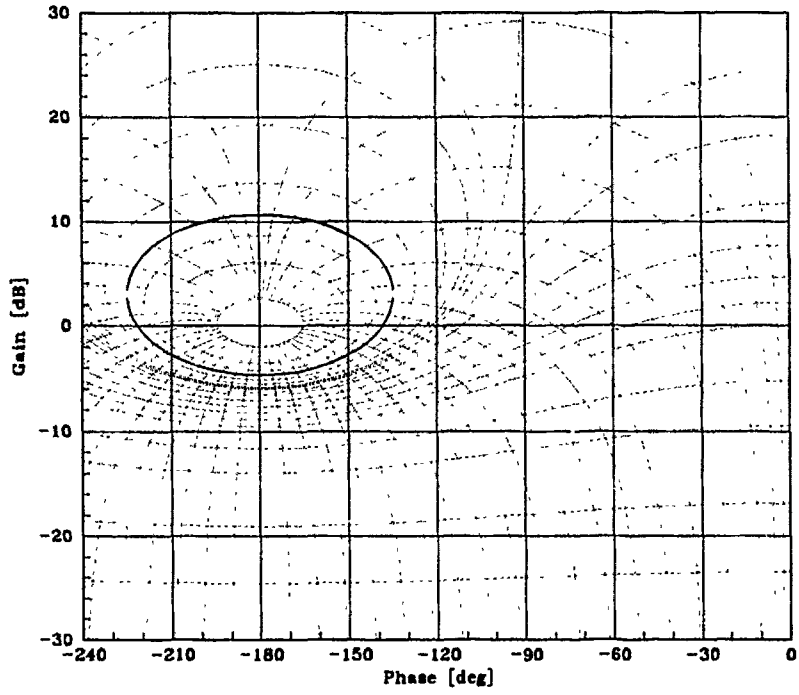


Figure 3.5. Nichols Chart With 3 dB Contour Highlighted

still accounting for their effects. The apf technique complicates the design; however, it allows the designer to rapidly determine the maximum possible loop transmission which is worth the additional complication. The phase of the apf $\phi_A$ is included when plotting the stability bounds. The apf used in the longitudinal SISO design is:

$$\text{apf} = \frac{(w' - 100)(w' - 130)}{(w' + 100)(w' + 130)} \tag{3.29}$$

The amount of phase associated with the template frequencies is summarized in Table 3.2. At low frequencies, below $v = 0.5$ (rad/sec)($\omega = 0.4999958$[rad/sec]), the shift is negligible. At higher frequencies, above $v = 0.5$ (rad/sec), the shift is incorporated in the stability bounds. The moving Nichols chart technique, which is slightly different from the method usually employed, is used to plot the stability bounds on the NC.

Table 3.2. All–Pass–Filter Used in the Longitudinal SISO System Design

| Template Frequency $v$ (rad/sec) | Phase $\phi_A$ (deg) |
|---|---|
| 0.001 | 0.002 |
| 0.005 | 0.01 |
| 0.05 | 0.10 |
| 0.10 | 0.20 |
| 0.20 | 0.40 |
| 0.30 | 0.61 |
| 0.40 | 0.81 |
| 0.50 | 1.01 |
| 0.60 | 1.21 |
| 0.70 | 1.41 |
| 1.00 | 2.02 |
| 2.00 | 4.04 |
| 3.00 | 6.06 |
| 4.00 | 8.08 |
| 5.00 | 10.1 |
| 6.00 | 12.1 |
| 8.00 | 16.1 |
| 10.0 | 20.2 |
| 20.0 | 40.0 |
| 50.0 | 94.9 |
| 100 | 165 |

*3.7.2 The Moving Nichols Chart Technique.* Two transparent NCs are created. The 3 dB $M_L$ contour is then plotted on each NC. Instead of cutting out the plant templates, a template which is plotted on a NC with the same scale as the transparent NCs, is placed beneath one of the transparent NCs, refered to as the top NC (TNC), (see Figure 3.6). In this way, the template orientations can be maintained by aligning the grid lines of the TNC with the grid lines on the template NC. For a particular location of the template, with the template contour touching the stability bound, the location of the nominal plant point is marked on the TNC (see Figure 3.6). The template is then moved to a new location with the template contour just touching the $M_L$ contour at another location. Again the location of the nominal plant point is marked on the TNC. This procedure continues until a

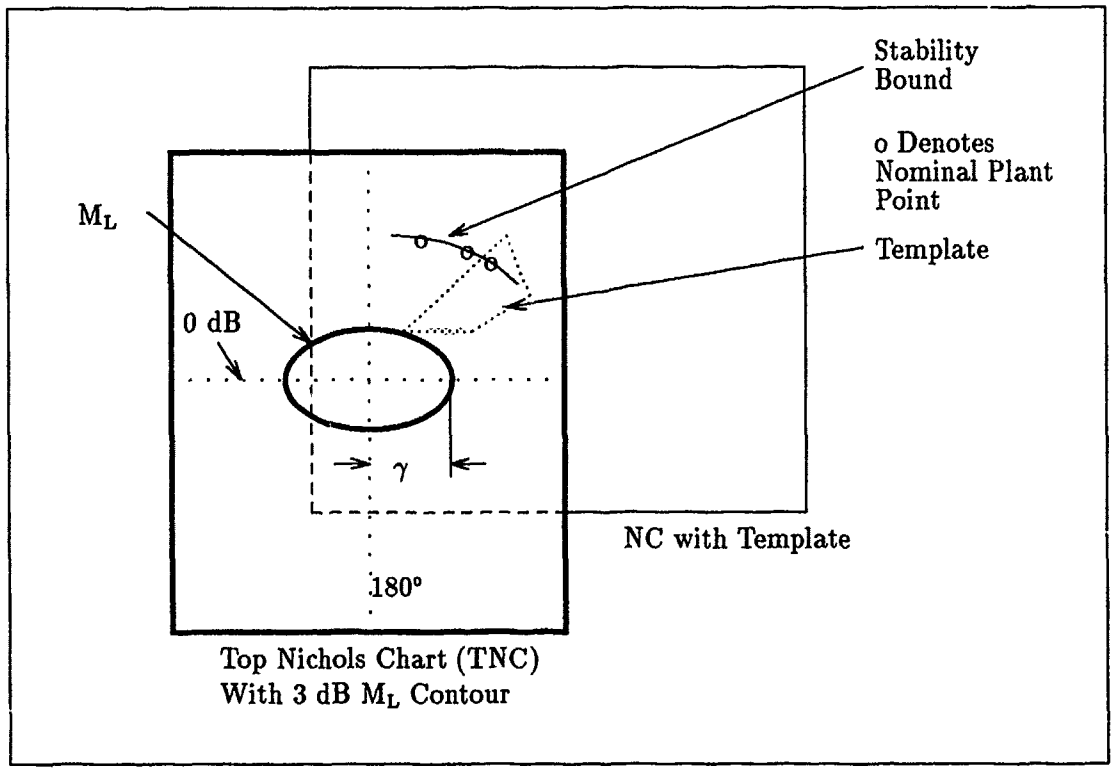


Figure 3.6. Plotting Stability Bound Using Moving Nichols Chart Technique

stability boundary is drawn through these points on the TNC. Once completed, the bound is marked with the appropriate template frequency. This procedure is followed for each template up to $v = 0.5$. For frequencies above $v = 0.5$, the second transparent NC is used and is refered to as the reference Nichols Chart, RNC. It is used to indicate the phase lead $\phi_A$ necessary to account for the lead contributed by the NMP elements removed from the design by the apf. The phase contribution must be incorporated in plotting the stability bounds. Before the stability bounds are plotted, the $M_L$ contour must be shifted to the right on the NC. This is readily accomplished by placing the RNC, with the $M_L$ contour marked, under the TNC. The RNC is then shifted to the right by the number of degrees contributed by $\phi_A$ associated with the template frequency $v_i$. Using the "shifted" $M_L$ contour on the RNC, stability bound plotting can continue. Next, the template is placed under the RNC. The stability bounds are obtained by moving the template boundaries about

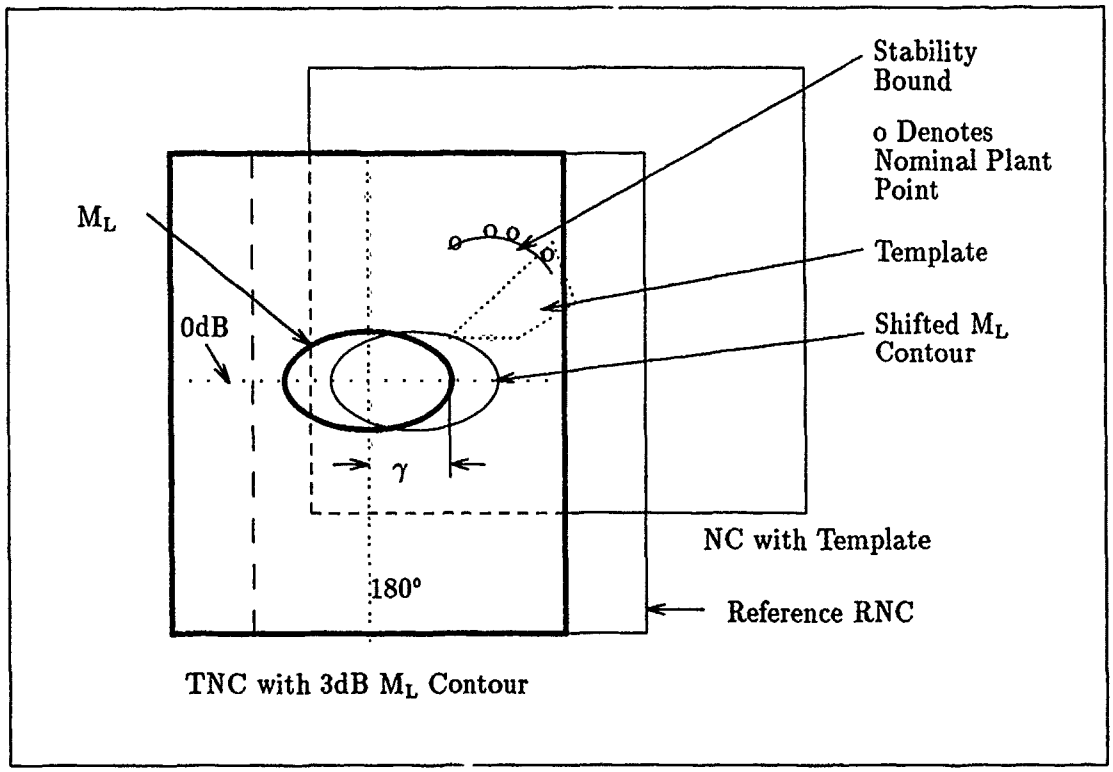


Figure 3.7. Plotting Stability Bound—Including Phase Contribution of apf

the shifted contour and marking the nominal plant point on the TNC as before (see Figure 3.7). The resulting stability bound is plotted through these points on the TNC which reflects this shift to the right of the stability bound by $\phi_A$, the number of degrees needed to account for the NMP character of the plant at the template frequency. As the process continues for each template frequency, the RNC is shifted further to the right by the appropriate $\phi_A$. This continues until the 180° line, of the RNC is on the 0° line on the TNC (see Figure 3.8). The bottom of the last stability bound dictates the amount of loop transmission gain available to the designer. A NC showing shifted stability bounds is included in Figure 3.9.

## *3.8* Loop Shaping

The stability bounds are used in shaping the loop transmission. The design can proceed using a variety of techniques. The two techniques outlined below are

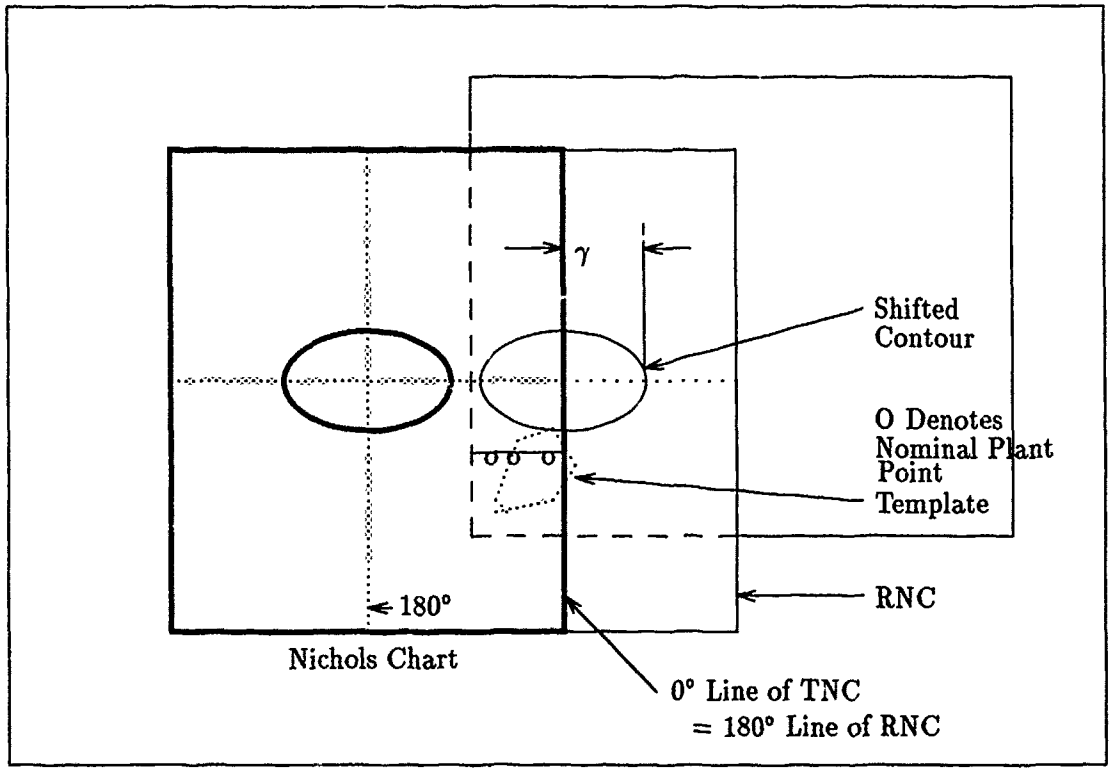


Figure 3.8. Plotting Stability Bound—Plotting the Last Bound

the "backward loop shaping technique" and "minimum order compensator design technique". A high order compensator is not desirable for Lambda and the "backward loop shaping technique" may produce a high order compensator, however, both loop shaping design techniques are used in this design. Although the final design is based on the "minimum order compensator technique", the "backward loop shaping technique" is used to determine the theoretical maximum loop transmission. In the lateral-directional MIMO design, covered in Chapter IV, the "backward loop shaping technique" is used as a performance baseline.

*3.8.1 Backward Loop Shaping Technique.* This technique takes full advantage of the minimum phase (MP) character of the plant with all of the NMP elements removed by the apf. In MP systems the phase lag is correlated with the slope of the gain (dB/octave).

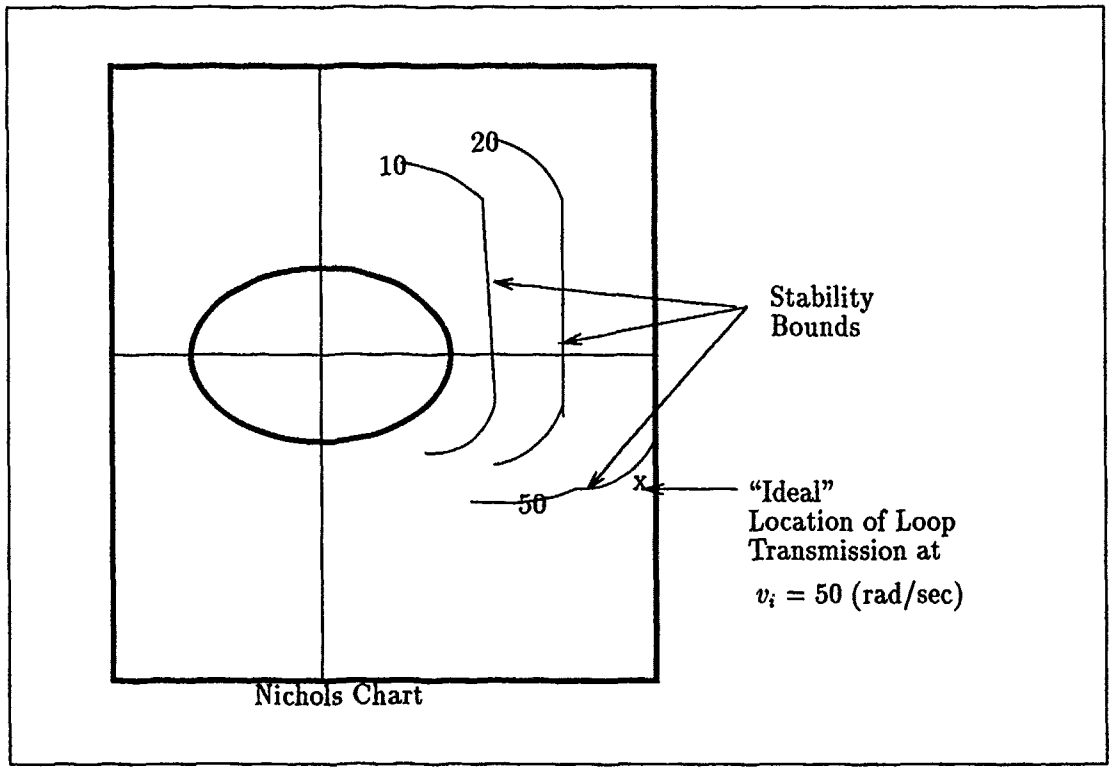


Figure 3.9. Nichols Chart With Stability Bounds Plotted

This characteristic allows the designer to quickly determine the maximum loop transmission gain possible. The maximum loop transmission gain is determined by starting at the frequency corresponding to the highest stability bound and working down (backward) in frequency. The first step is to select a point close to the zero degree line and slightly below the highest frequency boundary on the NC (see Figure 3.9). The point marked "Ideal" is the beginning point of the design. Using the fact that the dB/octave slope is determined by the amount of phase lag, the dB increase to the next lower bound is determined by calculating the average phase lag between the bounds. The average phase lag between the two points is determined by averaging the phase lag of each of the bounds:

$$\text{Phase Lag}_{av} = \frac{\text{Phase Lag}_{Bound\,1} + \text{Phase Lag}_{Bound\,2}}{2} \tag{3.30}$$

The MP character of the design allows the amount of dB increase to be determined based on the average phase lag. The relationship between phase and the gain slope is:

$$90°_{\text{Phase Lag}} \sim 6 \text{ dB/Octave} \tag{3.31}$$

This relationship is used to determine the slope at the average phase lag of the two bounds. For example, if the average phase lag between the two bounds is 10° the slope is:

$$(10°_{\text{Phase Lag}}) \left[ \frac{6 \text{ dB/Octave}}{90°_{\text{Phase Lag}}} \right] = 0.667 \text{ dB/Octave} \tag{3.32}$$

The number of octaves between the bounds is determined from:

$$\frac{\text{Frequency}_{(\text{Bound 1})}}{\text{Frequency}_{(\text{Bound 2})}} = 2^{(\text{Number of Octaves})} \tag{3.33}$$

Or more directly from:

$$\frac{\ln \left[ \frac{\text{Frequency}_{(\text{Bound 1})}}{\text{Frequency}_{(\text{Bound 2})}} \right]}{\ln 2} = \text{Number of Octaves} \tag{3.34}$$

For example, the number of octaves between $v = 50$ and $v = 40$ is:

$$\frac{\ln(\frac{50}{40})}{\ln 2} = 0.332 \text{ Octaves} \tag{3.35}$$

The maximum dB value at the next bound is the product of the number of octaves and the dB/octave slope. For the examples above, the maximum rise in dB from the bound at $v = 50$, to the bound at $v = 40$, is approximately 0.22 dB. This procedure is repeated until a point above the lowest frequency bound is reached or when the designer determines the design is not possible. If the design is not possible, the designer chooses a lower frequency bound, that is, for this example, a value of $v < 50$ (rad/sec)as a new starting point. When a satisfactory loop shape is determined by this method, it results in the highest loop transmission gain and the best performance

possible. The maximum loop transmission provides the most benefit from feedback [10]. However, the loop transmission formed using this procedure may produce a higher order compensator than desired. If the compensator is limited to a lower order, it can be reduced by absorbing some of the nominal plant poles and zeros into the loop transmission transfer function. If the order is still too high, the entire plant can be included for the final transmission loop design as described below. By using the above procedure, the loop shaping information obtained by excluding the nominal plant poles and zeros is useful in determining the theoretical maximum loop transmission gain that is achievable. In addition, the higher order design may be used as a performance baseline for comparison with lower order designs.

*3.8.2 Minimum Order Compensator Design Technique.* The previous technique is most useful if the loop is formed from scratch. That is, the nominal plant is not included in the design of the transmission loop. The drawback is the possibility of an unacceptably high order compensator. The order can be reduced somewhat by absorbing as many poles and zeros of the nominal plant as possible into the loop transmission equation. Therefore, a satisfactory lower-order compensator is obtained by including the nominal plant in the design. The nominal plant is first multiplied by the inverse of the all-pass-filter, $(\text{apf})^{-1}$, which produces a MP transfer function. Thus, the resulting MP transfer function, designated by $P_{mo}$, is plotted on the NC or on a set of Bode plots. Loop shaping begins at the lowest frequency and progresses until a point below the highest frequency bound is reached. The result of the backward loop shaping technique is used as the design goal. Loop shaping by this technique produces the following MP transmission loop shape and is used for the remainder of the longitudinal SISO design:

$$L_{mo} = \frac{0.0183(w' + 2)(w' + 5)(w' + 10)(w' + 50)P_{mo}}{(w')^2(w' + 160 \pm j120)(w' + 300)} \tag{3.36}$$

Figure 3.10 is the MP loop transmission $L_{mo}$ plotted on the NC. A NC showing a plot of all the plants including the NMP elements is shown in Figure 3.11.

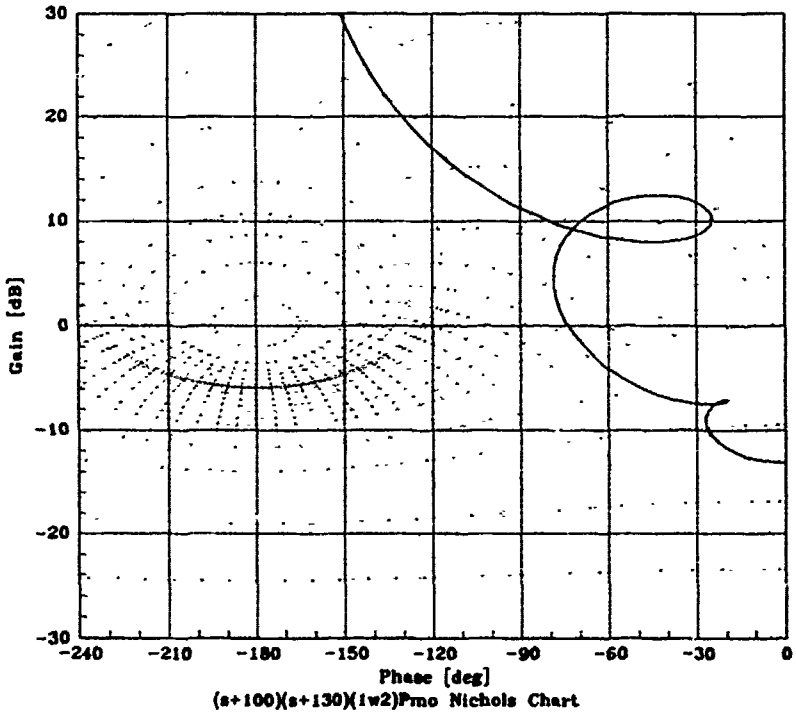


Figure 3.10. NC Showing MP Transmission Loop After Loop Shaping

## *3.9* w′ Compensator

The w′ compensator, G(w′), is found by dividing the loop transmission by the nominal plant. If the plant is included in the loop transmission, G(w′) is simply the poles, zeros, and gain added during loop shaping. If the nominal plant is not included in the transmission loop, the zero and poles not absorbed in $L_{mo}$ become poles and zeros, respectively, of G(w′). The longitudinal SISO G(w′) for this design is:

$$G(w') = \frac{5.5(w'/2+1)(w'/5+1)(w'/8+1)(w'/10+1)(w'/50+1)}{(w')^2(w'/200^2+1.6w'/200+1)(w'/300+1)} \qquad (3.37)$$

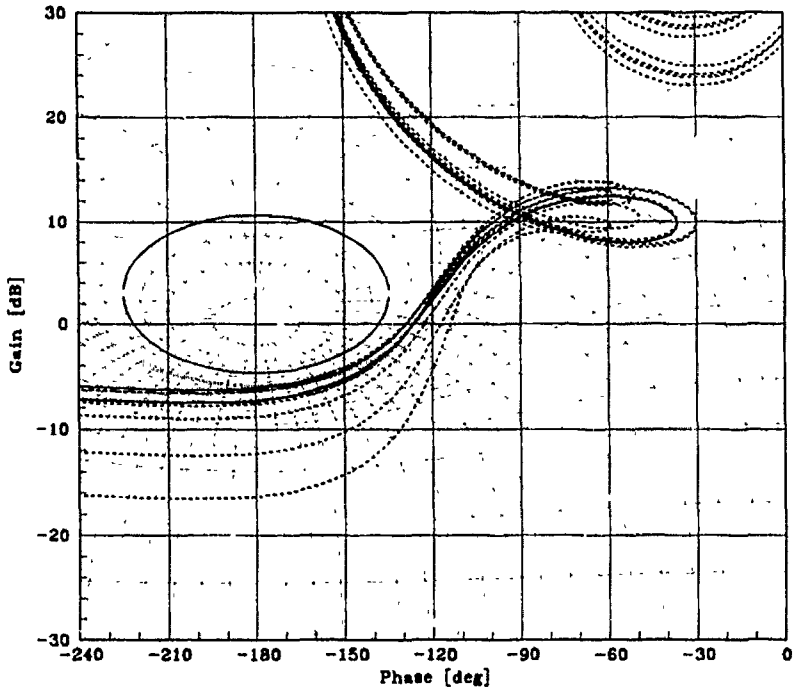


Figure 3.11. NC Including All Nineteen Plants and NMP Elements

or equivalently:

$$G(w') = \frac{0.0183(w'+2)(w'+5)(w'+8)(w'+10)(w'+50)}{(w')^2(w'+160 \pm j120)(w'+300)} \tag{3.38}$$

## *3.10* Prefilter Design

The prefilter, F(w'), is obtained by plotting the frequency response data of the closed loop system:

$$\left(\frac{L(w')}{1+L(w')}\right) = \left(\frac{G(w')P(w')}{1+G(w')P(w')}\right) \tag{3.39}$$

The frequency response bounds, developed from the specifications, are plotted over the closed loop response. A family of curves is produced. See the first plot in Figure 3.12. Poles and zeros are placed in front of the closed loop system until all of the responses are contained within the performance bounds, as in the second plot in Figure 3.12. The prefilter for the longitudinal SISO QFT design is:

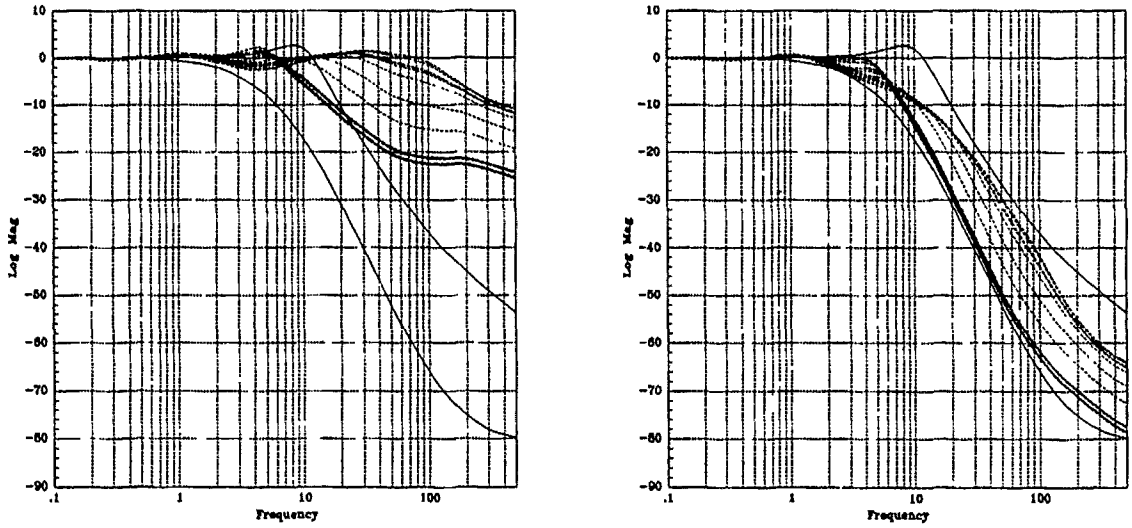


Figure 3.12. Closed Loop Response Without and With Prefilter, F(w′)

$$F(w') = \frac{0.001875(w' + 200)^2}{(w' + 5)(w' + 15)} \tag{3.40}$$

where:

$$\lim_{w' \to 0} = 1 \tag{3.41}$$

## *3.11* w′ Simulation

The w′–plane design is simulated to verify the performance before proceeding with the design. The w′ simulations are performed using the System Build capability of MATRIX$_X$ (see Figure 3.13). Time domain step responses are plotted along with the performance bounds (see Figure 3.14) which indicate that a robust design is achieved, that is, all responses lie between the upper and lower specified tracking bounds.

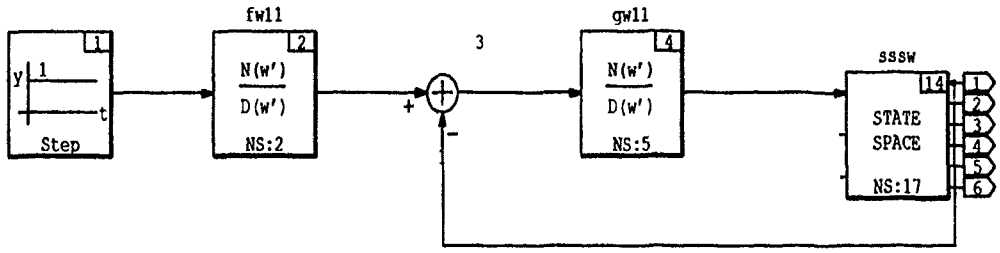


Figure 3.13. System Build w′ Simulation

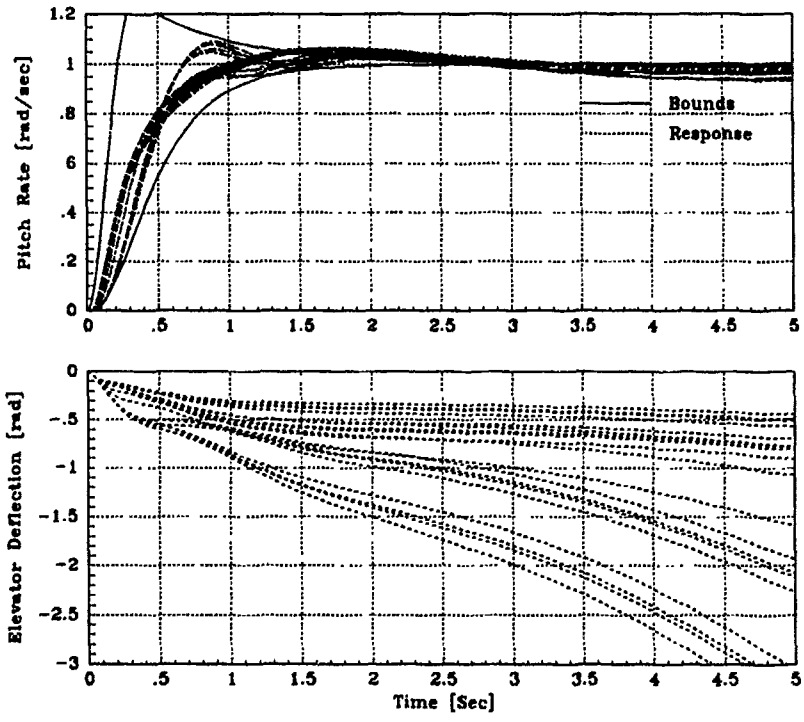


Figure 3.14. System Build w′ Simulation Frequency Response

### *3.12* z–Plane Transformations

F(w′) and G(w′) are transformed to the z–plane for digital implementation on Lambda. The z–plane representations are obtained by performing the bilinear transformation; see Equation (3.6). The MATRIX$_X$ user function below readily performs this transformation:

```
//[numz,denz]=w2z(num,den,dt)
//Function to take a {\rm w}' domain numerator and denominator into
//the z-domain.
sz=size(num);
n=sz(2)-1;
//multiply the (2/dt) factors into the num and den
for i=1:n;...
  num(i)=num(i)*(2/dt)**((N+1)-i);...
  den(i)=den(i)*(2/dt)**((N+1)-i);...
end;
//build the transformation matrix
tm=ones((n+1),(n+1));
facta=[1 -1];factb=[1];
for j=1:(n+1);...
  row=1;...
  for i=j:n;row=conv(row,facta);end;...
  for i=1:(j-1);row=conv(row,factb);end;...
  for i=1:(n+1);tm(j,i)=row(i);end;...
end;
tm,
//multiply the num and den vectors
//with the matrix
numz=num*tm;
denz=den*tm;
//normalize the transfer function
numz=numz/denz(1);denz=denz/denz(1);
```

In addition to performing the transformation, the above function divides the numerator and denominator by the denominator leading coefficient resulting in a normalized z–plane representation:

$$\mathrm{F}(z) = \frac{0.013975z^2 + 0.0093168z + 0.0015528}{z^2 - 1.6439z + 0.66874} \tag{3.42}$$

$$\mathrm{G}(z) = \frac{96.749z^5 - 374.31z^4 + 566.96z^3 - 417.22z^2 + 147.36z - 19.538}{z^5 - 0.76829z^4 - 0.87805z^3 + 0.17073z^2 - 0.36585z + 0.10976} \tag{3.43}$$

*3.12.1 Comparison of* w′ *and z–Plane F's and G's* . The required difference equations are obtained from the z–plane representations of the design and are included in Appendix F. The w′ and z–plane compensators and filters must be comparable up to frequencies greater than $\frac{1}{3}\omega_s$ (rad/sec) [11]. The sampling frequency on Lambda is 50 Hertz, which means $\omega_s = 314$ (rad/sec). Therefore, the w′ and Z–plane representations must be fairly close up to a $\omega = 105$ (rad/sec). The frequency response comparison of G(w′) and G(z) are plotted in Figure 3.16 for comparison. In addition, the frequency response of F(w′) and F(z) are plotted in Figure 3.15. The plots show a good comparison within the required frequency bandwidth $0 \leq \omega \leq 105$ (rad/sec).

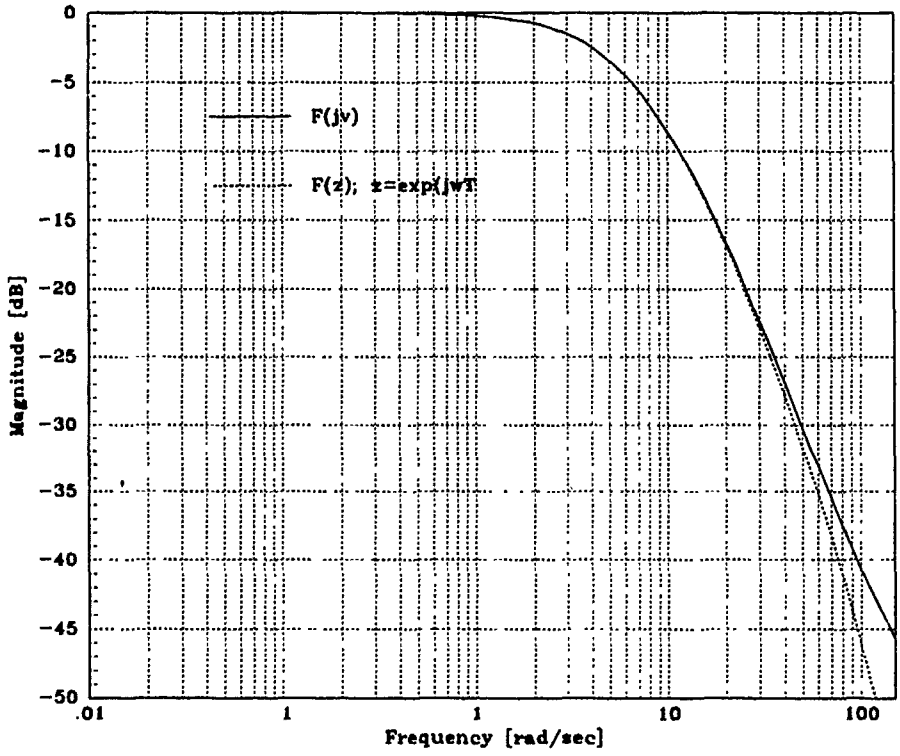


Figure 3.15. Comparison of F(w′) and F(z) Magnitude Frequency Response

## *3.13* Simulations

Simulation is the final step in the design. The design is simulated using the best model available. In this case, the best model available is the same one used in

the design with the additional non–linear elements added. The non–linear elements are due to the software and hardware limiters present on Lambda (see Figure 3.17). Figure 3.18 is the MATRIX$_X$ System Build representation of Lambda without the non-linear elements while, Figure 3.20 includes the non–linear elements. MATRIX$_X$ has the ability to simulate a system with both continuous and discrete elements. This "hybrid" simulation capability is used to verify the performance of the design. The design is simulated without the non–linear elements. The results are plotted in Figure 3.19. Adding the limiters produces the simulation results shown in Figure 3.21. The simulations predict the performance expected from Lambda in actual flight. They show good performance at all flight conditions for a step command of 10° per second for at least two seconds. After two seconds, the deflection limits on the actuators begin to affect the response.

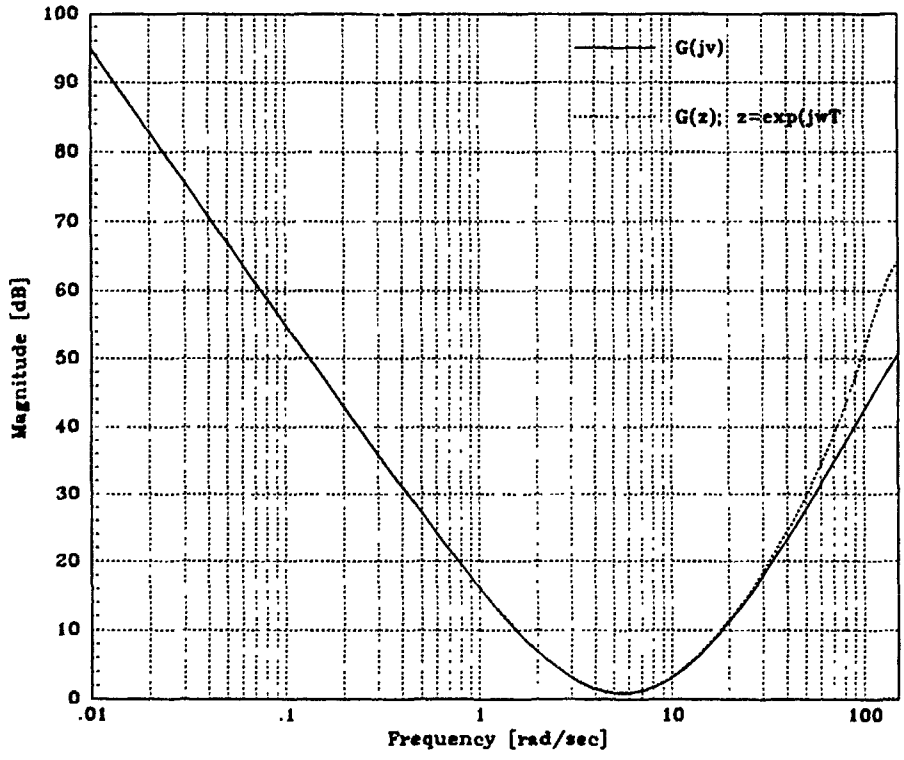


Figure 3.16. Comparison of G(w′) and G(z) Magnitude Frequency Response

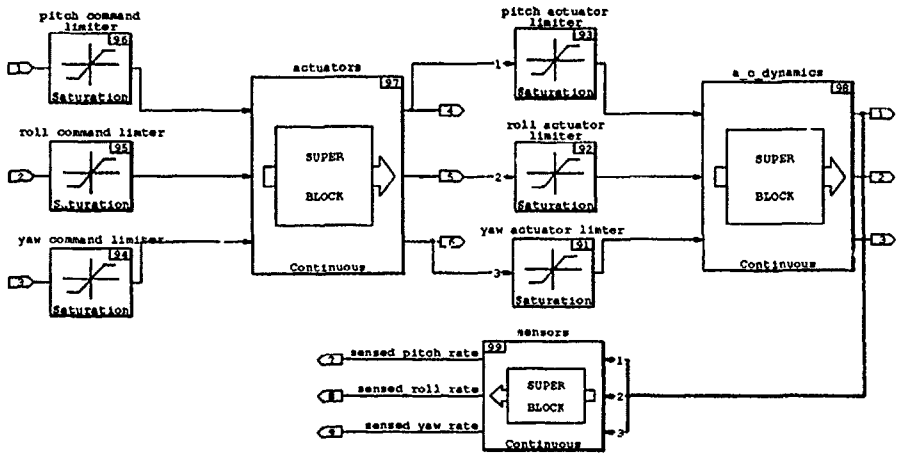


Figure 3.17. System Build Model of Lambda Including Non-Linear Elements

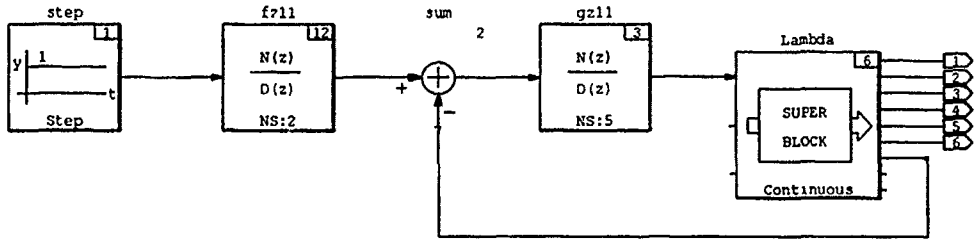


Figure 3.18. Model Used for Hybrid Simulation of Longitudinal SISO QFT Design

## *3.14* Summary

A single QFT controller was synthesized that produces satisfactory performance throughout the flight envelope of Lambda. It is important to note that no gain scheduling is necessary. Response of the system remains stable in spite of the inherent non-linearities present due to hardware and software control limiters. The hybrid simulation with non-linear elements (see Figure 3.21) is the final test of the design as it includes all that is known about the plant. Some of the performance limitations can be overcome if Lambda's speed is held constant. In the simulations, Lambda can hold a pitch rate constant until the speed drops. As the speed drops,

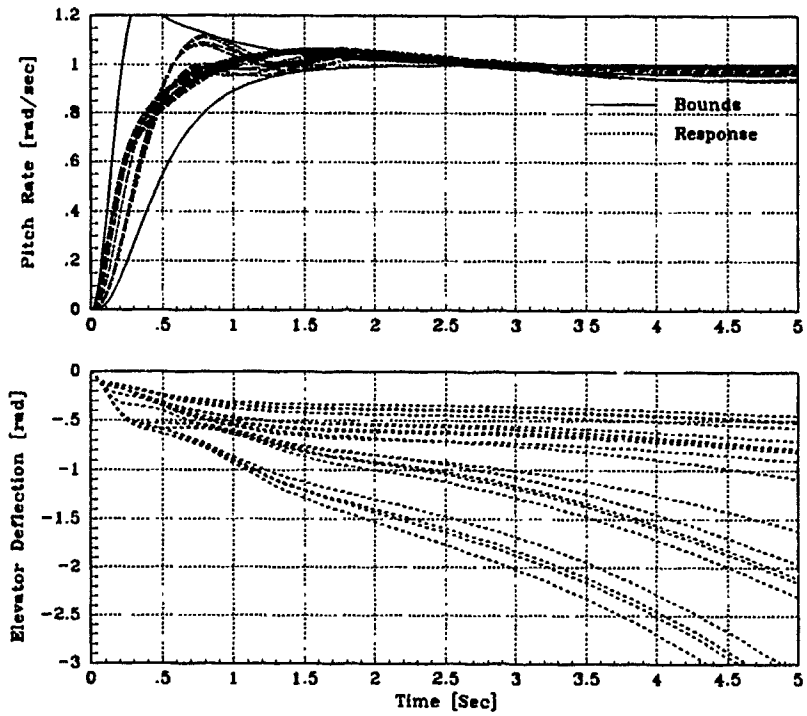


Figure 3.19. Hybrid Simulation of the Longitudinal SISO QFT Design

more elevator is needed than is available to the controller. Since the simulation results are good, within the performance limitations of Lambda, it is assumed that the aircraft will perform well with this controller design.

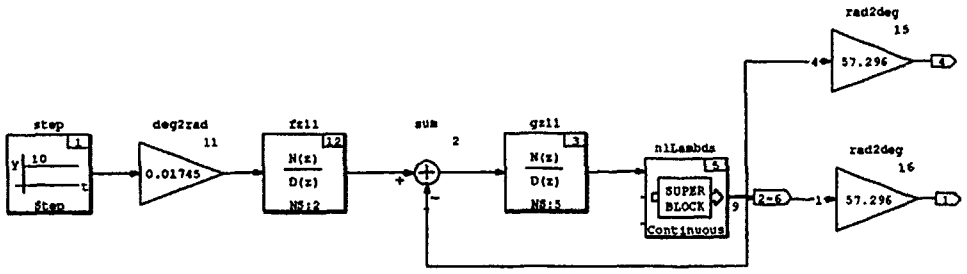


Figure 3.20. Model Used for Hybrid Simulation Including Non–Linear Elements

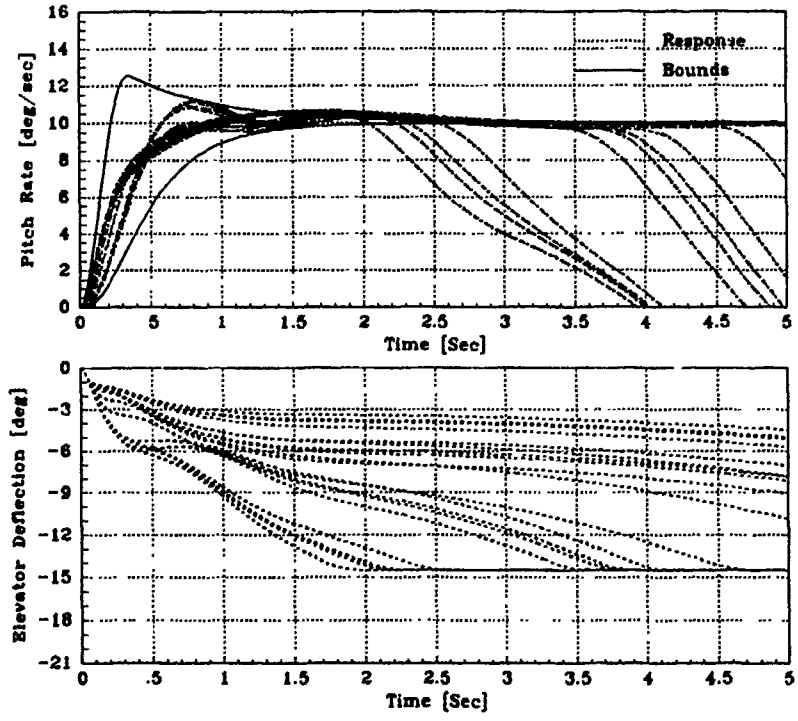


Figure 3.21. Hybrid Simulation With Non–Linear Elements

# *IV.* Lateral–Directional MIMO Design

This chapter covers the synthesis of the QFT compensators and prefilters for the two–by–two lateral–directional MIMO plants, and follows the steps outlined in Chapter 1 Section 1.7. The MIMO QFT design technique differs only slightly from the SISO QFT technique, and only the differences are covered in detail. Method Two requires sequential design of the yaw and roll loops; however, they are presented simultaneously.

## *4.1* Flight Conditions

The same flight conditions used in the longitudinal SISO design are used in this lateral-directional MIMO QFT design.

## *4.2* Plant Transfer Function Matrix

The plant transfer function matrix, $\mathbf{P}(w')$, is obtained from a MATRIX$_X$ simulation of the aircraft at the selected flight conditions. The **A** and **B** matrices are of the form:

$$\mathbf{A}_{lat} = \begin{bmatrix} \frac{Y_\beta}{u} & \frac{Y_p}{u} & \frac{32.174\cos\theta}{u} & \frac{Y_r}{u-1} & 0 \\ \frac{L_\beta+\left[\frac{I_{xz}}{I_{zz}}\right]N_\beta}{\left[\frac{I_{xz}}{I_{xx}}\right]\left[\frac{I_{xz}}{I_{zz}}\right]} & \frac{L_p+\left[\frac{I_{xz}}{I_{zz}}\right]N_r}{\left[\frac{I_{xz}}{I_{xx}}\right]\left[\frac{I_{xz}}{I_{zz}}\right]} & 0 & \frac{L_r+\left[\frac{I_{xz}}{I_{zz}}\right]N_r}{\left[\frac{I_{xz}}{I_{xx}}\right]\left[\frac{I_{xz}}{I_{zz}}\right]} & 0 \\ 0 & 1 & 0 & 0 & 0 \\ \frac{N_\beta+\left[\frac{I_{xz}}{I_{zz}}\right]L_\beta}{\left[\frac{I_{xz}}{I_{xx}}\right]\left[\frac{I_{xz}}{I_{zz}}\right]} & \frac{N_p+\left[\frac{I_{xz}}{I_{zz}}\right]L_p}{\left[\frac{I_{xz}}{I_{xx}}\right]\left[\frac{I_{xz}}{I_{zz}}\right]} & 0 & \frac{N_r+\left[\frac{I_{xz}}{I_{zz}}\right]L_r}{\left[\frac{I_{xz}}{I_{xx}}\right]\left[\frac{I_{xz}}{I_{zz}}\right]} & 0 \\ 0 & 0 & 0 & 1 & 0 \end{bmatrix} \tag{4.1}$$

and:

$$\mathbf{B}_{lat} = \begin{bmatrix} \frac{Y_{\delta_{ail}}}{u} & \frac{Y_{\delta_{rud}}}{u} \\ \frac{L_{\delta_{ail}} + \left[\frac{I_{xz}}{I_{zz}}\right] N_{\delta_{ail}}}{\left[\frac{I_{xz}}{I_{xx}}\right]\left[\frac{I_{xz}}{I_{zz}}\right]} & \frac{L_{\delta_{rud}} + \left[\frac{I_{xz}}{I_{zz}}\right] N_{\delta_r}}{\left[\frac{I_{xz}}{I_{xx}}\right]\left[\frac{I_{xz}}{I_{zz}}\right]} \\ 0 & 0 \\ \frac{L_{\delta_r} + \left[\frac{I_{xz}}{I_{xx}}\right] N_{\delta_r}}{\left[\frac{I_{xz}}{I_{xx}}\right]\left[\frac{I_{xz}}{I_{zz}}\right]} & \frac{N_{\delta_{rud}} + \left[\frac{I_{xz}}{I_{zz}}\right] L_{\delta_r}}{\left[\frac{I_{xz}}{I_{xx}}\right]\left[\frac{I_{xz}}{I_{zz}}\right]} \\ 0 & 0 \end{bmatrix} \tag{4.2}$$

The transfer function matrix resulting from the MATRIX$_X$ simulation, which includes the actuator and sensor dynamics, is a two–by–two matrix:

$$\mathbf{P} = \begin{bmatrix} \frac{p_{sen}(s)}{\delta_{ail_{cmd}}(s)} & \frac{p_{sen}(s)}{\delta_{rud_{cmd}}(s)} \\ \frac{r_{sen}(s)}{\delta_{ail_{cmd}}(s)} & \frac{r_{sen}(s)}{\delta_{rud_{cmd}}(s)} \end{bmatrix} = \begin{bmatrix} p_{22}(s) & p_{23}(s) \\ p_{32}(s) & p_{33}(s) \end{bmatrix} \tag{4.3}$$

where $p_{sen}$ is the roll rate sensed by the roll gyro and $r_{sen}$ is the yaw rate sensed by the yaw gyro. $\delta_{ail_{cmd}}$ and $\delta_{rud_{cmd}}$ are the commanded aileron and rudder deflections, respectively. At the nominal conditions, the elements of $\mathbf{P}$(s) are:

$p_{22}(s) = \frac{p_{sen}(s)}{\delta_{ail_{cmd}}(s)} =$

$$\frac{3.5051 \times 10^5 (s)(s + 0.9516 \pm j3.8448)}{(s + 0.0141)(s + 0.9734 \pm j3.9181)(s + 6.7492)(s + 9.0000 \pm j6.2450)(s + 50.0000)} \tag{4.4}$$

$p_{23}(s) = \frac{p_{sen}(s)}{\delta_{rud_{cmd}}(s)} =$

$$\frac{-72.7664 (s)(s + 3.9245)(s - 83.4616)}{(s + 0.0141)(s + 0.9734 \pm j3.9181)(s + 6.1996)(s + 6.7492)(s + 50.0000)} \tag{4.5}$$

$p_{32}(s) = \frac{r_{sen}(s)}{\delta_{ail_{cmd}}(s)} =$

$$\frac{-9.5335 \times 10^3 (s - 1.8300)(s + 2.3301)(s + 22.9473)}{(s + 0.0141)(s + 0.9734 \pm j3.9181)(s + 6.7492)(s + 9.0000 \pm j6.2450)(s + 50.0000)} \tag{4.6}$$

$p_{33}(s) = \frac{r_{sen}(s)}{\delta_{rud_{cmd}}(s)} =$

$$\frac{5.4760 \times 10^3 (s + 0.0658 \pm j0.3201)(s + 6.7753)}{(s + 0.0141)(s + 0.9734 \pm j3.9181)(s + 6.1996)(s + 6.7492)(s + 50.0000)} \tag{4.7}$$

A complete set of transfer functions is located in Appendix B.

## *4.3* w′ Plant Transfer Functions

The s–plane transfer functions of Equation 4.3 are transformed to the w′ domain as described in Section 3.3 using the Hofmann routine which takes into account the ZOH to yield $\mathbf{P}_e(w')$.

## *4.4* MIMO Plant Inversion, $\mathbf{P}^{-1}(w')$

The MIMO QFT technique requires an m×m MIMO plant be reduced to $m^2$ equivalent multiple–input single–output (MISO) loops in order to perform a QFT design [12]. The lateral–directional dynamics of Lambda are represented by a 2×2 MIMO plant which is converted to four equivalent loops. Since, a diagonal prefilter **F** is specified, the loops on the diagonal have two inputs—a desired input and a disturbance input and are MISO loops. The off–diagonal elements have only disturbance inputs and are represented as SISO loops (see Figure 4.1). The desired input is the control input from the compensator $g_{ii}$, while the disturbance input is due to the cross coupling in the MIMO plant. This design uses a compensator matrix **G** and the prefilter matrix **F**, which are diagonal, that is:

$$\mathbf{G}(w') = \begin{bmatrix} g_{11} & 0 & 0 \\ 0 & g_{22} & 0 \\ 0 & 0 & g_{33} \end{bmatrix} \tag{4.8}$$

and:

$$\mathbf{F}(w') = \begin{bmatrix} f_{11} & 0 & 0 \\ 0 & f_{22} & 0 \\ 0 & 0 & f_{33} \end{bmatrix} \tag{4.9}$$

Therefore, only the main diagonal MISO loops, elements $q_{22}$ and $q_{33}$, have desired control inputs. Disturbance inputs exist in each equivalent loop.

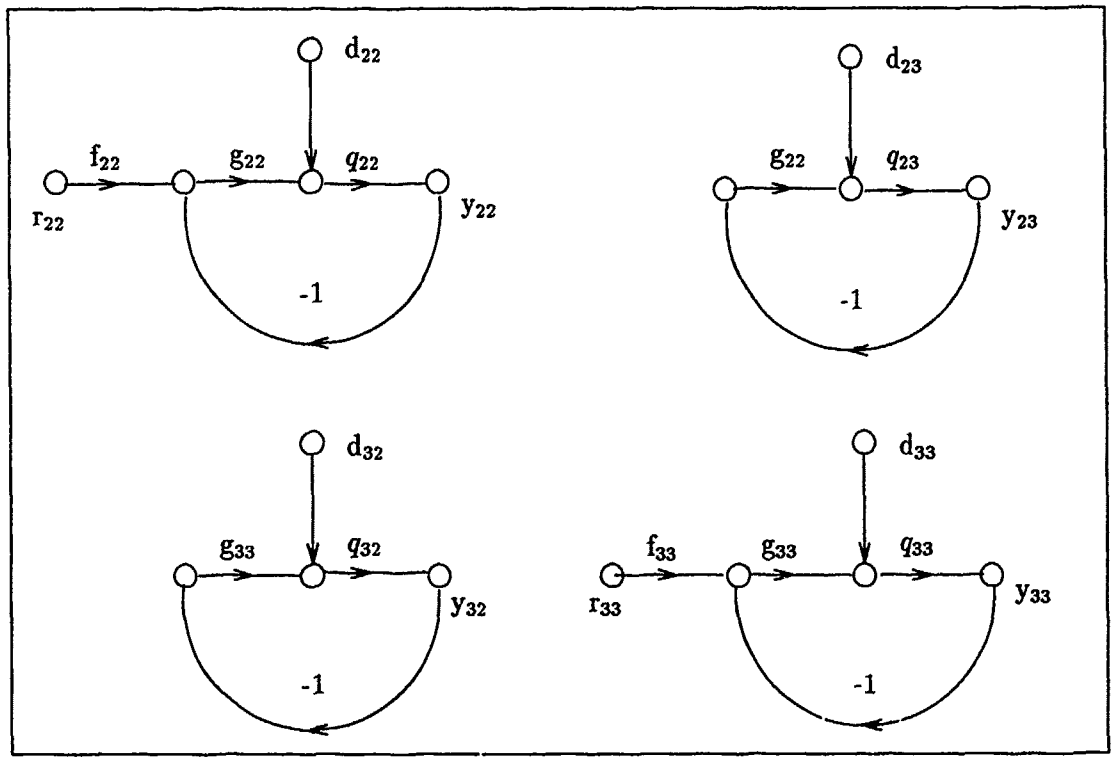


Figure 4.1. Equivalent Loops

The transfer functions used in the equivalent loops are obtained by first inverting the plant matrix $\mathbf{P}_e(w')$ and then inverting each element of $\mathbf{P}_e^{-1}(w')$. Symbolically:

$$\mathbf{P}_e^{-1}(w') = \begin{bmatrix} p_{11}^*(w') & p_{12}^*(w') \\ p_{12}^*(w') & p_{22}^*(w') \end{bmatrix} \tag{4.10}$$

and:

$$\mathbf{Q}(w') = \begin{bmatrix} \frac{1}{p_{11}^*(w')} & \frac{1}{p_{12}^*(w')} \\ \frac{1}{p_{12}^*(w')} & \frac{1}{p_{22}^*(w')} \end{bmatrix} = \begin{bmatrix} q_{11} & q_{12} \\ q_{21} & q_{22} \end{bmatrix} \tag{4.11}$$

The elements of $\mathbf{Q}(w')$ are the transfer functions of the equivalent loops (see Figure 4.1). Once the $q_{ii}$s are obtained, the design procedure is the same as the SISO design procedure with the plant transfer function replaced with $q_{ii}$ (see Figure 4.2).

*4.4.1 The Improved QFT Method.* The Improved Method [9] is used to reduce the uncertainty of the MISO disturbance inputs. The design starts with the loop with the least uncertainty due to the cross terms. The resulting loop transmission is used in the subsequent loops. In this case, the second loop is designed with a modified transfer function, $q_{22e}$.

Because the yaw channel has the lowest bandwidth , the design of the MISO loop associated with element (3,3) of **Q** is completed first, followed by the MISO loop associated with element (2,2). The following equation is used to find the effective transfer function, $q_{22e}$:

$$q_{22e} = q_{22}\frac{(1+L_3)}{1+L_3-\gamma_{32}} \tag{4.12}$$

where:

$$\gamma_{32} = \frac{q_{33}q_{22}}{q_{32}q_{23}} \tag{4.13}$$

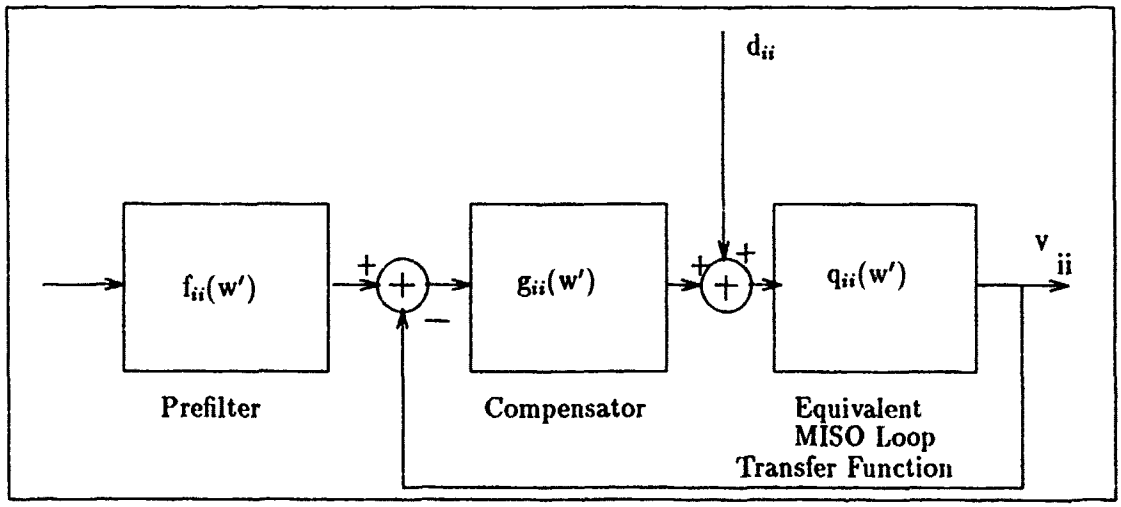


Figure 4.2. w'-domain QFT Design for Equivalent MISO Loops

## *4.5* Frequency Response Data

The frequency response data needed to obtain the plant templates, is obtained for all nineteen plants. Figures 4.3 and 4.4 are the Bode plots of $q_{33}(w')$ and $q_{22e}(w')$ respectively, from which the frequency response data are obtained.

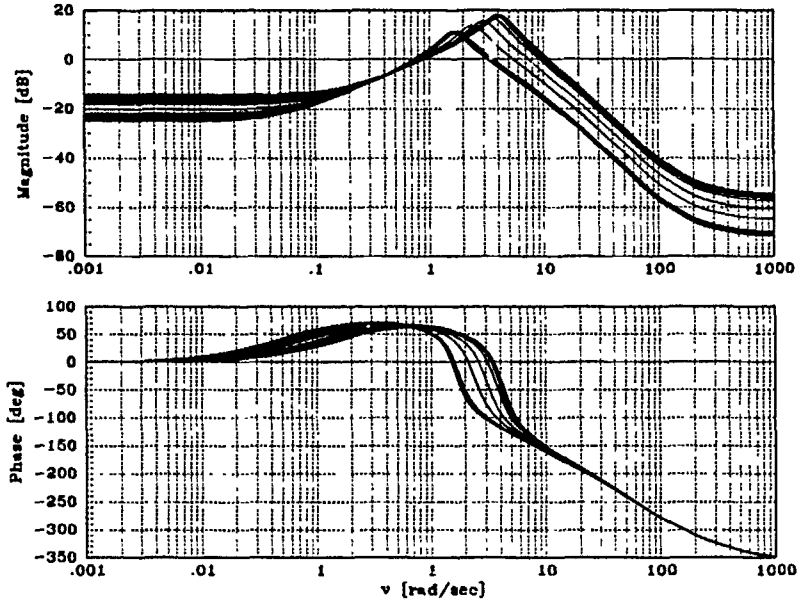


Figure 4.3. Frequency Response of the Nineteen Equivalent MISO Plants, $q_{33}$,

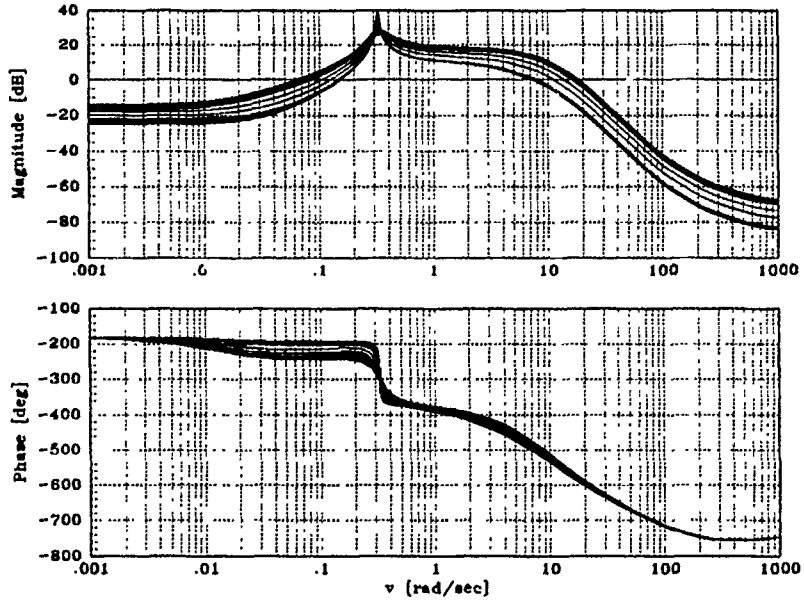


Figure 4.4. Frequency Response of the Nineteen Equivalent MISO Plants, $q_{22e}$,

## *4.6* Plant Templates

The plant template data for each template are taken from the frequency response by stripping out the magnitude and phase of each plant at the template frequency. The plant templates are then plotted in obtain the required stability bounds. A sample of a plant template is included in the previous chapter.

## *4.7* Nominal Plants

Since all $q_{ii}$ are all open loop stable, the same conditions used to create the nominal plant for the longitudinal SISO design are used to generate the nominal plants used in the lateral-directional MIMO system design. The nominal conditions are the first conditions listed in Table 3.1. The nominal equivalent MISO loop transfer functions used in the lateral-directional MIMO design are:
$q_{33}(w')=$

$$\frac{3.1345 \times 10^{-4}(w'+0.005)(w'+0.1523)(w'-100)(w'+115.9)(w-130.9)(w'+678.4)}{(w'+0.06488 \pm j0.3224)(w'+6.7661)(w'+9.0107 \pm j6.2026)(w'+46.37)} \quad (4.14)$$

and:
$q_{22e}(w') =$

$$\frac{1.6304 \times 10^{-3}(w'+0.1519)(w'-100)(w'+149.05)(w'-208.14)}{(w'+0.9748 \pm j3.9179)(w'+6.7389)(w'+46.212)} \quad (4.15)$$

A complete set of equivalent MISO loop transfer functions used in the design are included in Appendix C.

The NMP elements of the equivalent plants are removed to facilitate the application of the MP design technique, as in the longitudinal SISO design. The apf's used in the lateral-directional MIMO design are:

$$\text{apf}_{33} = \frac{(w' + 100)(w' + 208)}{(w' - 100)(w' - 208)} \tag{4.16}$$

and:

$$\text{apf}_{22} = \frac{(w' + 100)(w' + 131)}{(w' - 100)(w' - 131)} \tag{4.17}$$

## *4.8* Stability Bounds

Stability bounds are obtained using the moving Nichols chart technique discussed in Section 3.7.2.

## *4.9* Loop Shaping

Loop shaping is performed using both techniques discussed in Section 3.8. The backward loop shaping technique generates a maximum loop gain within the limits caused by the NMP character of the sampled data plant. Once the loop transmission is obtained, an attempt to reduce the order of the compensator is made by absorbing poles and zeros of the nominal plant into the loop. Failing to reduce the compensator sufficiently, the loop shape is reformed using the second loop shaping technique: the minimum order compensator design technique. Since the owners of Lambda, and sponsors of this thesis, desire low-order compensators, design by both methods is necessary. Only the designs resulting from the minimum order compensator design technique are presented.

Figures 4.5 and 4.6 are the MP transmission loops for $q_{33}$ and $q_{22e}$, respectively, using these minimum order compensators. The NMP transmission loops for all nineteen flight conditions are included in Figures 4.7 and 4.8. From the figures, it is apparent that the fifth order compensators are sufficient to maintain stability. However, the higher order compensators allow more loop transmission gain and result in better tracking and disturbance rejection.

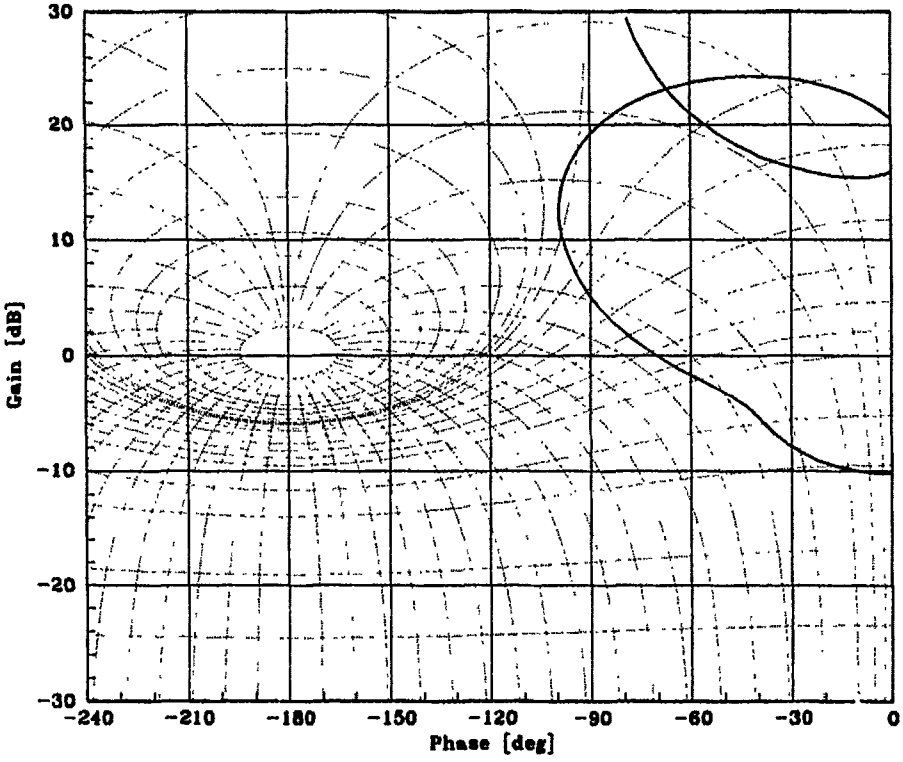


Figure 4.5. NC of MP Transmission Loop Shape for $q_{33}$

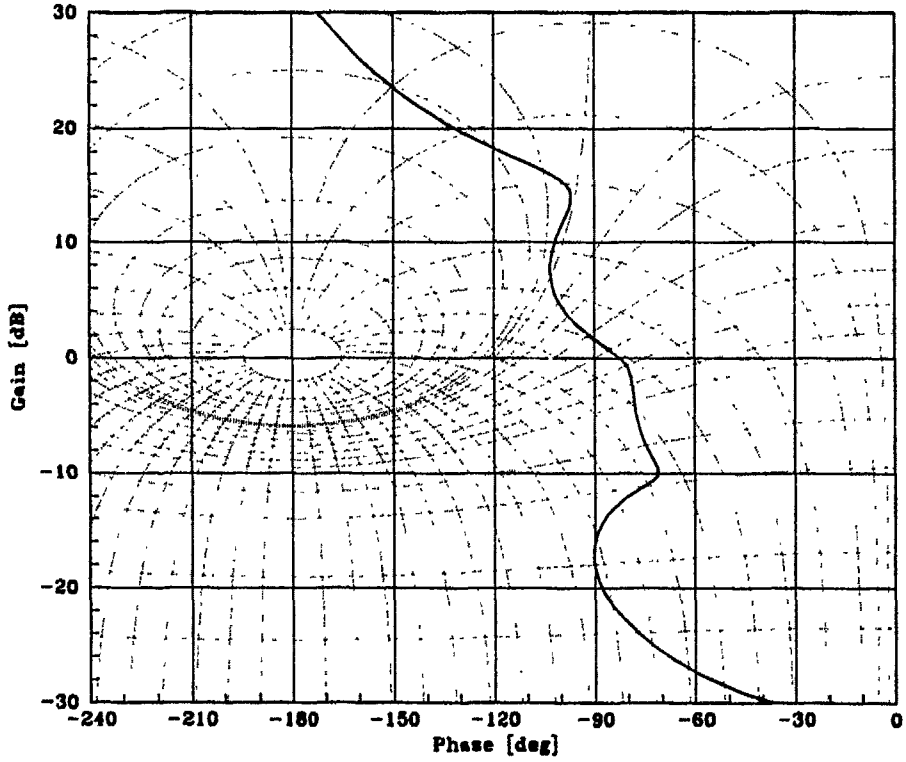


Figure 4.6. NC of MP Transmission Loop Shape for $q_{22e}$

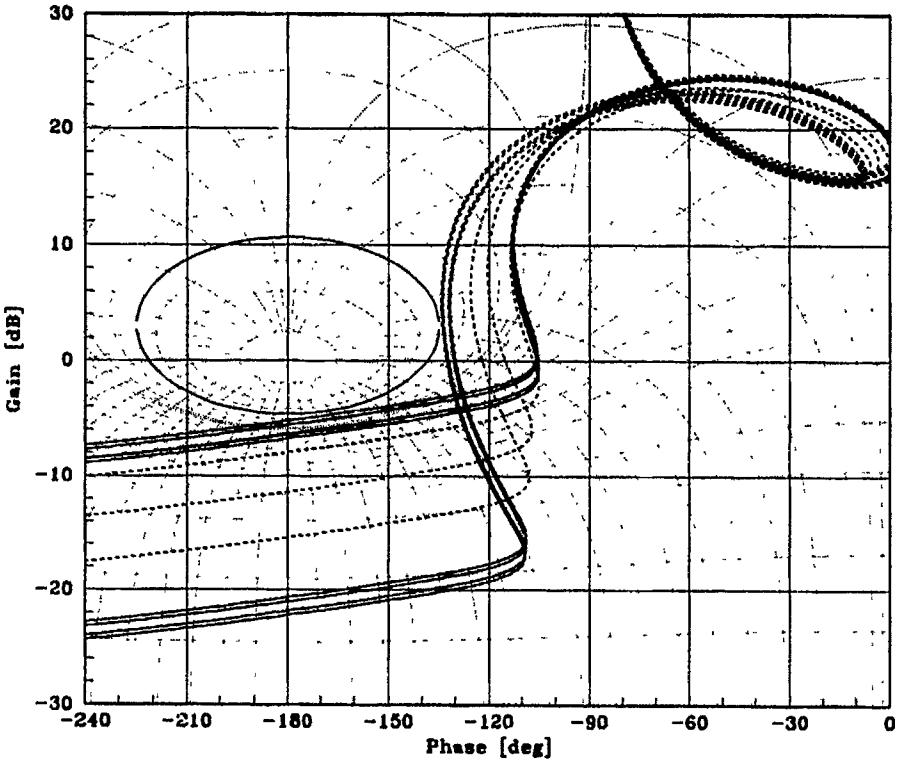


Figure 4.7. NMP Transmission Loops for All Nineteen $q_{33}$'s

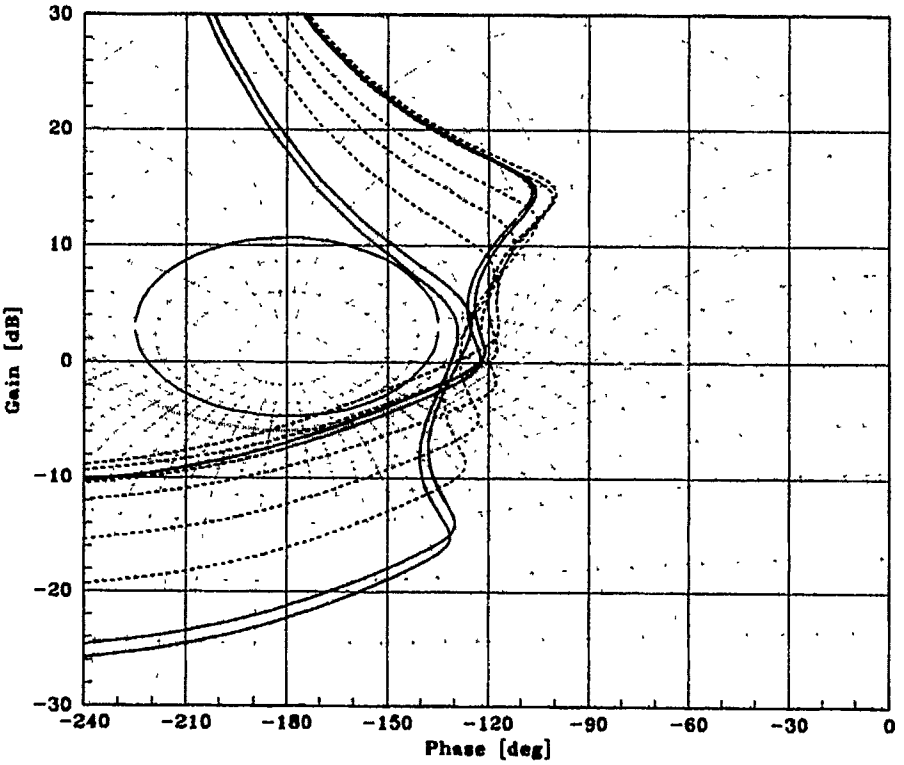


Figure 4.8. NMP Transmission Loops for All Nineteen $q_{22e}$'s

## *4.10* w′ Compensator

The compensators are extracted from the loop transmissions by dividing out the nominal plants. The resulting w′ compensators are:

$$g(w')_{33} = \frac{188.89(w'+1.5)(w'+5)(w'+15)(w'+20)(w'+33)}{(w')(w'+1.7)(w'+60)(w'+100)(w'+208)} \tag{4.18}$$

and:

$$g(w')_{22e} = \frac{86.097(w'+0.5)(w'+1.4 \pm j1.4283)(w'+7 \pm j12.124)}{(w')^3(w'+75 \pm j129.9)} \tag{4.19}$$

## *4.11* Prefilter Design

Synthesis of the prefilters follows the procedure discussed in Section 3.10. The closed-loop magnitude frequency responses of $L_{33}$ and $L_{22e}$ are plotted along with the frequency response tracking bounds. Poles and zeros are chosen for $f_{ii}(w')$ so that all of the responses of:

$$f(w')\left[\frac{g(w')q_{ii}(w')}{1+g(w')q_{ii}(w')}\right] \tag{4.20}$$

are contained within the bounds (see Figures 4.9 and 4.10).

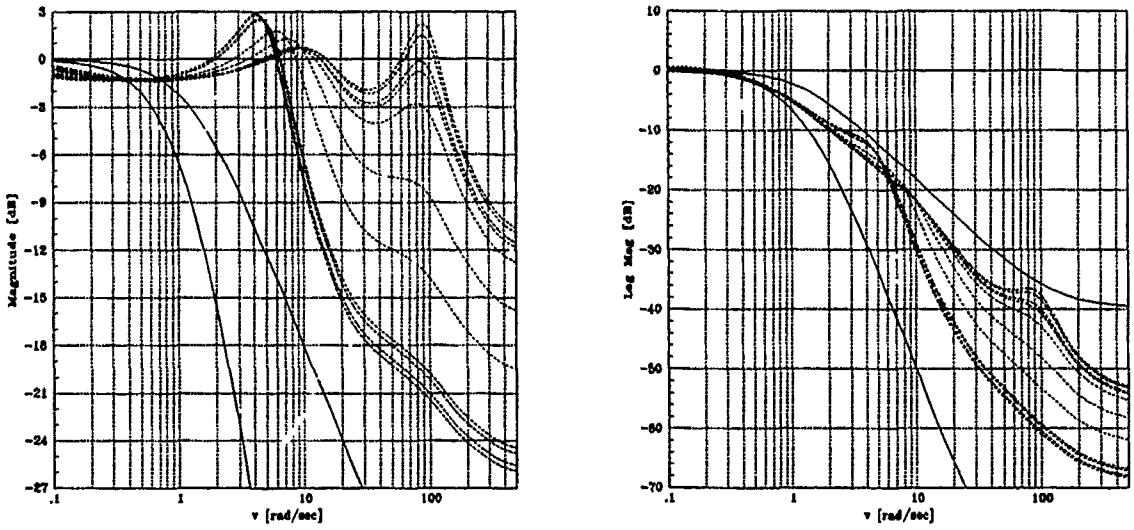


Figure 4.9. Closed–Loop Responses Without and With Prefilter, $f_{33}(w')$

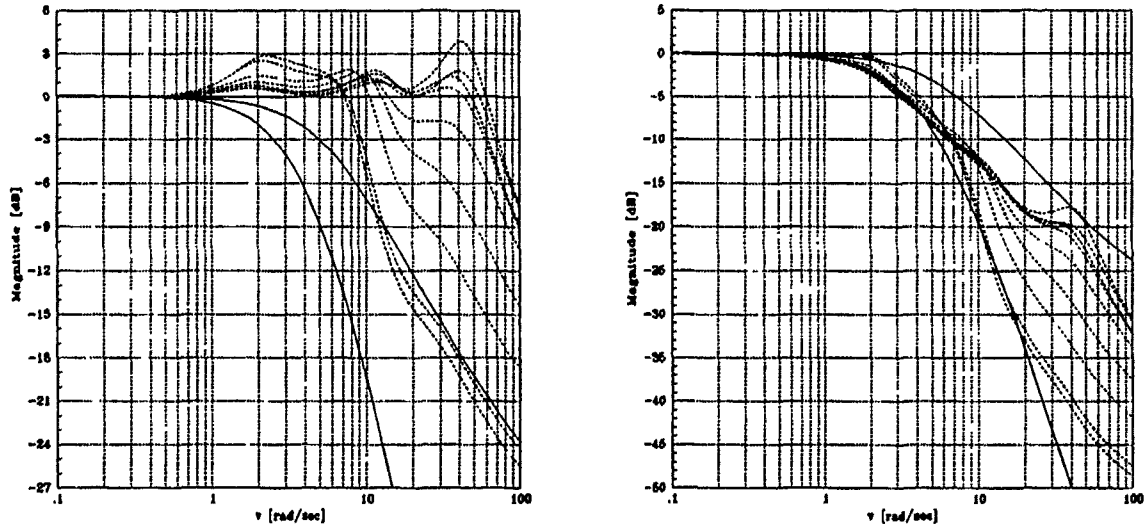


Figure 4.10. Closed–Loop Response Without and With Prefilter, $f_{22e}(w')$

## *4.12* z–Plane Transformations

The next step is to transform the compensators and prefilters into the z–plane.

Again, a $\text{MATRIX}_X$ user function is used for the transformation (see page 3-25). The resulting z–plane representations are:

$$\text{f}(z)_{33} = \frac{0.014908z^2 - 0.014884z}{z^2 - 1.9861z + 0.98610} \tag{4.21}$$

and:

$$\text{g}(z)_{33} = \frac{37.484z^5 - 142.55z^4 + 214.13z^3 - 158.66z^2 + 57.943z - 8.3350}{z^5 - 1.8832z^4 + 0.71935z^3 + 0.24443z^2 - 0.080547z} \tag{4.22}$$

and:

$$\text{f}(z)_{22} = \frac{0.084967z - 0.045752}{z - 0.96078} \tag{4.23}$$

and finally:

$$\text{g}(z)_{22} = \frac{21.724z^5 - 100.47z^4 + 186.60z^3 - 174.11z^2 + 81.682z - 15.426}{z^5 - 2.4737z^4 + 1.7895z^3 - 0.52632z^2 - 0.57895z - 0.36842} \tag{4.24}$$

*4.12.1 Comparison of* w′ *and z–Plane f's and g's* . The w′ and z–plane representations of the lateral–directional compensators and prefilters are compared. As in the longitudinal case, they must be comparable up to $\frac{1}{3}\omega_s = 105$ (rad/sec)(see Figures 4.11, 4.12, 4.13, and 4.14). As in the design for the longitudinal channel, there are differences in the w′ and z–plane representations. However, they are in good agreement up to the required frequency.

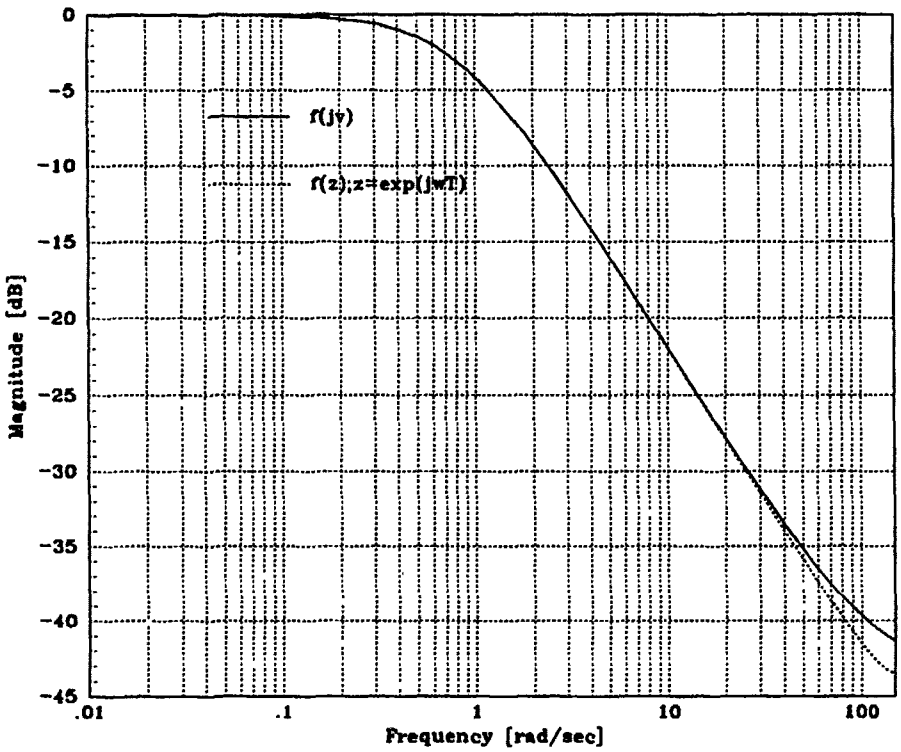


Figure 4.11. Comparison of $f_{33}(w')$ and $f_{33}(z)$ Magnitude Frequency Response

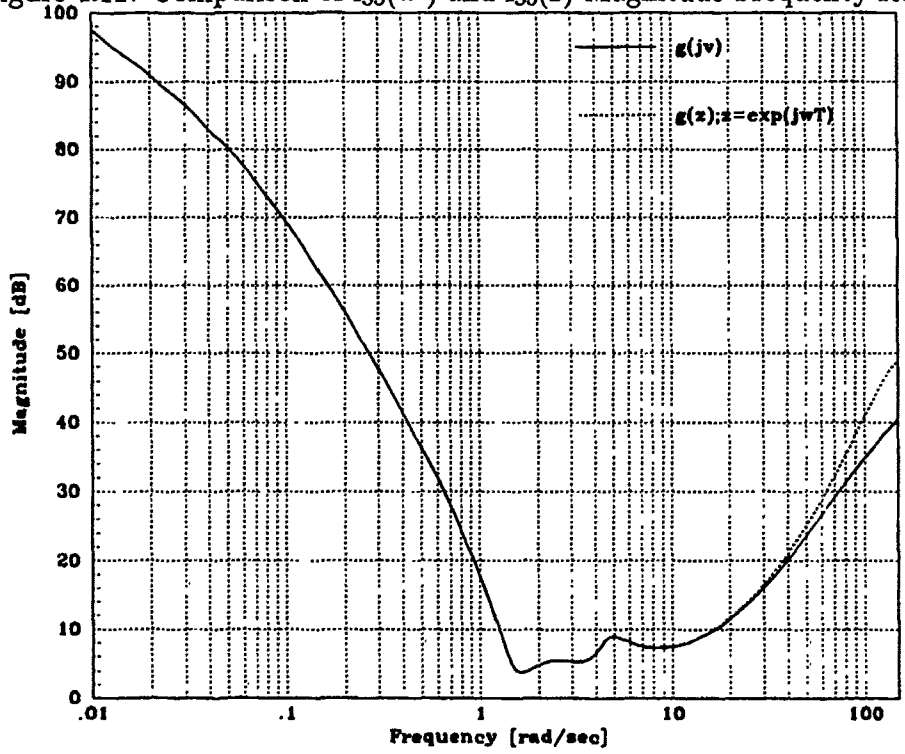


Figure 4.12. Comparison of $g_{33}(w')$ and $g_{33}(z)$ Magnitude Frequency Response

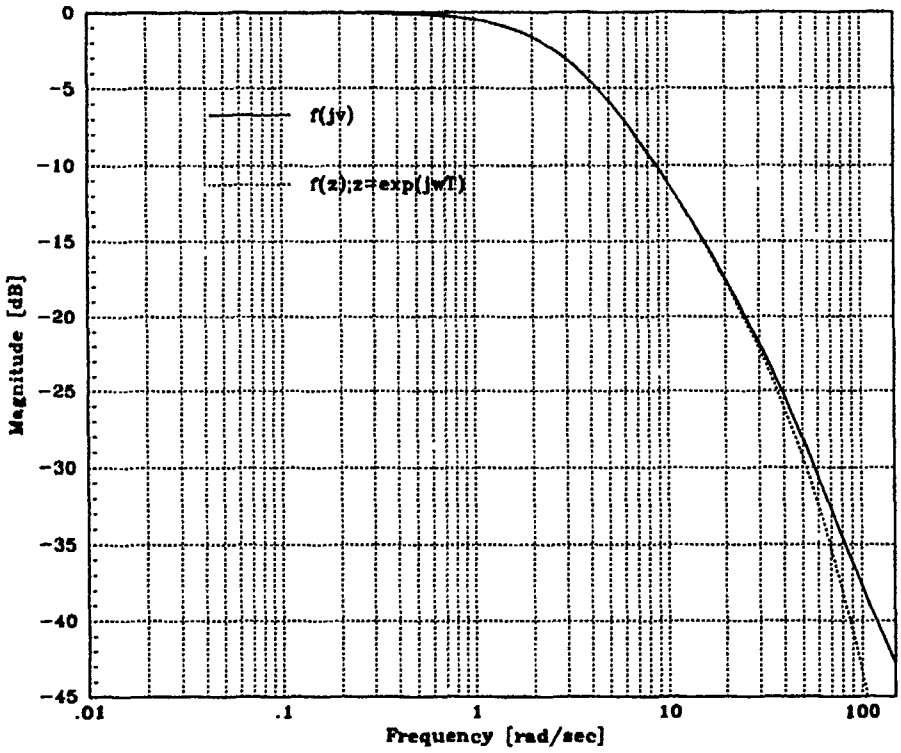


Figure 4.13. Comparison of $f_{22}(w')$ and $f_{22}(z)$ Magnitude Frequency Response

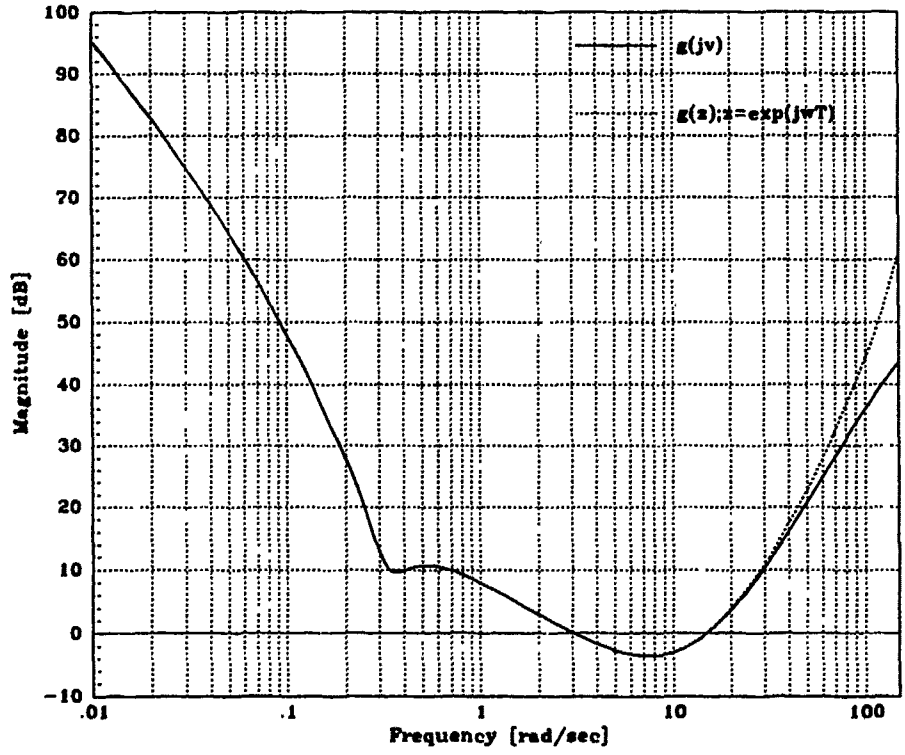


Figure 4.14. Comparison of $g_{22}(w')$ and $g_{22}(z)$ Magnitude Frequency Response

## *4.13* Simulations

The system was simulated on MATRIX$_X$ and the performance was verified by comparing the step response to the performance bounds. Once the performance was verified, the nonlinear limiter elements were added to the simulation. Again, the performance was verified. The results of the simulations are contained in Figures 4.15 and 4.16, and the results of the simulations containing the nonlinear elements are contained in Figures 4.17 and 4.18. In Figures 4.15 and 4.16, the units are radians per second for the roll and yaw rates and radians for the aileron and rudder deflections. A unit step input was used for the simulations. In Figures 4.17 and 4.18, the units for the roll and yaw rates are degrees per second, while the units of the aileron and rudder deflection are degrees. A step of 10° was used in the simulations which included the nonlinear elements. In the linear system, the size of the input does not effect the response of the system. For convenience, a unit step is used. After the nonlinear elements are added to the simulations, however, the level of the input directly affects the system response. For example, Lambda commands are limited by hardware and software limiters to a 15° maximum aileron deflection. Thus, an aileron command of 20° will have the same effect as a 15° command.

## *4.14* Summary

With the exception of generating the MISO equivalent transfer functions, the QFT design for the lateral–directional MIMO portion of Lambda follows the same procedure as the longitudinal SISO channel. The design is effective but somewhat limited by the low–order compensator requirement. Again, adding the nonlinear elements in the model limited the response but did not produce instabilities. Better performance could be obtained through faster sampling, higher bandwidth actuators, and higher–order compensation, all of which would allow higher loop transmission gain. In spite of the physical and imposed limitations, the QFT controller performs well.

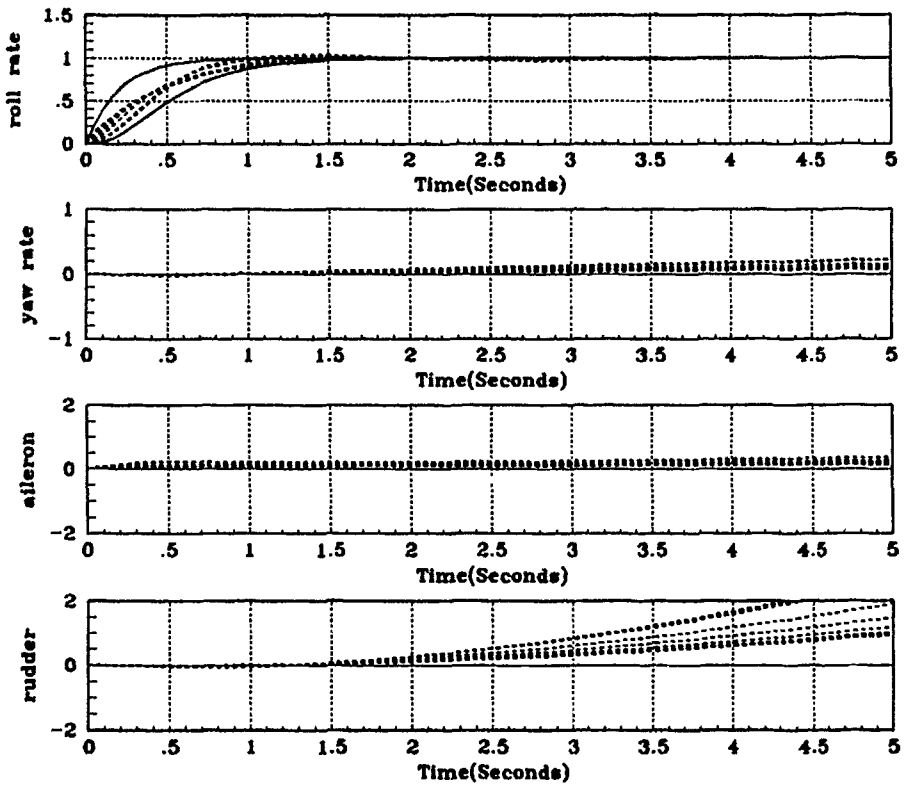


Figure 4.15. Simulation of Lateral–Directional Linear MIMO System With Step Roll Rate Command

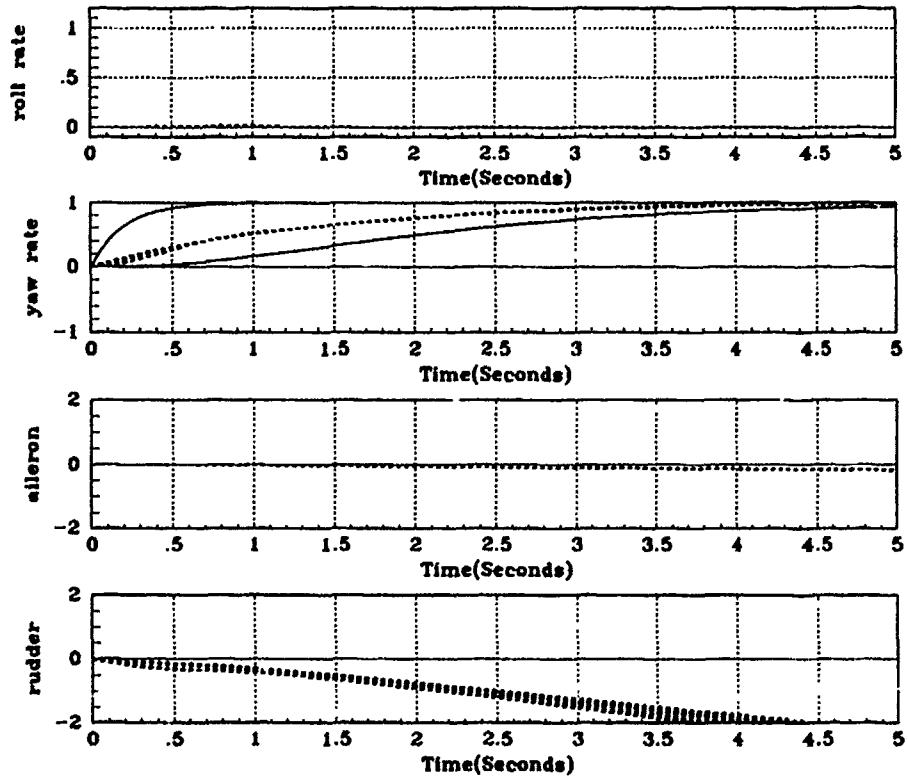


Figure 4.16. Simulation of Lateral–Directional Linear MIMO System With Step Yaw Rate Command

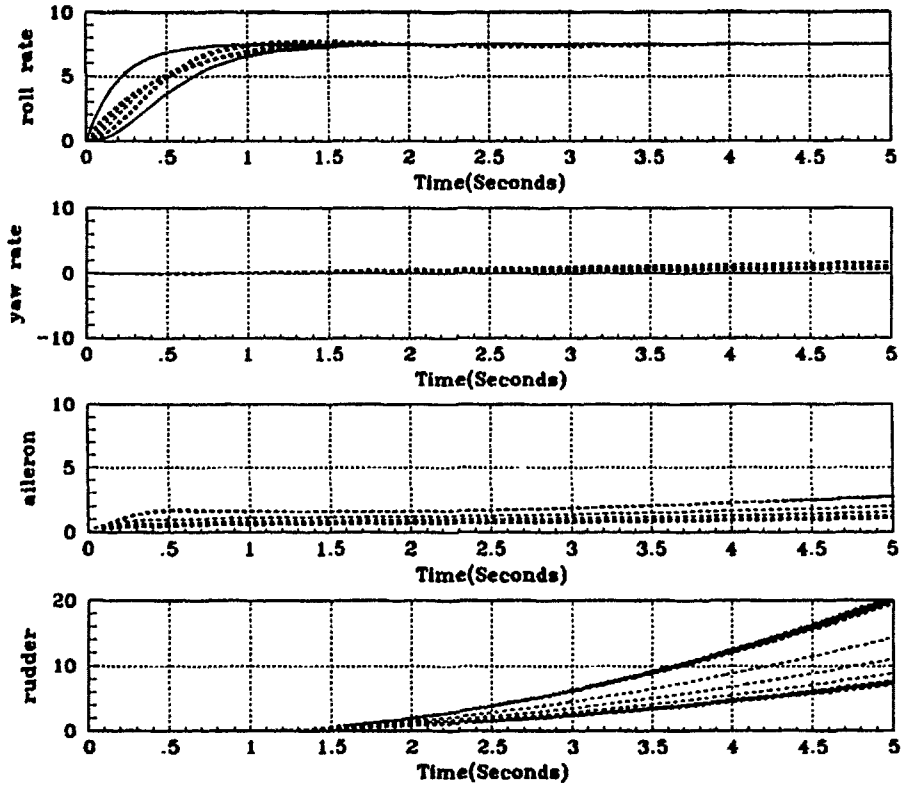


Figure 4.17. Simulation of Lateral–Directional MIMO System With Step Roll Rate Command Including Nonlinear Elements

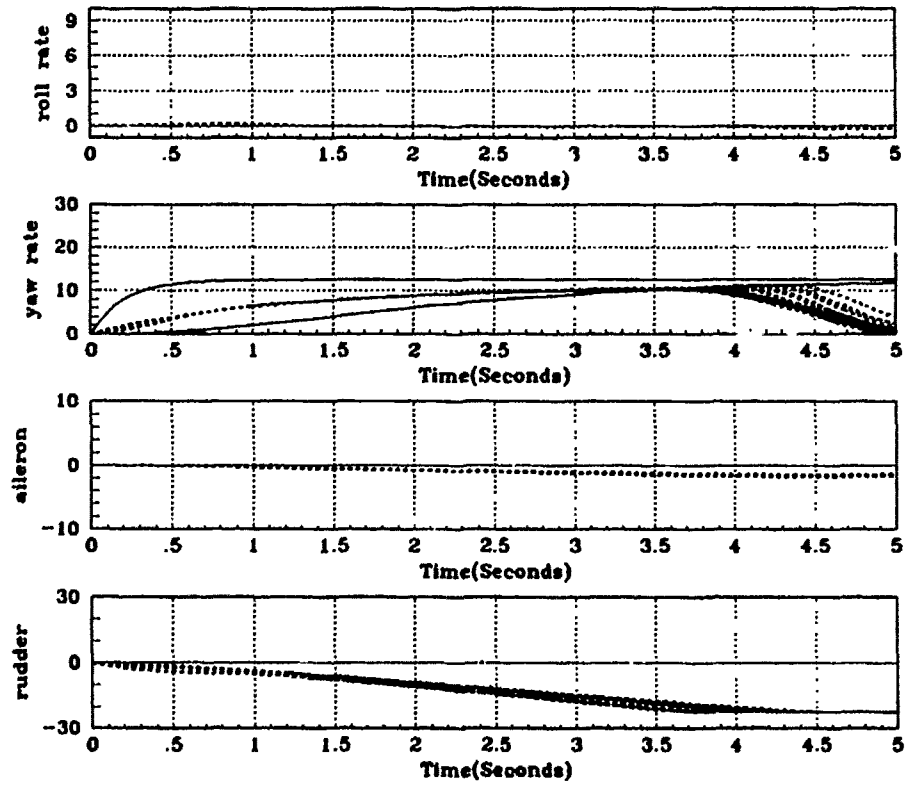


Figure 4.18. Simulation of Lateral–Directional MIMO System With Step Yaw Rate Command Including Nonlinear Elements

# V. Autopilot Design

This chapter presents an autopilot design for Lambda based on the QFT rate controller discussed in earlier chapters. Included are the design requirements, synthesis, and simulations.

## 5.1 Requirements

The Control Systems Development Branch of the Wright Laboratory requires a flight control system to aid the Lambda test pilot. The QFT rate controller meets part of the requirement by stabilizing the aircraft and guaranteeing performance throughout the flight envelope by reducing the effective plant variation. Thus tests can be conducted without redesigning or, at least, installing a new controller for each test flight. But, autopilot functions, such as turn coordination and attitude control, are also desired.

This design extends Capt Wheaton's [26] wing leveler to include turn coordination and roll attitude control. It is an outer loop for the QFT rate controller using specifications from MIL-C-18244A [17]. The standard requires the roll attitude remain within 0.5° of the commanded roll. Smooth and rapid return to commanded attitude after a disturbance is also specified. A disturbance of 20° will return to a commanded attitude with one overshoot or less with a peak overshoot less than 4° .

## 5.2 Synthesis

The autopilot is built as an outer loop around the QFT rate controller, (see Figure 5.1). It is designed directly on MATRIX$_X$ using System Build. For the purpose of simulation, the state space model of Lambda is modified to generate airspeed variations u as an output. The simulation requires total airspeed which is made up of the sum of the nominal airspeed $\bar{U}$ with the airspeed variations u. $C_{long}$ is changed and the state space is reconstructed. On the aircraft, the velocity sensor

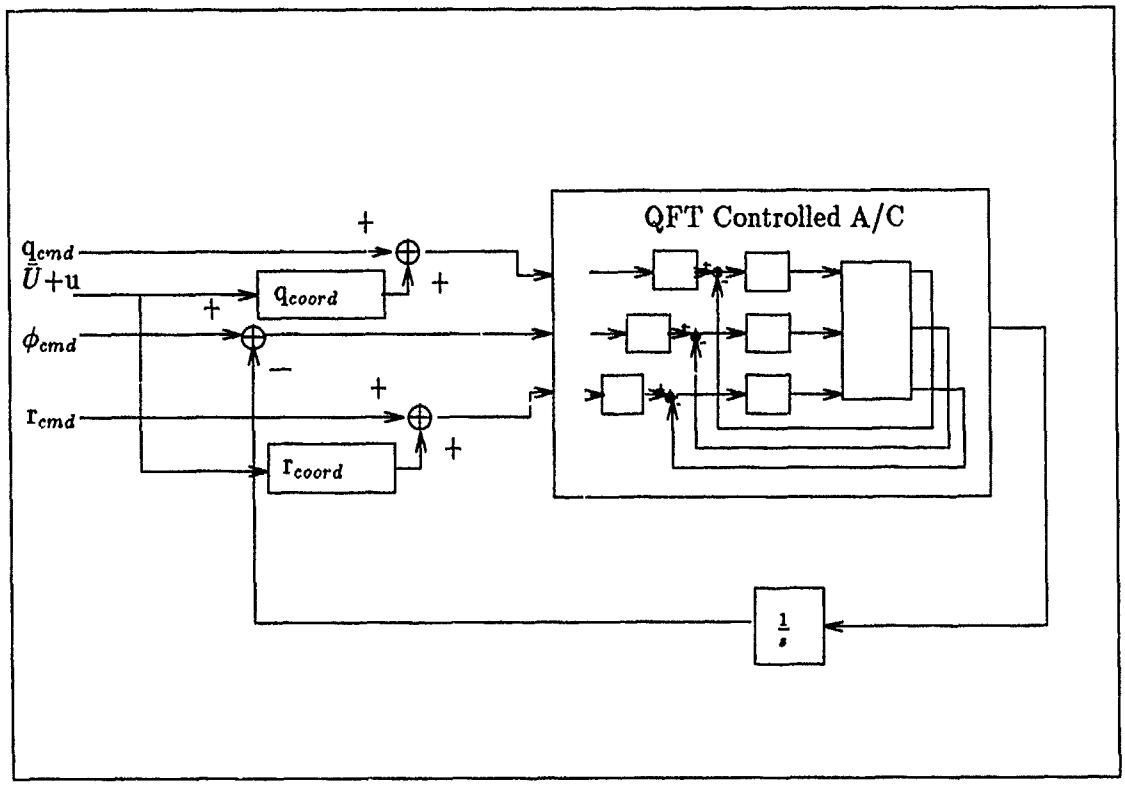


Figure 5.1. Block diagram of Autopilot Design Using QFT Controlled Lambda

provides total velocity $\bar{U}$+ u. Roll attitude $\phi$ is obtained by integrating the roll rate output $p$. Additional integrators generate simulation outputs for pitch and yaw attitude $\theta$ and $\psi$, respectively. On the aircraft the attitude is sensed with positional gyros. A disturbance input is added along with variable control inputs. Since the design must work throughout the flight envelope, the nominal speed of the aircraft is applied as an input to the system. The Lambda test pilot desires the ability to command bank angle [18]. Based on previous test flights, a wing leveler on the autopilot is also desirable. Rate control of pitch and yaw is desirable, particularly during landing. Landing is normally performed using pitch rate, making it the more natural choice. Yaw can be controlled with rate or attitude. Since there is no advantage to either methods and rate control of yaw will be simpler to implement because the turn coordination scheme in Reference [3] provides a yaw rate in response

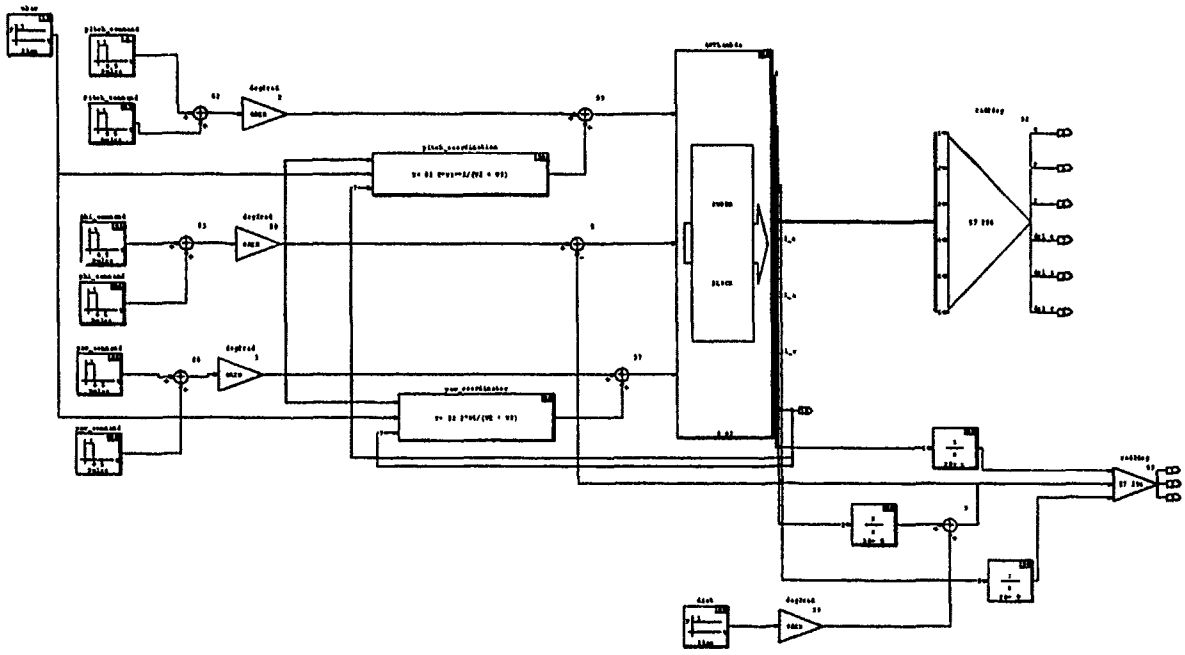

Figure 5.2. Lambda Autopilot Using QFT Compensated Aircraft

to a commanded roll, the autopilot design maintains rate control of pitch and yaw but allows the pilot to directly command $\phi$.

The QFT compensated Lambda does not require any additional compensation to enable the aircraft to respond to the pilot's command of $\phi$. A simple unity-feedback loop is added connecting the $\phi$ output to the $\phi_{cmd}$. Additional circuitry is needed for pitch and yaw turn coordination (see Figure 5.2). The pitch and yaw coordination equations are obtained from Reference [3] and are repeated below.

The pitch coordination equations are:

$$q_{coord} = \frac{g}{\bar{U} + \mathrm{u}} \tan\phi \sin\phi \tag{5.1}$$

and:

$$r_{coord} = \frac{g}{\bar{U} + \mathrm{u}} \sin\phi \tag{5.2}$$

where: q is the pitch rate (rad/sec), g is the acceleration due to gravity (32.1 ft/sec$^2$), $\bar{U}$ is the nominal speed (ft/sec), and r is the yaw rate (rad/sec). $\phi_{cmd}$ enters the

controller in degrees and is converted to radians. The equations are simplified for implementation on Lambda using a small angle approximation:

$$q_{coord} = \frac{g}{\bar{U} + \mathrm{u}}\phi^2 \tag{5.3}$$

and:

$$r_{coord} = \frac{g}{\bar{U} + \mathrm{u}}\phi \tag{5.4}$$

The $\phi$ input to the coordination circuits is taken from the pilot's command to prevent the coordination circuits from responding to bank angle disturbances caused by outside influences such as gusts. The nominal speed is entered from outside the controller, while the changes in speed u are fed back (for simulation). The model used in the autopilot simulations is the QFT–compensated Lambda that includes the nonlinear limiters (see Figure 3.17).

## *5.3* Simulations

Simulation was performed on MATRIX$_X$ . Each plant condition was included in the simulation through program iteration. The first simulation represented in Figure 5.3 is the response of the autopilot to a step disturbance of 20° . The autopilot returns the aircraft to the commanded roll angle of 0° within approximately 2 seconds, with little or no overshoot. A small error in yaw angle is created by the maneuver, which must be taken out by the rudder and ailerons. The error remains constant until the rudder actuator is saturated after about four seconds. Intervention by the pilot is required. This characteristic is due to the limit on the control surface and the lower–order compensator design.

The second simulation represented in Figure 5.4 shows the response of the autopilot to a -10° roll command with a +10° roll disturbance. Again, the aircraft model responds within specifications. In this simulation, it is evident that the system is more than a wings lever as it returns the aircraft to the commanded .oll angle of

-10° . As before, the pilot must intervene to keep from saturating the controls after about four seconds. In this case, the airspeed decreases as expected, because the turn coordination computer is commanding additional pitch rate. The additional pitch is required to keep the flight path horizontal throughout the turn. As Lambda slows, more elevator is needed to generate the required lift. Thus, the airspeed decreases steadily. An automatic throttle control may prevent this situation by holding the airspeed constant.

The third simulation (see Figure 5.5) shows the autopilot response to a constant 30° roll command. In this case, the autopilot very accurately responds to the command; the roll angle is established in about 2.5 seconds and held constant. Again, control saturation of the elevator and rudder actuators are reached. In this simulation, the rudder saturates for some conditions as early as 4.6 seconds, while for the high speed conditions it does not saturate within 10 seconds. The elevator actuator saturates at 6.5 seconds for a few of the conditions. Again, an automatic throttle control may extend the capability of holding a desired roll angle.

Figures 5.6 and Figures 5.7 show the autopilot response to a constant 10° pitch rate command and a 2 second 10° pulse pitch command, respectively. The response is the same as the QFT rate controller without the autopilot outer loop, which is to be expected. The 2 second 10° pulse pitch command is more realistic as it results in a 20° pitch angle.

The 10° constant yaw rate command simulation in Figure 5.8 and the 2 second 10° pulse yaw rate simulation in Figure 5.9 have the same response as the rate controller without the autopilot.

The next simulation, Figure 5.10, shows the autopilot response to a command consisting of a 4 second +10° roll angle command followed by a 4 second −10° roll angle command. The model follows the commands well and doesn't saturate the control actuators.

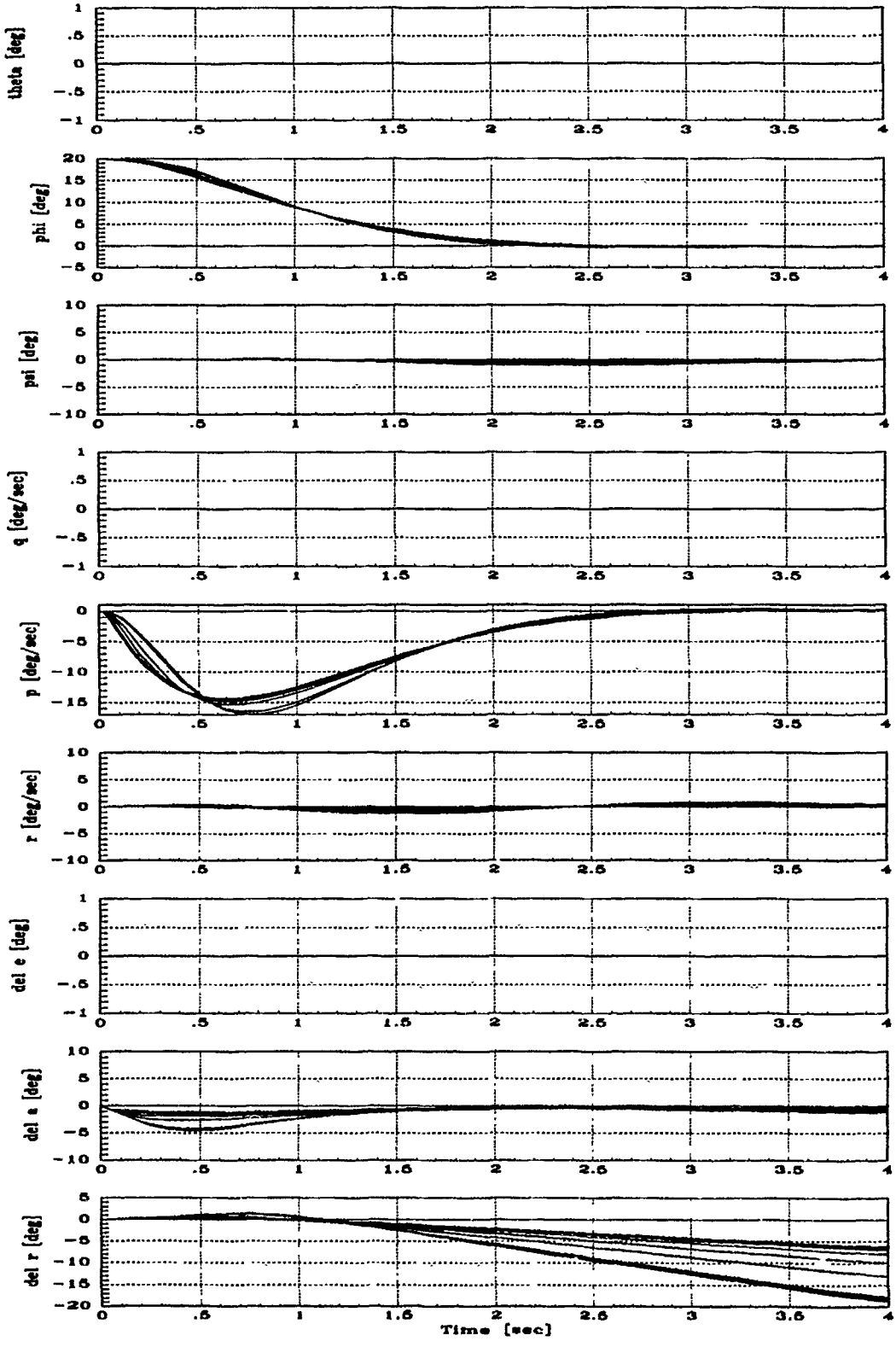


Figure 5.3. Autopilot Response to a 20° Roll Disturbance Input

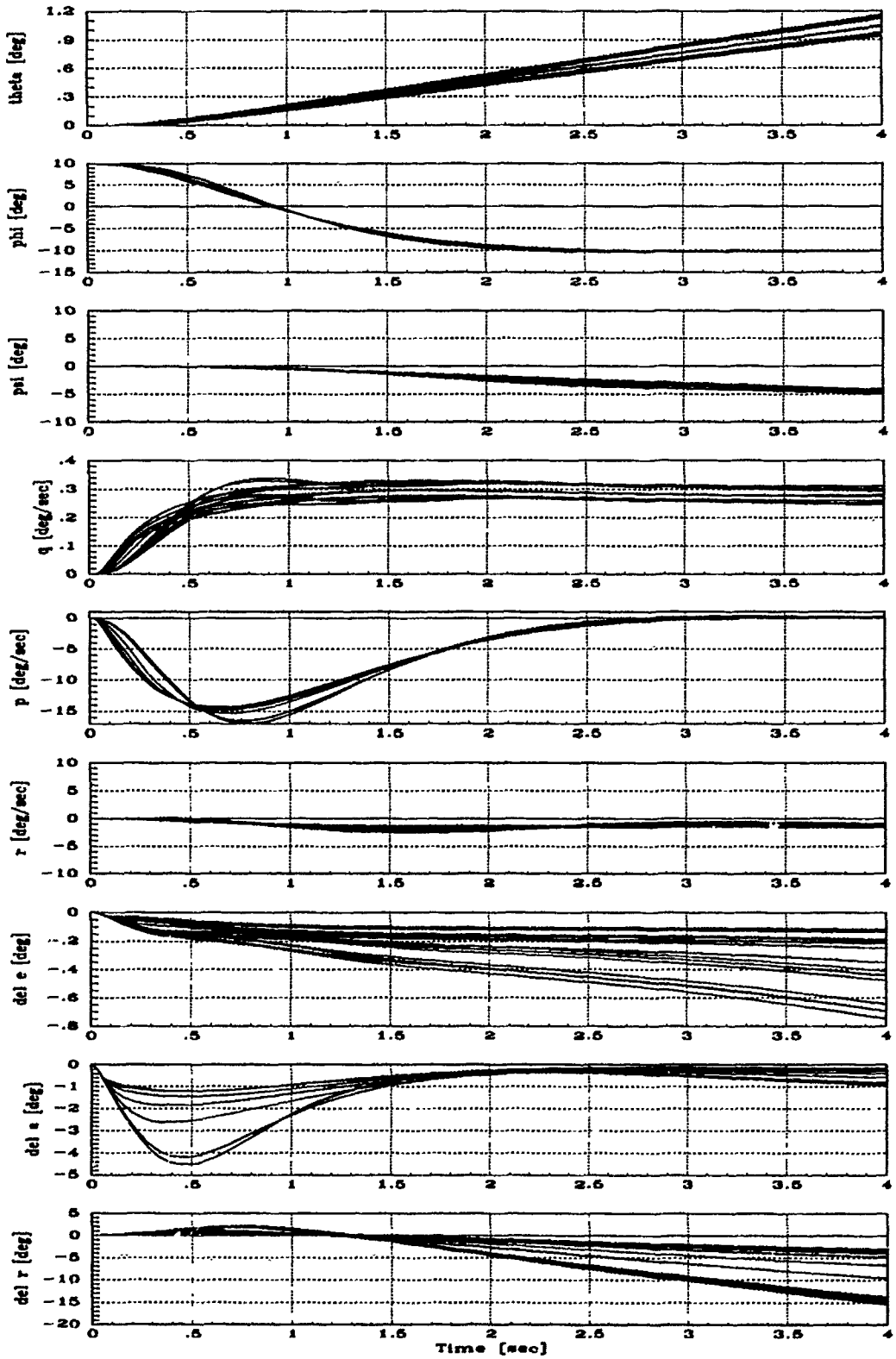


Figure 5.4. Autopilot Response to a -10° Roll Command With a +10° Roll Disturbance

The last three simulations involve a ramp roll position input.

Figure 5.11 is the autopilot response to a very slow (1°/sec) ramp. The rudder actuator begins to saturate for some of the plants after 18 seconds. Only four of the plants experience the saturation within the 20 second simulation.

Figure 5.12 response is due to a ramp with a peak of 20/dg and a slope of 5°/sec. The aircraft tracks the ramp well with a small (0.5 sec) delay. At 5 seconds, all of the nineteen plants achieve the desired roll angle and hold it throughout the simulation well within ± 0.5° specification of MIL–STD–18244A. Four of the plants saturate the elevator after 15 seconds. Eight plants exhibit rudder saturation starting after nine seconds.

The final simulation, Figure 5.13, demonstrates the autopilot response to a triangular shaped roll input. The peak input of 20 ° is realized at four seconds after the start of the simulation. At the peak, the slope is reversed until the input is zero at eight seconds. In this case, no actuators saturate.

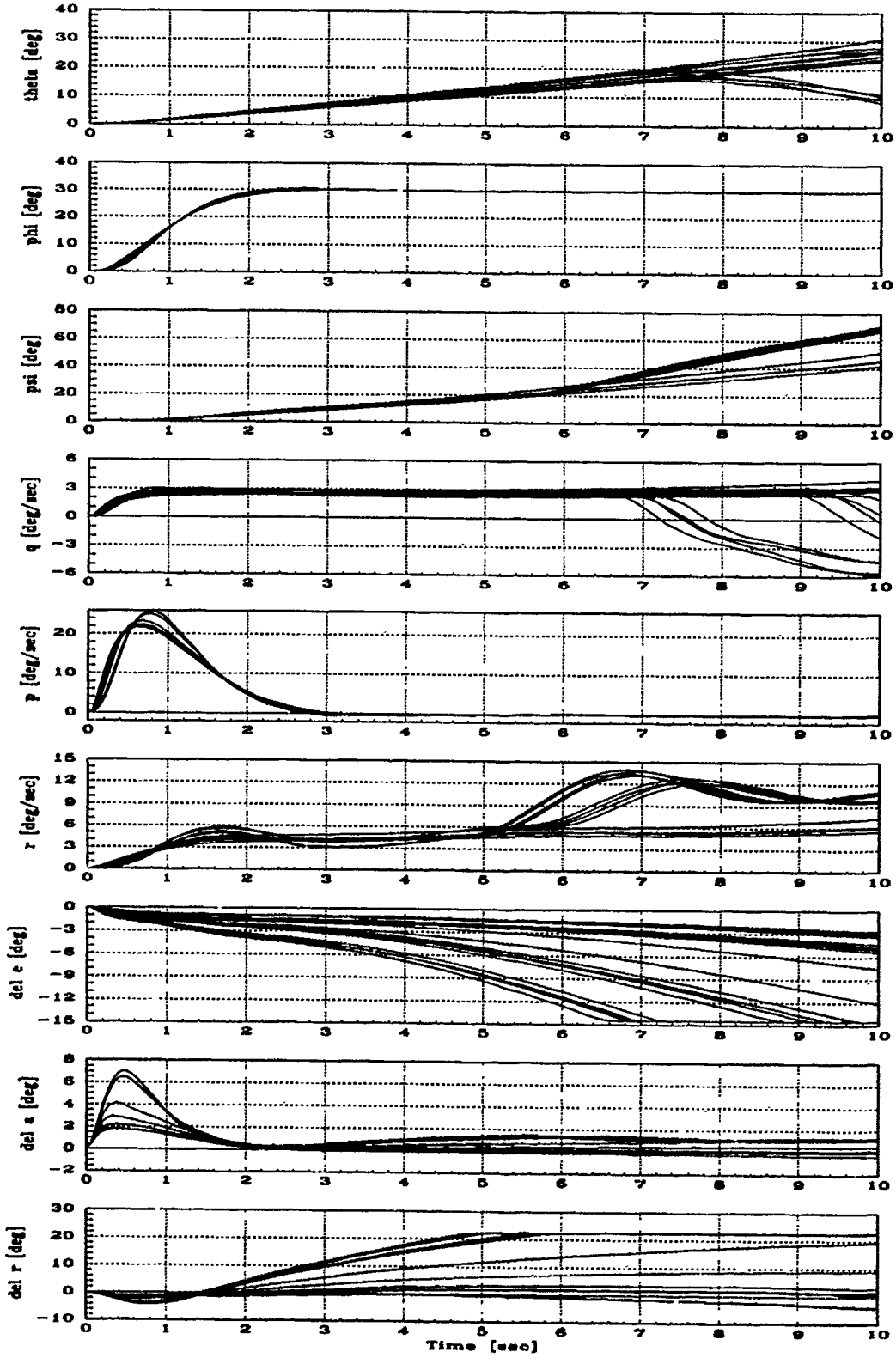


Figure 5.5. Autopilot Response to a Constant 30° Roll Command

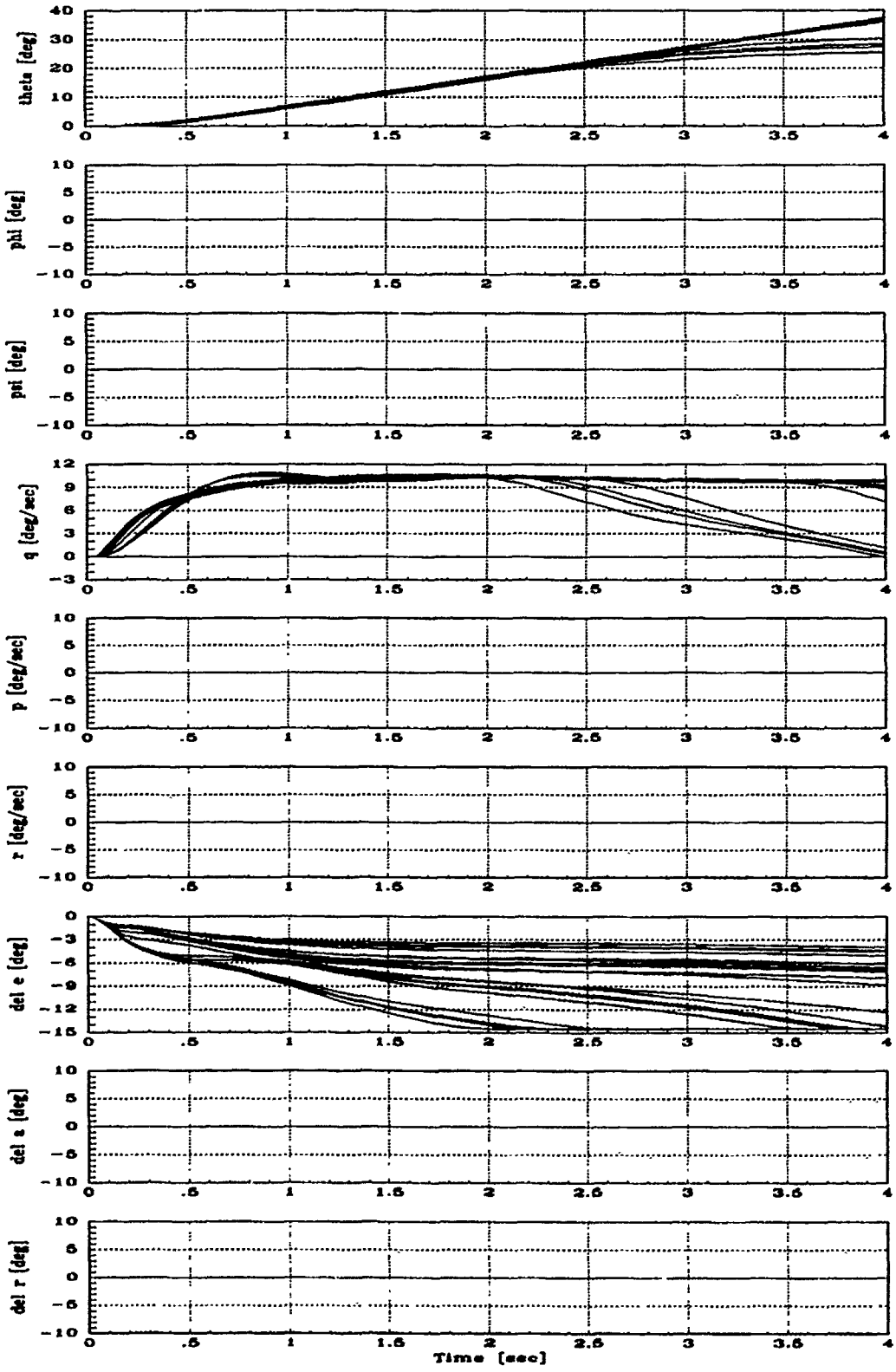


Figure 5.6. Autopilot Response to a Constant 10° Pitch Rate Command

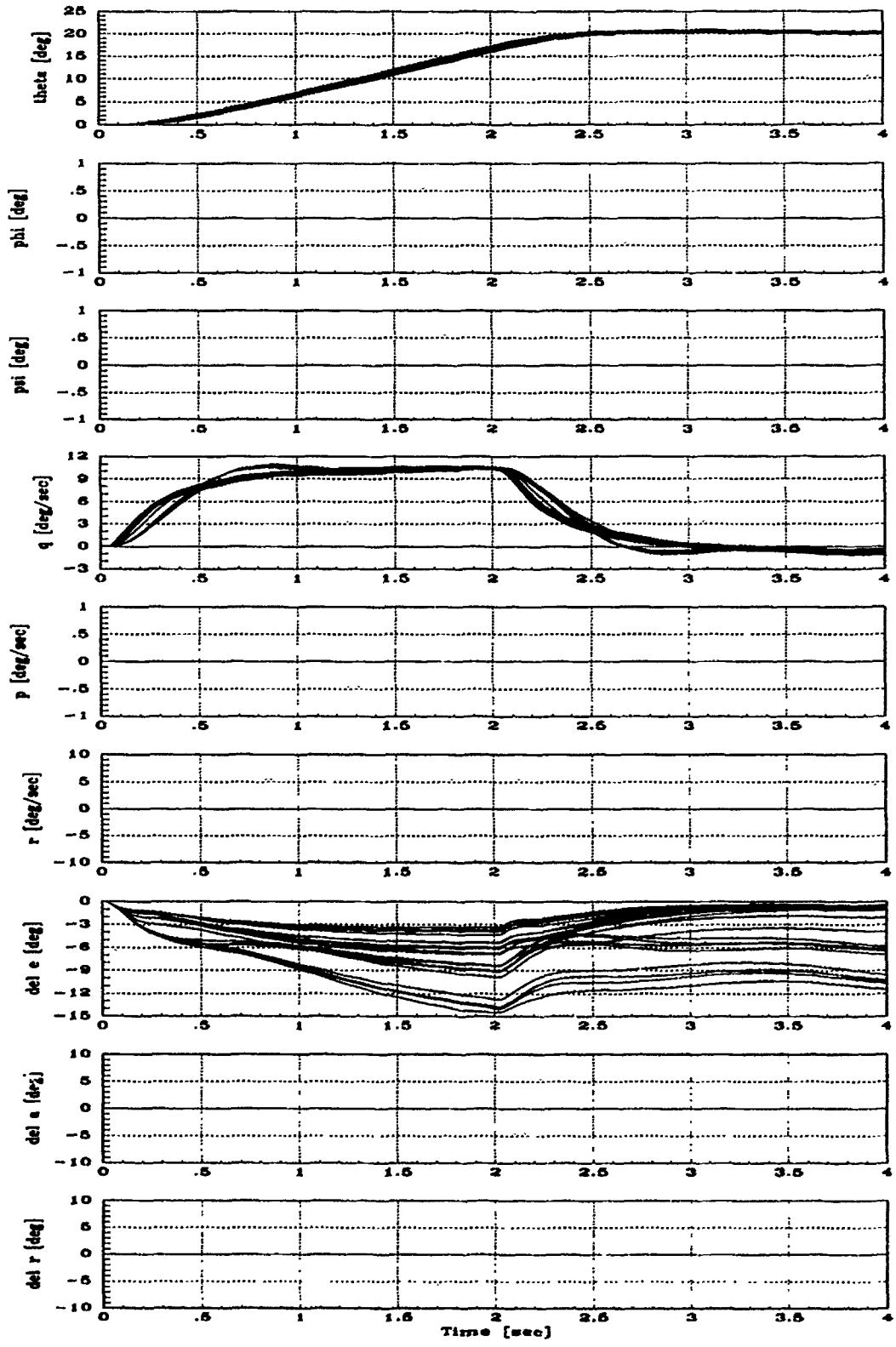


Figure 5.7. Autopilot Response to a 2 Second 10° Pulse Pitch Command

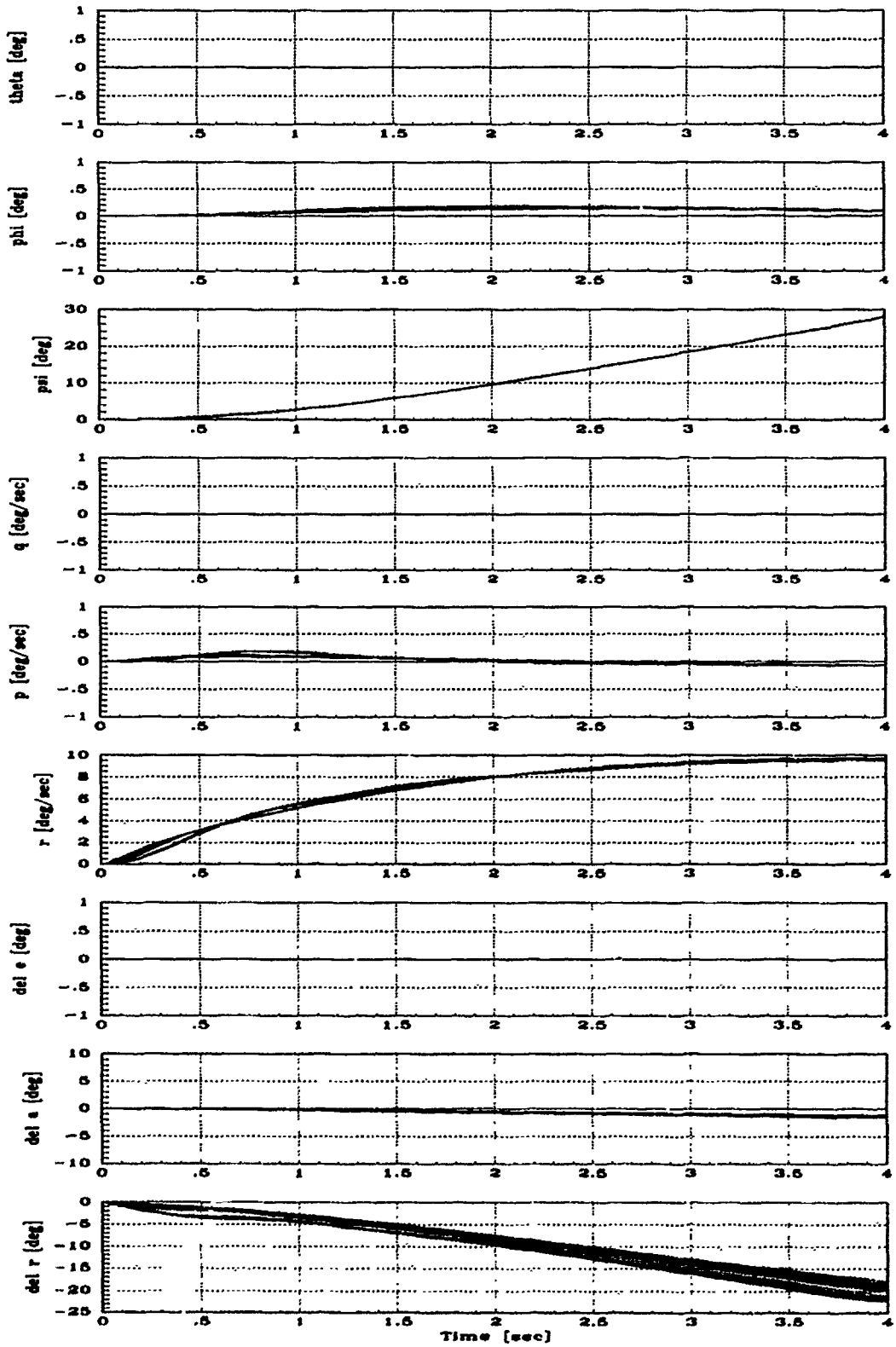


Figure 5.8. Autopilot Response to a Constant 10° Yaw Rate Command

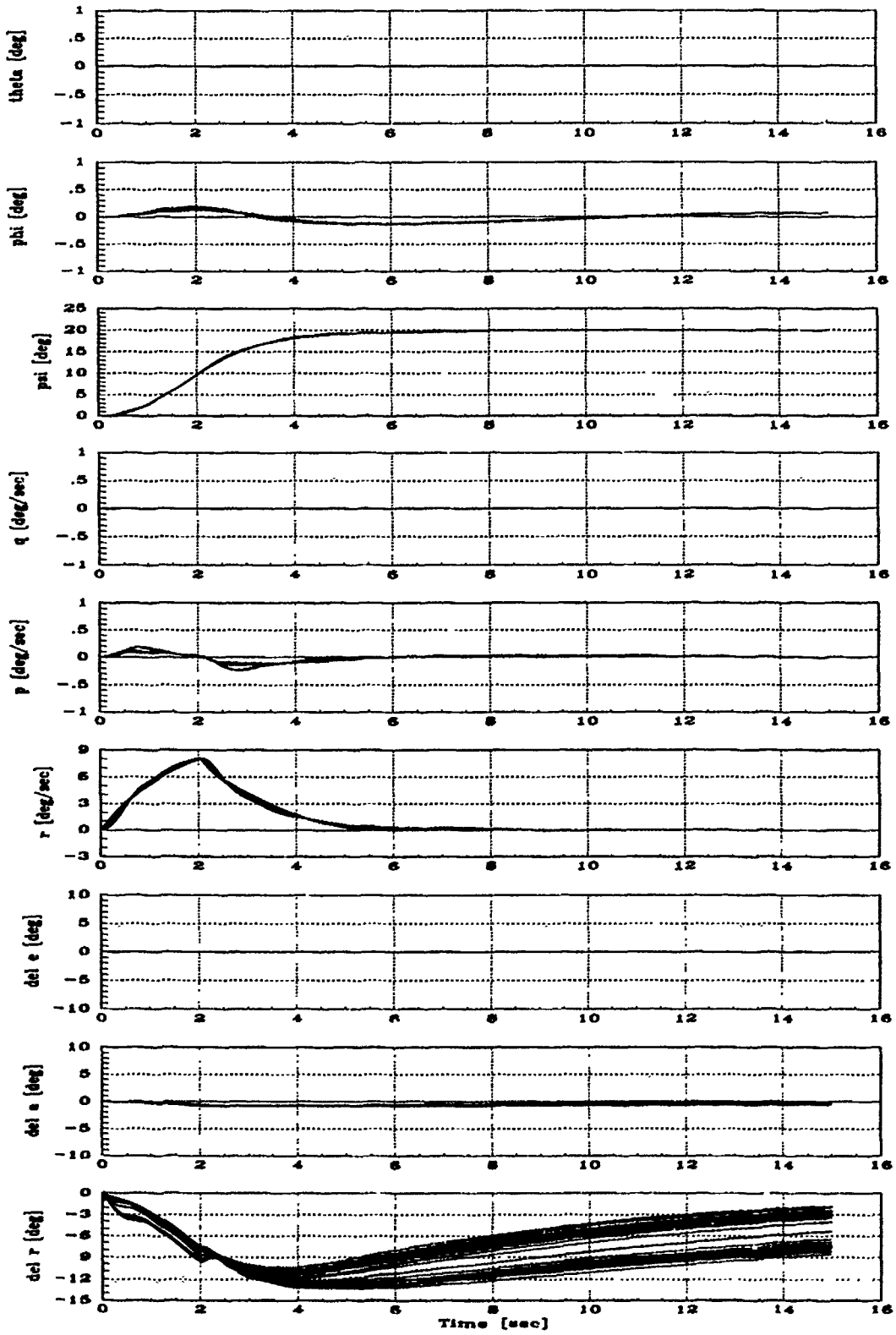


Figure 5.9. Autopilot Response to a 2 Second 10° Pulse Yaw Command

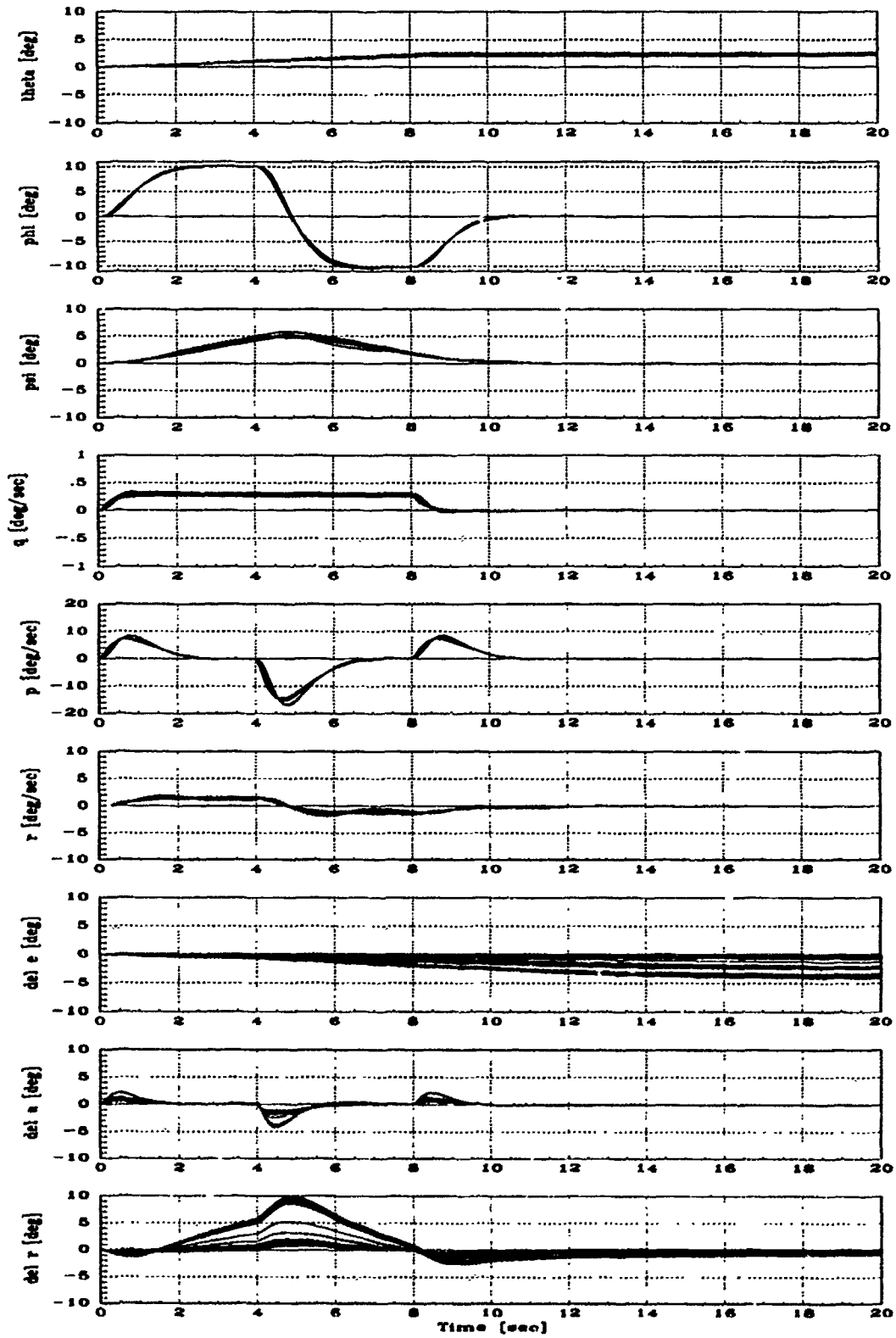


Figure 5.10. Autopilot Respon e to a 4 Second 10° Pulse Doublet Roll

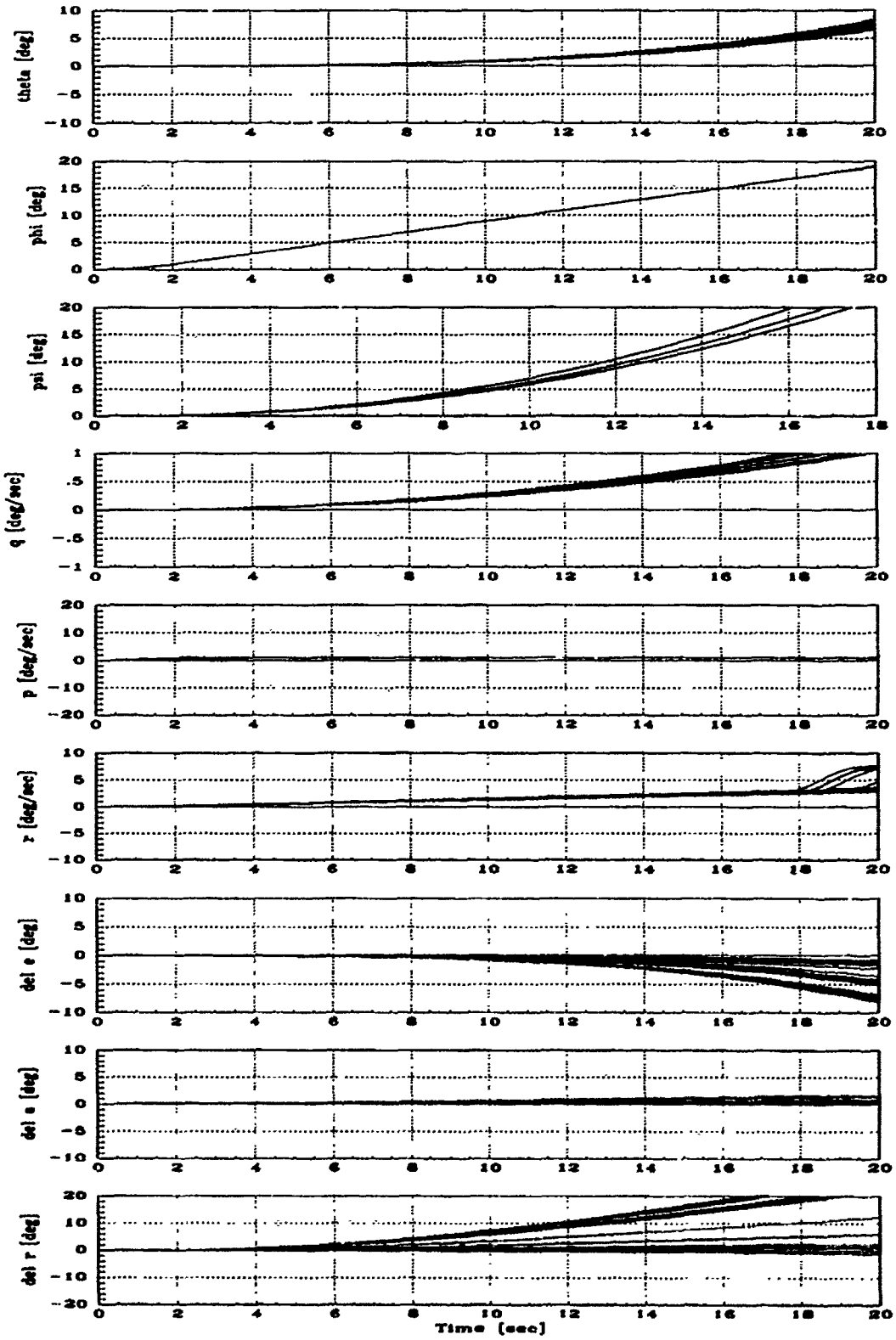


Figure 5.11. Autopilot Response to Ramp Roll Input With a 20° Peak and Slope of 1°/sec

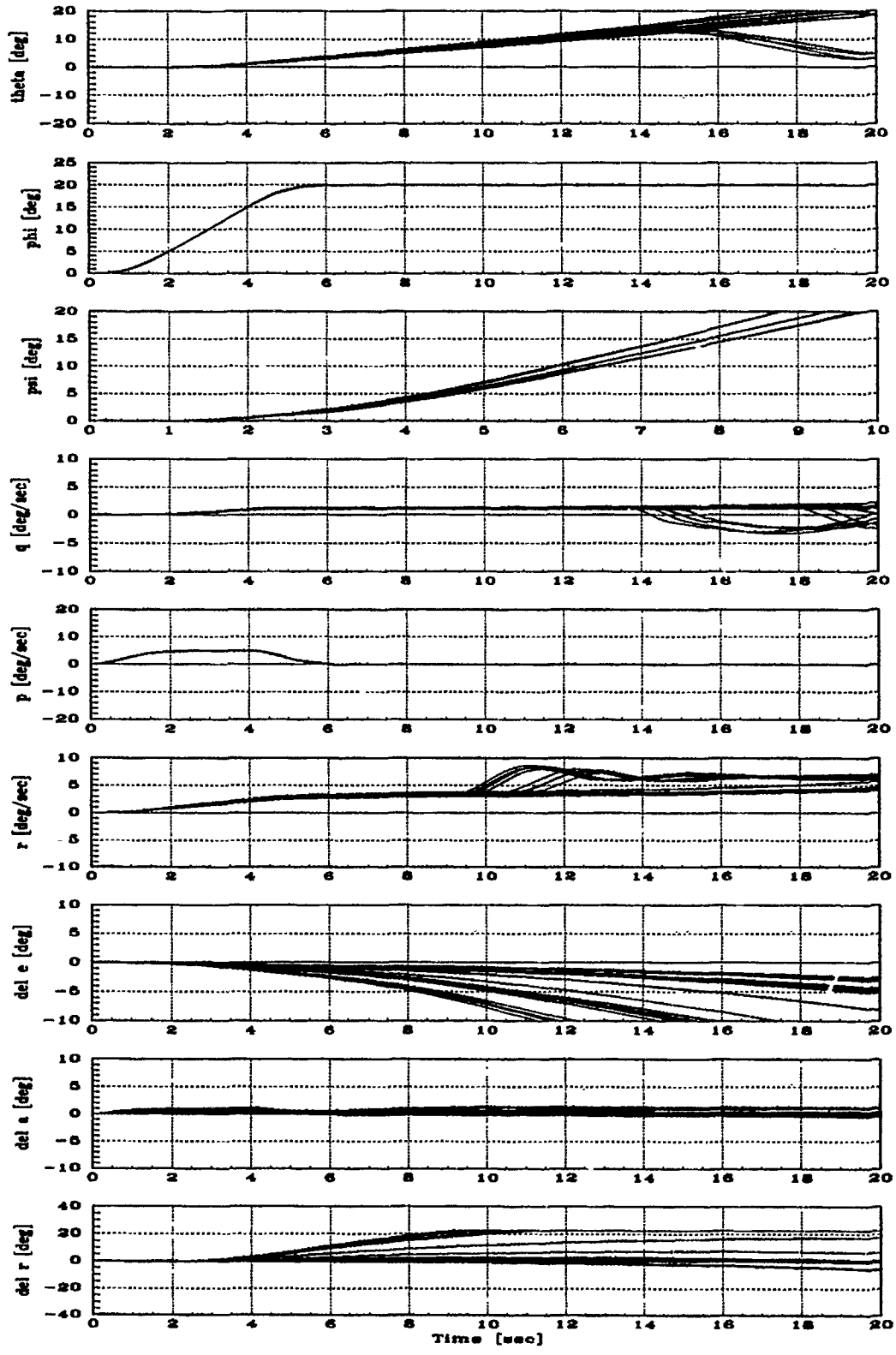


Figure 5.12. Autopilot Response to a Ramp Roll Input With a 20° Peak and a Slope of 5°/sec

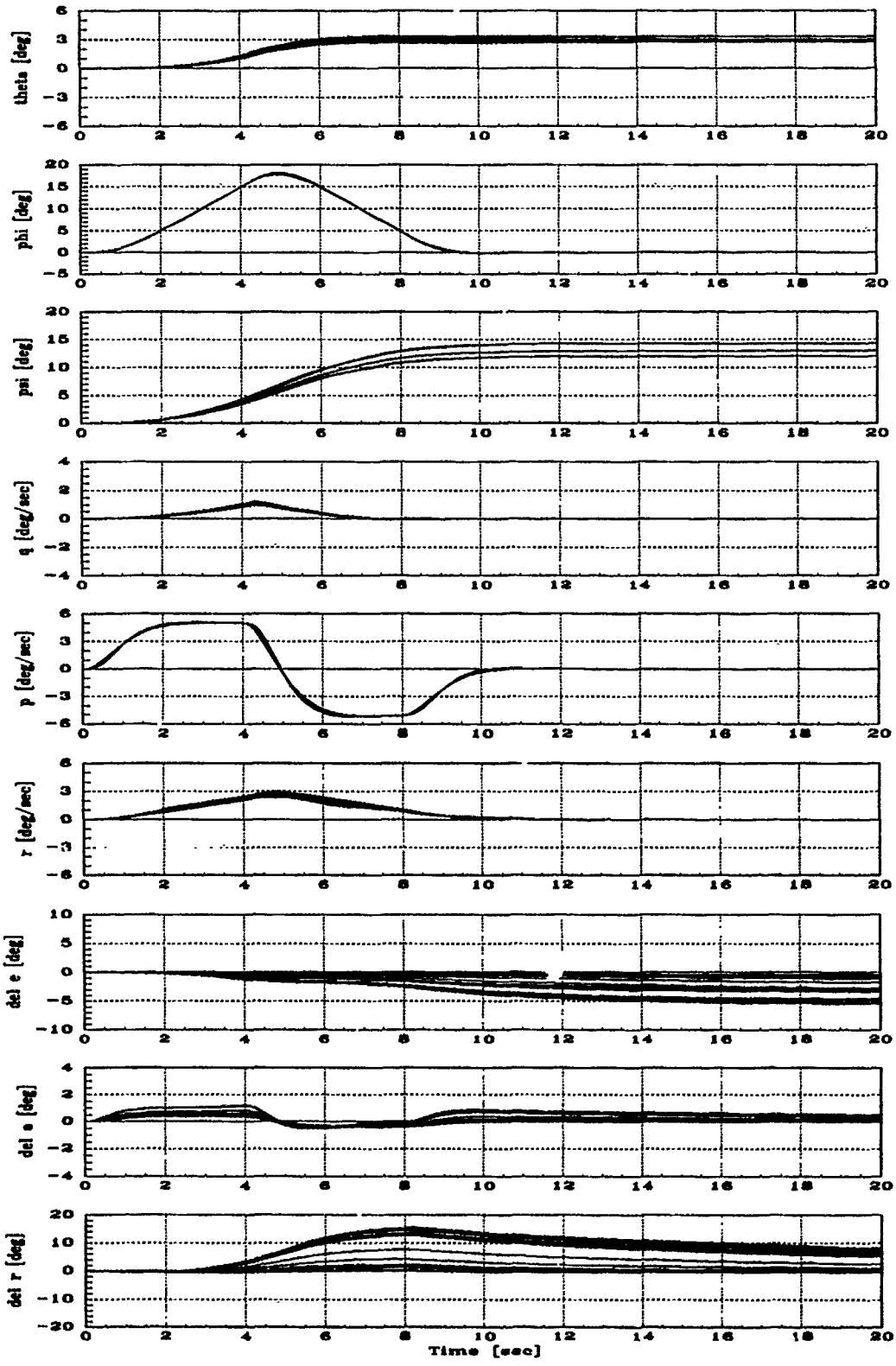


Figure 5.13. Autopilot Response to Rising and Falling Ramp Roll Input with a 20° Peak and a ± 5°/sec Slope

## *5.4* Summary

A satisfactory autopilot design was easily synthesized around the QFT controller due to the reduced uncertainty, stability, and predictable performance provided by the controller. The autopilot remained stable and responsive to commands until control saturation was reached. After one or more of the controls became saturated, the model did not go unstable. An autopilot can be a great aid to the pilot but, in this design, a pilot is still necessary. The better performance could be expected from a higher-order controller with a higher loop transmission gain. In addition, this autopilot uses one of four turn coordination schemes presented in Reference [3]. Another scheme may perform better or, possibly, the sine and tangent functions could be used instead of a small angle approximation. Of course, a higher loop transmission gain would be obtained with an increased sample rate or increased order compensator. The main benefit of the higher gain would be reduced variation in the responses particularly in the yaw channel.

# *VI.* Summary, Conclusions, and Recommendations

This chapter presents a summary of the thesis, draws conclusions, and recommends future actions.

## *6.1* Summary

The QFT design technique was applied to the Lambda URV and autopilot functions were added as an outer loop to the QFT controller. In contrast with previous efforts that used models developed from computer predictions from design specifications, this thesis employs a model developed from flight test data. In the model, aircraft dynamics of the Lambda model separate into two independent channels—the longitudinal channel and the lateral-directional channel. The longitudinal channel is a SISO system while the lateral-directional channel is a two-by-two MIMO system.

The longitudinal SISO QFT design follows the steps outlined in Chapter I Section 1.7 and proceeds from the choice of flight conditions through simulations using the SISO QFT technique in the w'domain. Flight conditions were chosen with great care to insure a realistic usable design with minimal over-design. Stability bounds were plotted using graphical techniques, while performance bounds are not used due to the reasons explained in Chapter III Section 3.7. The loop shaping is done with the entire nominal plant included in the loop as part of a minimum realization technique. The compensator is extracted by dividing the plant out of the resulting transmission loop. After the prefilter is formed, the design is transformed to the z-plane and simulated using the hybrid simulation capability of MATRIX$_X$ .

The lateral-directional MIMO QFT design proceeds in a similar manner. Only the differences in the design techniques are discussed in detail. The flight conditions used in the longitudinal SISO design are the same ones used in the longitudinal SISO QFT design, including the choice of the nominal plant. An equivalent transfer function matrix is developed and inverted to create the **Q** matrix with elements $q_{ii}$

which are the equivalent MISO loop transfer functions. Once the $q_{ii}$ are obtained, the design follows the SISO QFT design steps. The transmission loop is formed using two separate techniques—a backward loop shaping technique, Section (3.8.1), and a minimum order compensator design technique. The backward loop shaping technique is applied first to establish a theoretical maximum performance baseline for the design. Then, application of the minimum order compensator design technique produces a fifth order compensator required for implementation on Lambda's digital flight control computer. After the first loop of the MIMO system is designed, the subsequent loops are designed using modified $q_{ii}$'s. Comparing the results of simulations with specifications completes the design.

An autopilot is added as an outer loop built around the QFT compensated Lambda. It allows roll attitude control along with providing turn coordination, mode requested by the Wright Laboratory. The autopilot modes are designed to meet military specifications and the simulations prove the design. For example, the wings return to level in about 2 seconds after a 20° disturbance with little or no overshoot and meets MIL-STD-18244A. The QFT controller effectively minimized the parameter variations in the aircraft. Therefore, the design is simple, and only one set of controllers is necessary. The turn coordination modes work well but are limited by the performance of the aircraft. Control authority is exceeded in many cases, and though the design is stable throughout the envelope, pilot intervention is necessary.

## *6.2* Conclusions

The QFT design technique is powerful and perfect for the design of a rate controlled autopilot for URVs requiring robust autopilot systems. Lambda simulations show a *single* QFT controller can perform well throughout the entire flight envelope of Lambda without additional sensors. The technique is straightforward. Synthesis and simulations can be performed using a computer aided design package such as

$MATRIX_X$ using minimal computer resources compared with the hours of computer time devoured by fellow students using other control techniques. The method is completely transparent, in that the designer is able to predict the ultimate performance early in the design. More importantly, the designer is able to make engineering tradeoffs during loop shaping. For example, performance at certain frequencies can be increased by reducing the performance at frequencies of lower interest to the designer.

## *6.3* Recommendations

Working on a controller for Lambda is a unique opportunity. Simply knowing that the controller design will be used is highly motivating. The Wright Laboratory should continue to challenge AFIT students with thesis proposals involving Lambda. The students benefit by facing a real life challenge and the laboratory gets needed research. The effect is synergistic. This design should be implemented on Lambda and the performance should be compared with predictions. The Lambda model should be improved as more information becomes available and should be extended to include the effects of operating the ten flight control surfaces independently. The weight of Lambda should be reduced or ,at least, held to its current value since the heavier weights are the main source of plant variation and contain open loop unstable poles. An automatic throttle control should also be added. The Wright Laboratory should acquire the ability to run $MATRIX_X$ in order to use the computer software generated during this thesis to upgrade the controller if it becomes necessary. Additionally, other QFT controllers should be synthesized for Lambda. This design is aimed at stability throughout the envelope assuming no failures. Future efforts should consider the effects of component failure or battle damage on the controllability of the aircraft. Because of limited computer resources aboard Lambda, this controller is limited to fifth order compensation. Superior performance was achieved in simulation with higher order compensation due the higher available loop trans-

mission gain. Future efforts might add the computer resources, without additional weight, to Lambda to allow higher order compensation and a faster sampling rate. Finally, Lambda's performance could be improved by installing faster actuators since the present actuators severely limit the loop transmission gain.

# Appendix A. **Model Generating MATLAB macro File**

The following *MATLAB* "m" file was created by Lt Gerald Swift to generate a state space representation of Lambda [24]:

```
%  This macro calculates the longitudinal and lateral-
%  directional state space equations of motion for the
%  Lambda URV given Xcg, U1, q1, W and theta.
%
%  Input:  X=[Xcg,U1,q1,W,theta]
%
%          where, Xcg = inches
%                 U1 = feet/second
%                 q1 = pounds/sq foot
%                 W  = pounds
%                 theta = degrees
%
%  Outputs:
%
%    Clong=[CMu,CMa,CMad,CMq,CLu,CLa,CLad,CLq,CDa,CDu,
%                            CLde,CDde,CMde,CLdf,CDdf,CMdf]'
%
%    Clat=[Clb,Clp,Clr,Clda,Cldr,Cnb,Cnp,Cnr,Cnda,Cndr,
%                                    Cyb,Cyp,Cyr,Cyda,Cydr]'
%
%    Dlong = corresponding vector of dimensional
%                                           derivatives for Clong
%
%    Dlat = corresponding vector of dimensional derivatives for Clat
%
%    Along = A matrix for longitudinal equations of motion
%
%    Alat = A matrix for lateral-directional equations of motion
%
%    Blong = B matrix for longitudinal equations of motion
%
%    Blat = B matrix for lateral-directional equations of motion
%
CMu=0;
```

```
CMa=0.326643*X(1,1)-16.5189;
CMad=0.238235*X(1,1)-7.8977;
CMq=0.628420*X(1,1)-45.0582;
CLu=-0.0001719*X(1,1)+0.01518;
CLa=5.820;
CLad=-0.03838*X(1,1)+3.83508;
CLq=-0.65202*X(1,1)+37.8884;
CDa=0;
CDu=0;
CLde=0.2908;
CDde=0;
CMde=0.013464*X(1,1)-1.48039;
CLdf=1.419;
CDdf=0.08489;
CMdf=0.070932*X(1,1)-3.63838;
Clong1=[CMu,CMa,CMad,CMq,CLu,CLa,CLad,CLq,CDa,CDu];
Clong2=[CLde,CDde,CMde,CLdf,CDdf,CMdf];
Clong=[Clong1 Clong2]';
%
Clb=-0.01451;
Clp=-.5538;
Clr=0.08763;
Clda=0.2608;
Cldr=0.000213*X(1,1)-0.00783;
Cnb=-0.00038*X(1,1)+0.07834;
Cnp=-0.03601;
Cnr=0.003087*X(1,1)-0.31072;
Cnda=-0.01368;
Cndr=0.001633*X(1,1)-0.15208;    % updated 4/22/91
Cyb=-0.4372;
Cyp=-0.001600;
Cyr=-0.00424*X(1,1)+0.46047;
Cyda=0;
Cydr=0.2865;
Clat=[Clb,Clp,Clr,Clda,Cldr,Cnb,Cnp,Cnr,Cnda,Cndr,
%                                          Cyb,Cyp,Cyr,Cyda,Cydr]';
%
%  Calculation of Dimensional Derivatives
%
%    Dlong=[Mu,Ma,Mad,Mq,Zu,Za,Zad,Zq,Xa,Xu,Zde,
%                                          Xde,Mde,Zdf,Xdf,Mdf]'
%
```

```
%    Dlat=[Lb,Lp,Lr,Lda,Ldr,Nb,Np,Nr,Nda,Ndr,Yb,Yp,Yr,Yda,Ydr]'
%
xcg=X(1,1);
u=X(1,2);
q=X(1,3);
m=X(1,4)/32.174;
s=21.1;
c=1.51;
b=14.07;
Ixx=?2.502;
Iyy=26.666;
Izz=40.939;
Ixz=0.5922;
CL1=X(1,4)/(q*s);
CD1=0.027;
CM1=0.0;
A1=Ixz/Ixx;
B1=Ixz/Izz;
%
Mu=q*s*c*(CMu+2*CM1)/(Iyy*u);
Ma=q*s*c*CMa/Iyy;
Mad=q*s*c*c*CMad/(2*Iyy*u);
Mq=q*s*c*c*CMq/(2*Iyy*u);
Zu=-q*s*(CLu+2*CL1)/(m*u);
Za=-q*s*(CLa+CD1)/m;
Zad=-q*s*c*CLad/(2*m*u);
Zq=-q*s*c*CLq/(2*m*u);
Xu=-q*s*(CDu+2*CD1)/(m*u);
Xa=-q*s*(CDa-CL1)/m;
Zde=-q*s*CLde/m;
Xde=-q*s*CDde/m;
Mde=q*s*c*CMde/Iyy;
Zdf=-q*s*CLdf/m;
Xdf=-q*s*CDdf/m;
Mdf=q*s*c*CMdf/Iyy;
Dlong=[Mu,Ma,Mad,Mq,Zu,Za,Zad,Zq,Xa,Xu,Zde,Xde,Mde,Zdf,Xdf,Mdf]';
%
Lb=q*s*b*Clb/Ixx;
Lp=q*s*b*b*Clp/(2*Ixx*u);
Lr=q*s*b*b*Clr/(2*Ixx*u);
Lda=q*s*b*Clda/Ixx;
Ldr=q*s*b*Cldr/Ixx;
```

```
Nb=q*s*b*Cnb/Izz;
Np=q*s*b*b*Cnp/(2*Izz*u);
Nr=q*s*b*b*Cnr/(2*Izz*u);
Nda=q*s*b*Cnda/Izz;
Ndr=q*s*b*Cndr/Izz;
Yb=q*s*Cyb/m;
Yp=q*s*b*Cyp/(2*m*u);
Yr=q*s*b*Cyr/(2*m*u);
Yda=q*s*Cyda/m;
Ydr=q*s*Cydr/m;
Dlat=[Lb,Lp,Lr,Lda,Ldr,Nb,Np,Nr,Nda,Ndr,Yb,Yp,Yr,Yda,Ydr]';
%
%  Calculation of the Longitudinal A and B matrices
%
theta=X(1,5)/57.29578;
Along=[Xu,Xa,0,-32.174*cos(theta);
       Zu/(u-Zad),Za/(u-Zad),(u+Zq)/(u-Zad),-32.174*sin(theta);
       Mu+Mad*Zu/(u-Zad),Ma+Mad*Za/(u-Zad),Mq+Mad*(u+Zq)/(u-Zad),...
         -Mad*32.174*sin(theta);
       0,0,1,0];
Blong=[Xde,Xdf;
       Zde/(u-Zad),Zdf/(u-Zad);
       Mde+Mad*Zde/(u-Zad),Mdf+Mad*Zdf/(u-Zad);
       0,0];
%
%  Calculation of the Lateral Directional A and B matrices
%
BA=1-B1*A1;
Alat=[Yb/u,Yp/u,32.174*cos(theta)/u,Yr/u-1,0;
      (Lb+A1*Nb)/BA,(Lp+A1*Np)/BA,0,(Lr+A1*Nr)/BA,0;
      0,1,0,0,0;
      (Nb+B1*Lb)/BA,(Np+B1*Lp)/BA,0,(Nr+B1*Lr)/BA,0;
      0,0,0,1,0];
Blat=[Yda/u,Ydr/u;
      (Lda+A1*Nda)/BA,(Ldr+A1*Ndr)/BA;
      0,0;
      (Nda+B1*Lda)/BA,(Ndr+B1*Ldr)/BA;
      0,0];
```

# Appendix B. Transfer Functions

This appendix includes all transfer functions used in the rate controller design.

## *B.1* Longitudinal Transfer Functions

The flight conditions produce nineteen separate plants. The s-domain and w'-domain transfer functions used in the longitudinal SISO design are included below:

**Nominal s–Domain Transfer Function** $\left(\frac{q(s)}{\delta_{elev}(s)}\right)$:

$$p_{o_{11}} = p_{1_{11}} = \frac{K(s)(s+0.0548)(s+3.7340)}{(s+0.0178 \pm j0.2298)(s+3.2050 \pm j8.0129)(s+9 \pm j6.2450)(s+50)}$$

$(K = 1.5774 \times 10^5)$

**Off–Nominal s–Domain Transfer Functions** $\left(\frac{q(s)}{\delta_{elev}(s)}\right)$

$$p_{2_{11}} = \frac{K(s)(s+0.0519)(s+3.1423)}{(s+0.0150 \pm j0.2323)(s+2.8788 \pm j8.0423)(s+9 \pm j6.2450)(s+50)}$$

$(K = 1.5766 \times 10^5)$

$$p_{3_{11}} = \frac{K(s)(s+0.0583)(s+4.2689)}{(s+0.0206 \pm j0.2277)(s+3.6639 \pm j8.5618)(s+9 \pm j6.2450)(s+50)}$$

$(K = 1.8045 \times 10^5)$

$$p_{4_{11}} = \frac{K(s)(s+0.0540)(s+3.5946)}{(s+0.0173 \pm j0.2304)(s+3.2913 \pm j8.5978)(s+9 \pm j6.2450)(s+50)}$$

$(K = 1.8035 \times 10^5)$

$$p_{5_{11}} = \frac{K(s)(s+0.0542)(s+3.8754)}{(s+0.0173 \pm j0.2201)(s+3.0638 \pm j6.2369)(s+9 \pm j6.2450)(s+50)}$$

$(K = 1.5310 \times 10^5)$

$$p_{6_{11}} = \frac{K(s)(s+0.0511)(s+3.2619)}{(s+0.0145\pm j0.2238)(s+2.7374\pm j6.2664)(s+9\pm j6.2450)(s+50)}$$

$(K = 1.5301 \times 10^5)$

$$p_{7_{11}} = \frac{K(s)(s+0.0577)(s+4.4299)}{(s+0.0202\pm j0.2169)(s+3.5023\pm j6.6723)(s+9\pm j6.2450)(s+50)}$$

$(K = 1.7515 \times 10^5)$

$$p_{8_{11}} = \frac{K(s)(s+0.0534)(s+3.7308)}{(s+0.0169\pm j0.2210)(s+3.1295\pm j6.7084)(s+9\pm j6.2450)(s+50)}$$

$(K = 1.7504 \times 10^5)$

$$p_{9_{11}} = \frac{K(s)(s+0.1141)(s+2.1412)}{(s+0.0033\pm j0.4028)(s+1.9054\pm j4.3264)(s+9\pm j6.2450)(s+50)}$$

$(K = 5.5923 \times 10^4)$

$$p_{10_{11}} = \frac{K(s)(s+0.0729)(s+2.7725)}{(s+0.0102\pm j0.3199)(s+2.3980\pm j5.4539)(s+9\pm j6.2450)(s+50)}$$

$(K = 8.9051 \times 10^4)$

$$p_{11_{11}} = \frac{K(s)(s+0.0596)(s+3.4480)}{(s+0.0152\pm j0.2647)(s+2.9539\pm j6.6530)(s+9\pm j6.2450)(s+50)}$$

$(K = 1.3261 \times 10^5)$

$$p_{12_{11}} = \frac{K(s)(s+0.2872)(s+1.3270)}{(s+0.0178\pm j0.5275)(s+1.2835\pm j2.5894)(s+9\pm j6.2450)(s+50)}$$

$(K = 2.5836 \times 10^4)$

$$p_{13_{11}} = \frac{K(s)(s+0.3825)(s+0.9785)}{(s+0.0166\pm j0.5372)(s+1.1470\pm j2.5972)(s+9\pm j6.2450)(s+50)}$$

$(K = 2.5822 \times 10^4)$

$$p_{14_{11}} = \frac{K(s)(s+0.2427)(s+1.6011)}{(s+0.0147\pm j0.5207)(s+1.4620\pm j2.7686)(s+9\pm j6.2450)(s+50)}$$

$(K = 2.9564 \times 10^4)$

$$p_{15_{11}} = \frac{K(s)(s+0.3032)(s+1.2516)}{(s+0.0141 \pm j0.5310)(s+1.3068 \pm j2.7792)(s+9 \pm j6.2450)(s+50)}$$

$(K = 2.9545 \times 10^4)$

$$p_{16_{11}} = \frac{K(s)(s+0.3037)(s+1.2528)}{(s+0.0114 \pm j0.5544)(s+1.3354 \pm j3.3066)(s+9 \pm j6.2450)(s+50)}$$

$(K = 2.6619 \times 10^4)$

$$p_{17_{11}} = \frac{K(s)(s+0.4180)(s+0.8942)}{(s+0.0104 \pm j0.5608)(s+1.1991 \pm j3.3160)(s+9 \pm j6.2450)(s+50)}$$

$(K = 2.6607 \times 10^4)$

$$p_{18_{11}} = \frac{K(s)(s+0.2544)(s+1.5235)}{(s+0.0093 \pm j0.5494)(s+1.5232 \pm j3.5328)(s+9 \pm j6.2450)(s+50)}$$

$(K = 3.0457 \times 10^4)$

$$p_{19_{11}} = \frac{K(s)(s+0.3217)(s+1.1774)}{(s+0.0087 \pm j0.5565)(s+1.3681 \pm j3.5449)(s+9 \pm j6.2450)(s+50)}$$

$(K = 3.0441 \times 10^4)$

## Nominal w′–Domain Transfer Function $\left(\frac{q(w')}{\delta_{elev}(w')}\right)$

$p_{o_{11}} = p_{1_{11}} =$

$$\frac{K(w')(w'+0.0548)(w'+3.7323)(w'-100)(w'+116.1585)(w'-130.3470)(w'+718.6759)}{(w'+0.0178\pm j0.2298)(w'+3.2246\pm j8.0218)(w'+9.0106\pm j6.2026)(w'+46.2117)}$$

$(K = 1.3414 \times 10^{-4})$

## Off–Nominal w′–Domain Transfer Functions $\left(\frac{q(w')}{\delta_{elev}(w')}\right)$

$p_{2_{11}} =$

$$\frac{K(w')(w'+0.0519)(w'+3.1413)(w'-100)(w'+116.1627)(w'-130.3378)(w'+719.3433)}{(w'+0.0150\pm j0.2323)(w'+2.8967\pm j8.0529)(w'+9.0106\pm j6.2026)(w'+46.2117)}$$

$(K = 1.3397 \times 10^{-4})$

$p_{3_{11}} =$

$$\frac{K(w')(w'+0.0583)(w'+4.2663)(w'-100)(w'+116.1373)(w'-130.4125)(w'+714.8263)}{(w'+0.0206\pm j0.2277)(w'+3.6892\pm j8.5712)(w'+9.0106\pm j6.2026)(w'+46.2117)}$$

$(K = 1.5432 \times 10^{-4})$

$p_{4_{11}} =$

$$\frac{K(w')(w'+0.0540)(w'+3.5931)(w'-100)(w'+116.1422)(w'-130.4019)(w'+715.5924)}{(w'+0.0173\pm j0.2304)(w'+3.3145\pm j8.6096)(w'+9.0106\pm j6.2026)(w'+46.2117)}$$

$(K = 1.5408 \times 10^{-4})$

$p_{5_{11}} =$

$$\frac{K(w')(w'+0.0542)(w'+3.8735)(w'-100)(w'+116.1758)(w'-130.2617)(w'+722.8078)}{(w'+0.0173\pm j0.2201)(w'+3.0748\pm j6.2391)(w'+9.0106\pm j6.2026)(w'+46.2117)}$$

$(K = 1.2931 \times 10^{-4})$

$p_{6_{11}} =$

$$\frac{K(w')(w'+0.0511)(w'+3.2607)(w'-100)(w'+116.1785)(w'-130.2555)(w'+723.2503)}{(w'+0.0145\pm j0.2238)(w'+2.7475\pm j6.2699)(w'+9.0106\pm j6.2026)(w'+46.2117)}$$

$(K = 1.2917 \times 10^{-4})$

$p_{7_{11}} =$

$$\frac{K(w')(w'+0.0577)(w'+4.4270)(w'-100)(w'+116.1572)(w'-130.3152)(w'+719.5097)}{(w'+0.0202\pm j0.2169)(w'+3.5165\pm j6.6740)(w'+9.0106\pm j6.2026)(w'+46.2117)}$$

$(K = 1.4863 \times 10^{-4})$

$p_{8_{11}} =$

$$\frac{K(w')(w'+0.0534)(w'+3.7291)(w'-100)(w'+116.1603)(w'-130.3080)(w'+720.0226)}{(w'+0.0169\pm j0.2210)(w'+3.1426\pm j6.7119)(w'+9.0106\pm j6.2026)(w'+46.2117)}$$

$(K = 1.4844 \times 10^{-4})$

$p_{9_{11}} =$

$$\frac{K(w')(w'+0.1141)(w'+2.1408)(w'-100)(w'+116.2107)(w'-130.1436)(w'+729.6175)}{(w'+0.0033\pm j0.4028)(w'+1.9088\pm j4.3275)(w'+9.0106\pm j6.2026)(w'+46.2117)}$$

$(K = 4.6762 \times 10^{-5})$

$p_{10_{11}} =$

$$\frac{K(w')(w'+0.0729)(w'+2.7718)(w'-100)(w'+116.1888)(w'-130.2142)(w'+725.4450)}{(w'+0.0102\pm j0.3199)(w'+2.4047\pm j5.4562)(w'+9.0106\pm j6.2026)(w'+46.2117)}$$

$(K = 7.4917 \times 10^{-5})$

$p_{11_{11}} =$

$$\frac{K(w')(w'+0.0596)(w'+3.4467)(w'-100)(w'+116.1650)(w'-130.2956)(w'+720.8195)}{(w'+0.0152\pm j0.2647)(w'+2.9662\pm j6.6570)(w'+9.0106\pm j6.2026)(w'+46.2117)}$$

$(K = 1.1233 \times 10^{-4})$

$p_{12_{11}} =$

$$\frac{K(w')(w'+0.2872)(w'+1.3269)(w'-100)(w'+116.2475)(w'-130.0370)(w'+736.3425)}{(w'+0.0178\pm j0.5275)(w'+1.2842\pm j2.5895)(w'+9.0106\pm j6.2026)(w'+46.2117)}$$

$(K = 2.1401 \times 10^{-5})$

$p_{13_{11}} =$

$$\frac{K(w')(w'+0.3825)(w'+0.9784)(w'-100)(w'+116.2486)(w'-130.0345)(w'+736.5274)}{(w'+0.0166\pm j0.5372)(w'+1.1478\pm j2.5974)(w'+9.0106\pm j6.2026)(w'+46.2117)}$$

$(K = 2.1385 \times 10^{-5})$

$p_{14_{11}} =$

$$\frac{K(w')(w'+0.2427)(w'+1.6010)(w'-100)(w'+116.2393)(w'-130.0578)(w'+734.9239)}{(w'+0.0147\pm j0.5207)(w'+1.4630\pm j2.7687)(w'+9.0106\pm j6.2026)(w'+46.2117)}$$

$(K = 2.4535 \times 10^{-5})$

$p_{15_{11}} =$

$$\frac{K(w')(w'+0.3032)(w'+1.2516)(w'-100)(w'+116.2406)(w'-130.0548)(w'+735.1389)}{(w'+0.0141\pm j0.5311)(w'+1.3077\pm j2.7794)(w'+9.0106\pm j6.2026)(w'+46.2117)}$$

$(K = 2.4513 \times 10^{-5})$

$p_{16_{11}} =$

$$\frac{K(w')(w'+0.3037)(w'+1.2527)(w'-100)(w'+116.2380)(w'-130.0666)(w'+734.5254)}{(w'+0.0114\pm j0.5544)(w'+1.3368\pm j3.3072)(w'+9.0106\pm j6.2026)(w'+46.2117)}$$

$(K = 2.2107 \times 10^{-5})$

$p_{17_{11}} =$

$$\frac{K(w')(w'+0.4180)(w'+0.8941)(w'-100)(w'+116.2397)(w'-130.0628)(w'+734.8052)}{(w'+0.0104\pm j0.5608)(w'+1.2004\pm j3.3168)(w'+9.0106\pm j6.2026)(w'+46.2117)}$$

$(K = 2.2089 \times 10^{-5})$

$p_{18_{11}} =$

$$\frac{K(w')(w'+0.2544)(w'+1.5234)(w'-100)(w'+116.2283)(w'-130.0916)(w'+732.8558)}{(w'+0.0093\pm j0.5495)(w'+1.5250\pm j3.5334)(w'+9.0106\pm j6.2026)(w'+46.2117)}$$

$(K = 2.5352 \times 10^{-5})$

$p_{\Delta_{11}} =$

$$\frac{K(w')(w'+0.3217)(w'+1.1774)(w'-100)(w'+116.2303)(w'-130.0871)(w'+733.1781)}{(w'+0.0087 \pm j0.5565)(w'+1.3697 \pm j3.5457)(w'+9.0106 \pm j6.2026)(w'+46.?117)}$$

$(K = 2.5328 \times 10^{-5})$

## *B.2* Lateral-Directional Transfer Functions

The lateral-directional dynamics are represented by a two-by-two transfer function matrix:

$$\mathbf{P} = \begin{bmatrix} p_{22} & p_{23} \\ p_{32} & p_{33} \end{bmatrix} \tag{B.1}$$

The chosen flight conditions produce nineteen separate transfer function matrices. The s-domain and w'-domain transfer functions are included below:

**Nominal s–Domain Transfer Function** $p_{o22} = \left(\frac{p(s)}{\delta_{aileron}(s)}\right)$

$$p_{o_{22}} = p_{1_{22}} = \frac{K(s)(s + 0.9516 \pm j3.8448)}{(s + 0.0141)(s + 0.9734 \pm j3.9181)(s + 6.7492)(s + 9 \pm j6.2450)(s + 50)}$$

$$(K = 3.5051 \times 10^5)$$

**Off–Nominal s–Domain Transfer Functions** $p_{i_{22}} = \left(\frac{p(s)}{\delta_{aileron}(s)}\right)$

$$p_{2_{22}} = \frac{K(s)(s + 0.9271 \pm j3.8429)}{(s + 0.0142)(s + 0.9490 \pm j3.9158)(s + 6.7487)(s + 9 \pm j6.2450)(s + 50)}$$

$$(K = 3.5051 \times 10^5)$$

$$p_{3_{22}} = \frac{K(s)(s + 1.0882 \pm j4.1010)}{(s + 0.0141)(s + 1.1179 \pm j4.1789)(s + 7.7060)(s + 9 \pm j6.2450)(s + 50)}$$

$$(K = 4.0081 \times 10^5)$$

$$p_{4_{22}} = \frac{K(s)(s + 1.0601 \pm j4.0987)}{(s + 0.0141)(s + 1.0900 \pm j4.1761)(s + 7.7056)(s + 9 \pm j6.2450)(s + 50)}$$

$$(K = 4.0081 \times 10^5)$$

$$p_{5_{22}} = \frac{K(s)(s + 0.9230 \pm j3.8259)}{(s + 0.0144)(s + 0.9448 \pm j3.8997)(s + 6.7492)(s + 9 \pm j6.2450)(s + 50)}$$

$$(K = 3.5051 \times 10^5)$$

$$p_{6_{22}} = \frac{K(s)(s + 0.8984 \pm j3.8241)}{(s + 0.0144)(s + 0.9205 \pm j3.8975)(s + 6.7488)(s + 9 \pm j6.2450)(s + 50)}$$

$$(K = 3.5051 \times 10^5)$$

$$p_{7_{22}} = \frac{K(s)(s + 1.0554 \pm j4.0816)}{(s + 0.0144)(s + 1.0852 \pm j4.1600)(s + 7.7061)(s + 9 \pm j6.2450)(s + 50)}$$

$(K = 4.0081 \times 10^5)$

$$p_{8_{22}} = \frac{K(s)(s + 1.0573 \pm j4.0793)}{(s + 0.0144)(s + 1.0574 \pm j4.0793)(s + 7.7056)(s + 9 \pm j6.2450)(s + 50)}$$

$(K = 4.0081 \times 10^5)$

$$p_{9_{22}} = \frac{K(s)(s + 0.5961 \pm j2.2934)}{(s + 0.0251)(s + 0.6107 \pm j2.2934)(s + 4.3763)(s + 9 \pm j6.2450)(s + 50)}$$

$(K = 1.2610 \times 10^5)$

$$p_{10_{22}} = \frac{K(s)(s + 0.7521 \pm j2.8941)}{(s + 0.0201)(s + 0.7723 \pm j2.9610)(s + 5.5062)(s + 9 \pm j6.2450)(s + 50)}$$

$(K = 2.0060 \times 10^5)$

$$p_{11_{22}} = \frac{K(s)(s + 0.9273 \pm j3.5301)}{(s + 0.0167)(s + 0.9540 \pm j3.6026)(s + 6.7772)(s + 9 \pm j6.2450)(s + 50)}$$

$(K = 2.9901 \times 10^5)$

$$p_{12_{22}} = \frac{K(s)(s + 0.3791 \pm j1.5717)}{(s + 0.0333)(s + 0.3819 \pm j1.6351)(s + 2.8124)(s + 9 \pm j6.2450)(s + 50)}$$

$(K = 5.9151 \times 10^4)$

$$p_{13_{22}} = \frac{K(s)(s + 0.3691 \pm j1.5709)}{(s + 0.0334)(s + 0.3720 \pm j1.6341)(s + 2.8120)(s + 9 \pm j6.2450)(s + 50)}$$

$(K = 5.9151 \times 10^4)$

$$p_{14_{22}} = \frac{K(s)(s + 0.4336 \pm j1.6769)}{(s + 0.0334)(s + 0.4413 \pm j1.7419)(s + 3.2028)(s + 9 \pm j6.2450)(s + 50)}$$

$(K = 6.7651 \times 10^4)$

$$p_{15_{22}} = \frac{K(s)(s + 0.4221 \pm j1.6759)}{(s + 0.0335)(s + 0.4300 \pm j1.7407)(s + 3.2024)(s + 9 \pm j6.2450)(s + 50)}$$

$(K = 6.7651 \times 10^4)$

$$p_{16_{22}} = \frac{K(s)(s+0.3909 \pm j1.5795)}{(s+0.0326)(s+0.3933 \pm j1.6424)(s+2.8125)(s+9 \pm j6.2450)(s+50)}$$

$(K = 5.9151 \times 10^4)$

$$p_{17_{22}} = \frac{K(s)(s+0.3808 \pm j1.5787)}{(s+0.0328)(s+0.3835 \pm j1.6414)(s+2.8121)(s+9 \pm j6.2450)(s+50)}$$

$(K = 5.9151 \times 10^4)$

$$p_{18_{22}} = \frac{K(s)(s+0.4471 \pm j1.6849)}{(s+0.0327)(s+0.4544 \pm j1.7495)(s+3.2028)(s+9 \pm j6.2450)(s+50)}$$

$(K = 6.7651 \times 10^4)$

$$p_{19_{22}} = \frac{K(s)(s+0.4356 \pm j1.6839)}{(s+0.0329)(s+0.4431 \pm j1.7482)(s+3.2025)(s+9 \pm j6.2450)(s+50)}$$

$(K = 6.7651 \times 10^4)$

## Nominal s–Domain Transfer Function $p_{o_{23}} = \left(\frac{p(s)}{\delta_{rudder}(s)}\right)$

$$p_{o_{23}} = p_{1_{23}} = \frac{K(s)(s+3.9245)(s-83.4616)}{(s+0.0141)(s+0.9734 \pm j3.9181)(s+6.1996)(s+6.7492)(s+50)}$$

$(K = -72.7664)$

## Off–Nominal s–Domain Transfer Functions $\left(\frac{p(s)}{\delta_{rudder}(s)}\right)$

$$p_{2_{23}} = \frac{K(s)(s+3.9202)(s-82.9677)}{(s+0.0142)(s+0.9490 \pm j3.9158)(s+6.1996)(s+6.7487)(s+50)}$$

$(K = -72.7664)$

$$p_{3_{23}} = \frac{K(s)(s+3.9710)(s-94.9224)}{(s+0.0141)(s+1.1179 \pm j4.1789)(s+6.1996)(s+7.7060)(s+50)}$$

$(K = -83.2091)$

$$p_{4_{23}} = \frac{K(s)(s+3.9631)(s-94.3546)}{(s+0.0141)(s+1.0900 \pm j4.1761)(s+6.1996)(s+7.7056)(s+50)}$$

$(K = -83.2091)$

$$p_{5_{23}} = \frac{K(s)(s+3.7525)(s-52.1859)}{(s+0.0144)(s+0.9448 \pm j3.8997)(s+6.1996)(s+6.7492)(s+50)}$$

$(K = -113.3549)$

$$p_{6_{23}} = \frac{K(s)(s+3.7479)(s-51.8844)}{(s+0.0144)(s+0.9205 \pm j3.8975)(s+6.1996)(s+6.7488)(s+50)}$$

$(K = -113.3549)$

$$p_{7_{23}} = \frac{K(s)(s+3.8071)(s-59.1913)}{(s+0.0144)(s+1.0852 \pm j4.1600)(s+6.1996)(s+7.7061)(s+50)}$$

$(K = -129.6224)$

$$p_{8_{23}} = \frac{K(s)(s+3.7992)(s-58.8138)}{(s+0.0144)(s+1.0574 \pm j4.1573)(s+6.1996)(s+7.7056)(s+50)}$$

$(K = -129.6224)$

$$p_{9_{23}} = \frac{K(s)(s+2.1658)(s-41.1729)}{(s+0.0251)(s+0.6107 \pm j2.3573)(s+4.3763)(s+6.1996)(s+50)}$$

$(K = -33.4806)$

$$p_{10_{23}} = \frac{K(s)(s+2.7334)(s-51.9471)}{(s+0.0201)(s+0.7723 \pm j2.9610)(s+5.5062)(s+6.1996)(s+50)}$$

$(K = -53.3141)$

$$p_{11_{23}} = \frac{K(s)(s+3.3076)(s-63.9864)}{(s+0.0167)(s+0.9540 \pm j3.6026)(s+6.1996)(s+6.7772)(s+50)}$$

$(K = -79.3870)$

$$p_{12_{23}} = \frac{K(s)(s+1.5416)(s-21.4378)}{(s+0.0333)(s+0.3819 \pm j1.6351)(s+2.8124)(s+6.1996)(s+50)}$$

$(K = -19.1297)$

$$p_{13_{23}} = \frac{K(s)(s+1.5397)(s-21.3139)}{(s+0.0334)(s+0.3720 \pm j1.6341)(s+2.8120)(s+6.1996)(s+50)}$$

$(K = -19.1297)$

$$p_{14_{23}} = \frac{K(s)(s+1.5640)(s-24.3194)}{(s+0.0334)(s+0.4413 \pm j1.7419)(s+3.2028)(s+6.1996)(s+50)}$$

$(K = -21.8786)$

$$p_{15_{23}} = \frac{K(s)(s+1.5608)(s-24.1766)}{(s+0.0335)(s+0.4300 \pm j1.7407)(s+3.2024)(s+6.1996)(s+50)}$$

$(K = -21.8786)$

$$p_{16_{23}} = \frac{K(s)(s+1.6122)(s-34.2857)}{(s+0.0326)(s+0.3933 \pm j1.6424)(s+2.8125)(s+6.1996)(s+50)}$$

$(K = -12.2800)$

$$p_{17_{23}} = \frac{K(s)(s+1.6105)(s-34.0828)}{(s+0.0328)(s+0.3835 \pm j1.6414)(s+2.8121)(s+6.1996)(s+50)}$$

$(K = -12.2800)$

$$p_{18_{23}} = \frac{K(s)(s+1.6314)(s-39)}{(s+0.0327)(s+0.4544 \pm j1.7495)(s+3.2028)(s+6.1996)(s+50)}$$

$(K = -14.0446)$

$$p_{19_{23}} = \frac{K(s)(s+1.6281)(s-38.7667)}{(s+0.0329)(s+0.4431 \pm j1.7482)(s+3.2025)(s+6.1996)(s+50)}$$

$(K = -14.0446)$

## Nominal s–Domain Transfer Function $p_{o_{32}} = \left(\frac{r(s)}{\delta_{aileron}(s)}\right)$

$$p_{o_{32}} = p_{1_{32}} = \frac{K(s-1.8300)(s+2.3301)(s+22.9473)}{(s+0.0141)(s+0.9734 \pm j3.9181)(s+6.7492)(s+9 \pm j6.2450)(s+50)}$$

$$(K = -9.5335 \times 10^3)$$

## Off–Nominal s–Domain Transfer Functions $\left(\frac{r(s)}{\delta_{aileron}(s)}\right)$

$$p_{2_{32}} = \frac{K(s-1.8520)(s+2.3024)(s+22.9479)}{(s+0.0142)(s+0.9490 \pm j3.9158)(s+6.7487)(s+9 \pm j6.2450)(s+50)}$$

$$(K = -9.5335 \times 10^3)$$

$$p_{3_{32}} = \frac{K(s-1.8190)(s+2.3396)(s+26.2918)}{(s+0.0141)(s+1.1179 \pm j4.1789)(s+7.7060)(s+9 \pm j6.2450)(s+50)}$$

$$(K = -1.0902 \times 10^4)$$

$$p_{4_{32}} = \frac{K(s-1.8440)(s+2.3079)(s+26.2923)}{(s+0.0141)(s+1.0900 \pm j4.1761)(s+7.7056)(s+9 \pm j6.2450)(s+50)}$$

$$(K = -1.0902 < 10^4)$$

$$p_{5_{32}} = \frac{K(s-1.8185)(s+2.3163)(s+22.9496)}{(s+0.0144)(s+0.9448 \pm j3.8997)(s+6.7492)(s+9 \pm j6.2450)(s+50)}$$

$$(K = -9.5335 \times 10^3)$$

$$p_{6_{32}} = \frac{K(s-1.8405)(s+2.2885)(s+22.9502)}{(s+0.0144)(s+0.9205 \pm j3.8975)(s+6.7488)(s+9 \pm j6.2450)(s+50)}$$

$$(K = -9.5335 \times 10^3)$$

$$p_{7_{32}} = \frac{K(s-1.8074)(s+2.3260)(s+26.2938)}{(s+0.0144)(s+1.0852 \pm j4.1600)(s+7.7061)(s+9 \pm j6.2450)(s+50)}$$

$$(K = -1.0902 \times 10^4)$$

$$p_{8_{32}} = \frac{K(s-1.8324)(s+2.2942)(s+26.2943)}{(s+0.0144)(s+1.0574 \pm j4.1573)(s+7.7056)(s+9 \pm j6.2450)(s+50)}$$

$$(K = -1.0902 \times 10^4)$$

$$p_{9_{32}} = \frac{K(s-1.8454)(s+2.3241)(s+14.6538)}{(s+0.0251)(s+0.6107\pm j2.3573)(s+4.3763)(s+9\pm j6.2450)(s+50)}$$

$(K = -3.4299\times 10^3)$

$$p_{10_{32}} = \frac{K(s-1.8452)(s+2.3065)(s+18.6307)}{(s+0.0201)(s+0.7723\pm j2.9610)(s+5.5062)(s+9\pm j6.2450)(s+50)}$$

$(K = -5.4617\times 10^3)$

$$p_{11_{32}} = \frac{K(s-1.8371)(s+2.3067)(s+23.0703)}{(s+0.0167)(s+0.9540\pm j3.6026)(s+6.7772)(s+9\pm j6.2450)(s+50)}$$

$(K = -8.1327\times 10^3)$

$$p_{12_{32}} = \frac{K(s-1.8105)(s+2.4350)(s+9.0075)}{(s+0.0333)(s+0.3819\pm j1.6351)(s+2.8124)(s+9\pm j6.2450)(s+50)}$$

$(K = -1.6089\times 10^3)$

$$p_{13_{32}} = \frac{K(s-1.8195)(s+2.4225)(s+9.0089)}{(s+0.0334)(s+0.3720\pm j1.6341)(s+2.8120)(s+9\pm j6.2450)(s+50)}$$

$(K = -1.6089\times 10^3)$

$$p_{14_{32}} = \frac{K(s-1.8200)(s+2.3884)(s+10.4478)}{(s+0.0334)(s+0.4413\pm j1.7419)(s+3.2028)(s+9\pm j6.2450)(s+50)}$$

$(K = -1.8401\times 10^3)$

$$p_{15_{32}} = \frac{K(s-1.8304)(s+2.3746)(s+10.4489)}{(s+0.0335)(s+0.4300\pm j1.7407)(s+3.2024)(s+9\pm j6.2450)(s+50)}$$

$(K = -1.8401\times 10^3)$

$$p_{16_{32}} = \frac{K(s-1.8210)(s+2.4524)(s+9.0007)}{(s+0.0326)(s+0.3933\pm j1.6424)(s+2.8125)(s+9\pm j6.2450)(s+50)}$$

$(K = -1.6089\times 10^3)$

$$p_{17_{32}} = \frac{K(s-1.8301)(s+2.4399)(s+9.0020)}{(s+0.0328)(s+0.3835\pm j1.6414)(s+2.8121)(s+9\pm j6.2450)(s+50)}$$

$(K = -1.6089\times 10^3)$

$$p_{18_{32}} = \frac{K(s-1.8308)(s+2.4048)(s+10.4421)}{(s+0.0327)(s+0.4544 \pm j1.7495)(s+3.2028)(s+9 \pm j6.2450)(s+50)}$$

$(K = -1.8401 \times 10^3)$

$$p_{19_{32}} = \frac{K(s-1.8411)(s+2.3910)(s+10.4433)}{(s+0.0329)(s+0.4431 \pm j1.7482)(s+3.2025)(s+9 \pm j6.2450)(s+50)}$$

$(K = -1.8401 \times 10^3)$

## Nominal s–Domain Transfer Function $p_{o_{33}} = \left(\frac{r(s)}{\delta_{rudder}(s)}\right)$

$$p_{o_{33}} = p_{1_{33}} = \frac{K(s + 0.0658 \pm j0.3201)}{(s + 0.0141)(s + 0.9734 \pm j3.9181)(s + 6.1996)(s + 50)}$$

$$(K = 5.4760 \times 10^3)$$

## Off–Nominal s–Domain Transfer Functions $\left(\frac{r(s)}{\delta_{rudder}(s)}\right)$

$$p_{2_{33}} = \frac{K(s + 0.0542 \pm j0.3222)}{(s + 0.0142)(s + 0.9490 \pm j3.9158)(s + 6.1996)(s + 50)}$$

$$(K = 5.4760 \times 10^3)$$

$$p_{3_{33}} = \frac{K(s + 0.0774 \pm j0.3175)}{(s + 0.0141)(s + 1.1179 \pm j4.1789)(s + 6.1996)(s + 50)}$$

$$(K = 6.2618 \times 10^3)$$

$$p_{4_{33}} = \frac{K(s + 0.0641 \pm j0.3205)}{(s + 0.0141)(s + 1.0900 \pm j4.1761)(s + 6.1996)(s + 50)}$$

$$(K = 6.2618 \times 10^3)$$

$$p_{5_{33}} = \frac{K(s + 0.0637 \pm j0.3156)}{(s + 0.0144)(s + 0.9448 \pm j3.8997)(s + 6.1996)(s + 50)}$$

$$(K = 5.2531 \times 10^3)$$

$$p_{6_{33}} = \frac{K(s + 0.0524 \pm j0.3176)}{(s + 0.0144)(s + 0.9205 \pm j3.8975)(s + 6.1996)(s + 50)}$$

$$(K = 5.2531 \times 10^3)$$

$$p_{7_{33}} = \frac{K(s + 0.0749 \pm j0.3132)}{(s + 0.0144)(s + 1.0852 \pm j4.1600)(s + 6.1996)(s + 50)}$$

$$(K = 6.0069 \times 10^3)$$

$$p_{8_{33}} = \frac{K(s + 0.0620 \pm j0.3160)}{(s + 0.0144)(s + 1.0574 \pm j4.1573)(s + 6.1996)(s + 50)}$$

$$(K = 6.0069 \times 10^3)$$

$$p_{9_{33}} = \frac{K(s+0.0303 \pm j0.3224)}{(s+0.0251)(s+0.6107 \pm j2.3573)(s+6.1996)(s+50)}$$

$(K = 1.9300 \times 10^3)$

$$p_{10_{33}} = \frac{K(s+0.0440 \pm j0.3212)}{(s+0.0201)(s+0.7723 \pm j2.9610)(s+6.1996)(s+50)}$$

$(K = 3.0733 \times 10^3)$

$$p_{11_{33}} = \frac{K(s+0.0583 \pm j0.3191)}{(s+0.0167)(s+0.9540 \pm j3.6026)(s+6.1996)(s+50)}$$

$(K = 4.5763 \times 10^3)$

$$p_{12_{33}} = \frac{K(s+0.0108 \pm j0.3200)}{(s+0.0333)(s+0.3819 \pm j1.6351)(s+6.1996)(s+50)}$$

$(K = 886.5021)$

$$p_{13_{33}} = \frac{K(s+0.0062 \pm j0.3201)}{(s+0.0334)(s+0.3720 \pm j1.6341)(s+6.1996)(s+50)}$$

$(K = 886.5021)$

$$p_{14_{33}} = \frac{K(s+0.0172 \pm j0.3202)}{(s+0.0334)(s+0.4413 \pm j1.7419)(s+6.1996)(s+50)}$$

$(K = 1.0139 \times 10^3)$

$$p_{15_{33}} = \frac{K(s+0.0120 \pm j0.3204)}{(s+0.0335)(s+0.4300 \pm j1.7407)(s+6.1996)(s+50)}$$

$(K = 1.0139 \times 10^3)$

$$p_{16_{33}} = \frac{K(s+0.0112 \pm j0.3247)}{(s+0.0326)(s+0.3933 \pm j1.6424)(s+6.1996)(s+50)}$$

$(K = 924.1210)$

$$p_{17_{33}} = \frac{K(s+0.0065 \pm j0.3249)}{(s+0.0328)(s+0.3835 \pm j1.6414)(s+6.1996)(s+50)}$$

$(K = 924.1210)$

$p_{18_{33}} =$

$$\frac{K(s+0.0179 \pm j0.3249)}{(s+0.0327)(s+0.4544 \pm j1.7495)(s+6.1996)(s+50)}$$

$(K = 1.0569 \times 10^3)$

$p_{19_{33}} =$

$$\frac{K(s+0.0124 \pm j0.3252)}{(s+0.0329)(s+0.4431 \pm j1.7482)(s+6.1996)(s+50)}$$

$(K = 1.0569 \times 10^3)$

## Nominal w′–Domain Transfer Function $p_{o_{22}} = \left(\frac{p(w')}{\delta_{aileron}(w')}\right)$

$p_{o_{22}} = p_{1_{22}} =$

$$\frac{K(w')(w' + 0.9530 \pm j3.8464)(w' - 100)(w' + 115.8649)(w' - 130.9057)(w' + 678.4573)}{(w' + 0.0141)(w' + 0.9748 \pm j3.9197)(w' + 6.7389)(w' + 9.0106 \pm j6.2026)(w' + 46.2117)}$$

$(K = 3.1346 \times 10^{-4})$

## Off–Nominal w′–Domain Transfer Functions $\left(\frac{p(w')}{\delta_{aileron}(w')}\right)$

$p_{2_{22}} =$

$$\frac{K(w')(w' + 0.9284 \pm j3.8445)(w' - 100)(w' + 115.8649)(w' - 130.9057)(w' + 678.4573)}{(w' + 0.0142)(w' + 0.9505 \pm j3.9175)(w' + 6.7385)(w' + 9.0106 \pm j6.2026)(w' + 46.2117)}$$

$(K = 3.1346 \times 10^{-4})$

$p_{3_{22}} =$

$$\frac{K(w')(w' + 1.0900 \pm j4.1029)(w' - 100)(w' + 115.8017)(w' - 131.0513)(w' + 669.7337)}{(w' + 0.0141)(w' + 1.1198 \pm j4.1808)(w' + 7.6908)(w' + 9.0106 \pm j6.2026)(w' + 46.2117)}$$

$(K = 3.6274 \times 10^{-4})$

$p_{4_{22}} =$

$$\frac{K(w')(w' + 1.0618 \pm j4.1005)(w' - 100)(w' + 115.8017)(w' - 131.0513)(w' + 669.7337)}{(w' + 0.0141)(w' + 1.0919 \pm j4.1780)(w' + 7.6904)(w' + 9.0106 \pm j6.2026)(w' + 46.2117)}$$

$(K = 3.6274 \times 10^{-4})$

$p_{5_{22}} =$

$$\frac{K(w')(w' + 0.9243 \pm j3.8275)(w' - 100)(w' + 115.8649)(w' - 130.9057)(w' + 678.4571)}{(w' + 0.0144)(w' + 0.9462 \pm j3.9014)(w' + 6.7390)(w' + 9.0106 \pm j6.2026)(w' + 46.2117)}$$

$(K = 3.1346 \times 10^{-4})$

$p_{6_{22}} =$

$$\frac{K(w')(w' + 0.8997 \pm j3.8256)(w' - 100)(w' + 115.8649)(w' - 130.9057)(w' + 678.4571)}{(w' + 0.0144)(w' + 0.9219 \pm j3.8992)(w' + 6.7385)(w' + 9.0106 \pm j6.2026)(w' + 46.2117)}$$

$(K = 3.1346 \times 10^{-4})$

$p_{7_{22}} =$

$$\frac{K(w')(w' + 1.0571 \pm j4.0834)(w' - 100)(w' + 115.8017)(w' - 131.0513)(w' + 669.7335)}{(w' + 0.0144)(w' + 1.0870 \pm j4.1620)(w' + 7.6909)(w' + 9.0106 \pm j6.2026)(w' + 46.2117)}$$

$(K = 3.6274 \times 10^{-4})$

$p_{8_{22}} =$

$$\frac{K(w')(w' + 1.0290 \pm j4.0812)(w' - 100)(w' + 115.8017)(w' - 131.0513)(w' + 669.7335)}{(w' + 0.0144)(w' + 1.0592 \pm j4.1593)(w' + 7.6904)(w' + 9.0106 \pm j6.2026)(w' + 46.2117)}$$

$(K = 3.6274 \times 10^{-4})$

$p_{9_{22}} =$

$$\frac{K(w')(w' + 0.5964 \pm j2.2938)(w' - 100)(w' + 116.0205)(w' - 130.5472)(w' + 700.9747)}{(w' + 0.0251)(w' + 0.6110 \pm j2.3577)(w' + 4.3735)(w' + 9.0106 \pm j6.2026)(w' + 46.2117)}$$

$(K = 1.0940 \times 10^{-4})$

$p_{10_{22}} =$

$$\frac{K(w')(w' + 0.7527 \pm j2.8948)(w' - 100)(w' + 115.9461)(w' - 130.7184)(w' + 690.0289)}{(w' + 0.0201)(w' + 0.7729 \pm j2.9617)(w' + 5.5006)(w' + 9.0106 \pm j6.2026)(w' + 46.2117)}$$

$(K = 1.7678 \times 10^{-4})$

$p_{11_{22}} =$

$$\frac{K(w')(w' + 0.9285 \pm j3.5313)(w' - 100)(w' + 115.8626)(w' - 130.9109)(w' + 678.1364)}{(w' + 0.0167)(w' + 0.9552 \pm j3.6039)(w' + 6.7669)(w' + 9.0106 \pm j6.2026)(w' + 46.2117)}$$

$(K = 2.6752 \times 10^{-4})$

$p_{12_{22}} =$

$$\frac{K(w')(w' + 0.3792 \pm j1.5718)(w' - 100)(w' + 116.1239)(w' - 130.3092)(w' + 716.8074)}{(w' + 0.0333)(w' + 0.3820 \pm j1.6352)(w' + 2.8117)(w' + 9.0106 \pm j6.2026)(w' + 46.2117)}$$

$(K = 5.0247 \times 10^{-5})$

$p_{13_{22}} =$

$$\frac{K(w')(w' + 0.3691 \pm j1.5711)(w' - 100)(w' + 116.1239)(w' - 130.3092)(w' + 716.8074)}{(w' + 0.0334)(w' + 0.3721 \pm j1.6342)(w' + 2.8113)(w' + 9.0106 \pm j6.2026)(w' + 46.2117)}$$

$(K = 5.0247 \times 10^{-5})$

$p_{14_{22}} =$

$$\frac{K(w')(w' + 0.4338 \pm j1.6770)(w' - 100)(w' + 116.0980)(w' - 130.3689)(w' + 712.7699)}{(w' + 0.0334)(w' + 0.4414 \pm j1.7420)(w' + 3.2017)(w' + 9.0106 \pm j6.2026)(w' + 46.2117)}$$

$(K = 5.7776 \times 10^{-5})$

$p_{15_{22}} =$

$$\frac{K(w')(w' + 0.4222 \pm j1.6761)(w' - 100)(w' + 116.0980)(w' - 130.3689)(w' + 712.7699)}{(w' + 0.0335)(w' + 0.4301 \pm j1.7408)(w' + 3.2013)(w' + 9.0106 \pm j6.2026)(w' + 46.2117)}$$

$(K = 5.7776 \times 10^{-5})$

$p_{16_{22}} =$

$$\frac{K(w')(w' + 0.3910 \pm j1.5796)(w' - 100)(w' + 116.1239)(w' - 130.3092)(w' + 716.8075)}{(w' + 0.0326)(w' + 0.3934 \pm j1.6425)(w' + 2.8117)(w' + 9.0106 \pm j6.2026)(w' + 46.2117)}$$

$(K = 5.0247 \times 10^{-5})$

$p_{17_{22}} =$

$$\frac{K(w')(w' + 0.3809 \pm j1.5788)(w' - 100)(w' + 116.1239)(w' - 130.3092)(w' + 716.8075)}{(w' + 0.0328)(w' + 0.3836 \pm j1.6415)(w' + 2.8113)(w' + 9.0106 \pm j6.2026)(w' + 46.2117)}$$

$(K = 5.0247 \times 10^{-5})$

$p_{18_{22}} =$

$$\frac{K(w')(w' + 0.4472 \pm j1.6850)(w' - 100)(w' + 116.0980)(w' - 130.3689)(w' + 712.7700)}{(w' + 0.0327)(w' + 0.4545 \pm j1.7496)(w' + 3.2017)(w' + 9.0106 \pm j6.2026)(w' + 46.2117)}$$

$(K = 5.7776 \times 10^{-5})$

## Nominal w′–Domain Transfer Function $p_{o_{23}} = \left(\frac{p(w')}{\delta_{rudder}(w')}\right)$

$p_{o_{23}} = p_{1_{23}} =$

$$\frac{K(w')(w'+3.9225)(w'-68.1828)(w'-100)(w'+133.9606)(w'-360.3213)}{(w'+0.0141)(w'+0.9748 \pm j3.9197)(w'+6.1917)(w'+6.7389)(w'+46.2117)}$$

$(K = -1.7033 \times 10^{-5})$

## Off–Nominal w′–Domain Transfer Functions $\left(\frac{p(w')}{\delta_{rudder}(w')}\right)$

$p_{2_{23}} =$

$$\frac{K(w')(w'+3.9182)(w'-67.9158)(w'-100)(w'+134.0174)(w'-358.7702)}{(w'+0.0142)(w'+0.9505 \pm j3.9175)(w'+6.1917)(w'+6.7385)(w'+46.2117)}$$

$(K = -1.7065 \times 10^{-5})$

$p_{3_{23}} =$

$$\frac{K(w')(w'+3.9689)(w'-73.9404)(w'-100)(w'+132.6917)(w'-399.6571)}{(w'+0.0141)(w'+1.1198 \pm j4.1808)(w'+6.1917)(w'+7.6908)(w'+46.2117)}$$

$(K = -1.8586 \times 10^{-5})$

$p_{4_{23}} =$

$$\frac{K(w')(w'+3.9610)(w'-73.6741)(w'-100)(w'+132.7492)(w'-397.6120)}{(w'+0.0141)(w'+1.0919 \pm j4.1780)(w'+6.1917)(w'+7.6904)(w'+46.2117)}$$

$(K = -1.8629 \times 10^{-5})$

$p_{5_{23}} =$

$$\frac{K(w')(w'+3.7507)(w'-47.8329)(w'-100)(w'+137.6547)(w'-284.7205)}{(w'+0.0144)(w'+0.9462 \pm j3.9014)(w'+6.1917)(w'+6.7390)(w'+46.2117)}$$

$(K = -2.9123 \times 10^{-5})$

$p_{6_{23}} =$

$$\frac{K(w')(w'+3.7462)(w'-47.6015)(w'-100)(w'+137.7062)(w'-284.0332)}{(w'+0.0144)(w'+0.9219 \pm j3.8992)(w'+6.1917)(w'+6.7385)(w'+46.2117)}$$

$(K = -2.9155 \times 10^{-5})$

$p_{7_{23}} =$

$$\frac{K(w')(w'+3.8053)(w'-53.0185)(w'-100)(w'+136.4773)(w'-301.8984)}{(w'+0.0144)(w'+1.0870 \pm j4.1620)(w'+6.1917)(w'+7.6909)(w'+46.2117)}$$

$(K = -3.2407 \times 10^{-5})$

$p_{19_{22}} =$

$$\frac{K(\mathrm{w}')(\mathrm{w}' + 0.4357 \pm j1.6840)(\mathrm{w}' - 100)(\mathrm{w}' + 116.0980)(\mathrm{w}' - 130.3689)(\mathrm{w}' + 712.7700)}{(\mathrm{w}' + 0.0329)(\mathrm{w}' + 0.4433 \pm j1.7484)(\mathrm{w}' + 3.2014)(\mathrm{w}' + 9.0106 \pm j6.2026)(\mathrm{w}' + 46.2117)}$$

$(K = 5.7776 \times 10^{-5})$

$$p_{8_{23}} = \frac{K(w')(w'+3.7974)(w'-52.7699)(w'-100)(w'+136.5313)(w'-301.0226)}{(w'+0.0144)(w'+1.0592 \pm j4.1593)(w'+6.1917)(w'+7.6904)(w'+46.2117)}$$

$$(K = -3.2449 \times 10^{-5})$$

$$p_{9_{23}} = \frac{K(w')(w'+2.1655)(w'-38.9545)(w'-100)(w'+139.6278)(w'-261.8448)}{(w'+0.0251)(w'+0.6110 \pm j2.3577)(w'+4.3735)(w'+6.1917)(w'+46.2117)}$$

$$(K = -8.9330 \times 10^{-06})$$

$$p_{10_{23}} = \frac{K(w')(w'+2.7328)(w'-47.6504)(w'-100)(w'+137.7989)(w'-283.1456)}{(w'+0.0201)(w'+0.7729 \pm j2.9617)(w'+5.5006)(w'+6.1917)(w'+46.2117)}$$

$$(K = -1.3747 \times 10^{-5})$$

$$p_{11_{23}} = \frac{K(w')(w'+3.3064)(w'-56.3575)(w'-100)(w'+136.0025)(w'-311.2883)}{(w'+0.0167)(w'+0.9552 \pm j3.6039)(w'+6.1917)(w'+6.7669)(w'+46.2117)}$$

$$(K = -1.9645 \times 10^{-5})$$

$$p_{12_{23}} = \frac{K(w')(w'+1.5414)(w'-21.1115)(w'-100)(w'+143.6447)(w'-231.0659)}{(w'+0.0333)(w'+0.3820 \pm j1.6352)(w'+2.8117)(w'+6.1917)(w'+46.2117)}$$

$$(K = -5.4021 \times 10^{-06})$$

$$p_{13_{23}} = \frac{K(w')(w'+1.5326)(w'-20.9932)(w'-100)(w'+143.6756)(w'-230.8901)}{(w'+0.0334)(w'+0.3721 \pm j1.6342)(w'+2.8113)(w'+6.1917)(w'+46.2117)}$$

$$(K = -5.4041 \times 10^{-06})$$

$$p_{14_{23}} = \frac{K(w')(w'+1.5639)(w'-23.8448)(w'-100)(w'+142.9244)(w'-235.3338)}{(w'+0.0334)(w'+0.4414 \pm j1.7420)(w'+3.2017)(w'+6.1917)(w'+46.2117)}$$

$$(K = -6.1233 \times 10^{-06})$$

$$p_{15_{23}} = \frac{K(w')(w'+1.5607)(w'-23.7103)(w'-100)(w'+142.9584)(w'-235.1224)}{(w'+0.0335)(w'+0.4301 \pm j1.7408)(w'+3.2013)(w'+6.1917)(w'+46.2117)}$$

$$(K = -6.1259 \times 10^{-06})$$

$$p_{16_{23}} = \frac{K(w')(w'+1.6121)(w'-32.9818)(w'-100)(w'+141.1287)(w'-248.6719)}{(w'+0.0326)(w'+0.3934 \pm j1.6425)(w'+2.8117)(w'+6.1917)(w'+46.2117)}$$

$$(K = -3.3575 \times 10^{-06})$$

$$p_{17_{23}} = \frac{K(w')(w'+1.6103)(w'-32.8013)(w'-100)(w'+141.1695)(w'-248.3407)}{(w'+0.0328)(w'+0.3836 \pm j1.6415)(w'+2.8113)(w'+6.1917)(w'+46.2117)}$$

$$(K = -3.3595 \times 10^{-06})$$

$$p_{18_{23}} = \frac{K(w')(w'+1.6312)(w'-37.1036)(w'-100)(w'+140.1946)(w'-256.7633)}{(w'+0.0327)(w'+0.4545 \pm j1.7496)(w'+3.2017)(w'+6.1917)(w'+46.2117)}$$

$$(K = -3.7852 \times 10^{-06})$$

$$p_{19_{23}} = \frac{K(w')(w'+1.6279)(w'-36.9029)(w'-100)(w'+140.2385)(w'-256.3556)}{(w'+0.0329)(w'+0.4433 \pm j1.7484)(w'+3.2014)(w'+6.1917)(w'+46.2117)}$$

$$(K = -3.7879 \times 10^{-06})$$

## Nominal w′–Domain Transfer Function $p_{o_{32}} = \left(\frac{r(w')}{\delta_{aileron}(w')}\right)$

$p_{o_{32}} = p_{1_{32}} =$

$$\frac{K(w'-1.8298)(w'+2.3297)(w'+22.5528)(w'-100)(w'+117.4175)(w'-128.0109)(w'+956.6060)}{(w'+0.0141)(w'+0.9748\pm j3.9197)(w'+6.7389)(w'+9.0106\pm j6.2026)(w'+46.2117)}$$

$(K = -6.2160 \times 10^{-06})$

## Off–Nominal w′–Domain Transfer Functions $\left(\frac{r(w')}{\delta_{aileron}(w')}\right)$

$p_{2_{32}} =$

$$\frac{K(w'-1.8518)(w'+2.3020)(w'+22.5534)(w'-100)(w'+117.4175)(w'-128.0109)(w'+956.6068)}{(w'+0.0142)(w'+0.9505\pm j3.9175)(w'+6.7385)(w'+9.0106\pm j6.2026)(w'+46.2117)}$$

$(K = -6.2160 \times 10^{-06})$

$p_{3_{32}} =$

$$\frac{K(w'-1.8188)(w'+2.3392)(w'+25.7023)(w'-100)(w'+117.6049)(w'-127.7843)(w'+996.5365)}{(w'+0.0141)(w'+1.1198\pm j4.1808)(w'+7.6908)(w'+9.0106\pm j6.2026)(w'+46.2117)}$$

$(K = -6.8587 \times 10^{-06})$

$p_{4_{32}} =$

$$\frac{K(w'-1.8438)(w'+2.3075)(w'+25.7028)(w'-100)(w'+117.6050)(w'-127.7844)(w'+996.5376)}{(w'+0.0141)(w'+1.0919\pm j4.1780)(w'+7.6904)(w'+9.0106\pm j6.2026)(w'+46.2117)}$$

$(K = -6.8587 \times 10^{-06})$

$p_{5_{32}} =$

$$\frac{K(w'-1.8183)(w'+2.3158)(w'+22.5550)(w'-100)(w'+117.4215)(w'-128.0031)(w'+957.6502)}{(w'+0.0144)(w'+0.9462\pm j3.9014)(w'+6.7390)(w'+9.0106\pm j6.2026)(w'+46.2117)}$$

$(K = -6.2094 \times 10^{-06})$

$p_{6_{32}} =$

$$\frac{K(w'-1.8402)(w'+2.2881)(w'+22.5556)(w'-100)(w'+117.4215)(w'-128.0031)(w'+957.6509)}{(w'+0.0144)(w'+0.9219\pm j3.8992)(w'+6.7385)(w'+9.0106\pm j6.2026)(w'+46.2117)}$$

$(K = -6.2094 \times 10^{-06})$

$p_{7_{32}} =$

$$\frac{K(w' - 1.8072)(w' + 2.3255)(w' + 25.7042)(w' - 100)(w' + 117.6096)(w' - 127.7755)(w' + 997.8334)}{(w' + 0.0144)(w' + 1.0870 \pm j4.1620)(w' + 7.6909)(w' + 9.0106 \pm j6.2026)(w' + 46.2117)}$$

$(K = -6.8499 \times 10^{-06})$

$p_{8_{32}} =$

$$\frac{K(w' - 1.8322)(w' + 2.2938)(w' + 25.7047)(w' - 100)(w' + 117.6096)(w' - 127.7755)(w' + 997.8345)}{(w' + 0.0144)(w' + 1.0592 \pm j4.1593)(w' + 7.6904)(w' + 9.0106 \pm j6.2026)(w' + 46.2117)}$$

$(K = -6.8499 \times 10^{-06})$

$p_{9_{32}} =$

$$\frac{K(w' - 1.8452)(w' + 2.3236)(w' + 14.5498)(w' - 100)(w' + 116.9860)(w' - 128.6073)(w' + 870.0983)}{(w' + 0.0251)(w' + 0.6110 \pm j2.3577)(w' + 4.3735)(w' + 9.0106 \pm j6.2026)(w' + 46.2117)}$$

$(K = -2.4320 \times 10^{-06})$

$p_{10_{32}} =$

$$\frac{K(w' - 1.8450)(w' + 2.3061)(w' + 18.4181)(w' - 100)(w' + 117.1871)(w' - 128.3112)(w' + 909.7099)}{(w' + 0.0201)(w' + 0.7729 \pm j2.9617)(w' + 5.5006)(w' + 9.0106 \pm j6.2026)(w' + 46.2117)}$$

$(K = -3.7217 \times 10^{-06})$

$p_{11_{32}} =$

$$\frac{K(w' - 1.8369)(w' + 2.3063)(w' + 22.6695)(w' - 100)(w' + 117.4252)(w' - 127.9967)(w' + 958.4968)}{(w' + 0.0167)(w' + 0.9552 \pm j3.6039)(w' + 6.7669)(w' + 9.0106 \pm j6.2026)(w' + 46.2117)}$$

$(K = -5.2925 \times 10^{-06})$

$p_{12_{32}} =$

$$\frac{K(w' - 1.8103)(w' + 2.4345)(w' + 8.9833)(w' - 100)(w' + 116.7232)(w' - 129.0453)(w' + 820.4626)}{(w' + 0.0333)(w' + 0.3820 \pm j1.6352)(w' + 2.8117)(w' + 9.0106 \pm j6.2026)(w' + 46.2117)}$$

$(K = -1.2033 \times 10^{-06})$

$p_{13_{32}} =$

$$\frac{K(w' - 1.8193)(w' + 2.4220)(w' + 8.9846)(w' - 100)(w' + 116.7232)(w' - 129.0453)(w' + 820.4627)}{(w' + 0.0334)(w' + 0.3721 \pm j1.6342)(w' + 2.8113)(w' + 9.0106 \pm j6.2026)(w' + 46.2117)}$$

$$(K = -1.2033 \times 10^{-06})$$

$p_{14_{32}} =$

$$\frac{K(w' - 1.8198)(w' + 2.3880)(w' + 10.4099)(w' - 100)(w' + 116.7876)(w' - 128.9316)(w' + 832.4270)}{(w' + 0.0334)(w' + 0.4414 \pm j1.7420)(w' + 3.2017)(w' + 9.0106 \pm j6.2026)(w' + 46.2117)}$$

$$(K = -1.3581 \times 10^{-06})$$

$p_{15_{32}} =$

$$\frac{K(w' - 1.8302)(w' + 2.3742)(w' + 10.4110)(w' - 100)(w' + 116.7876)(w' - 128.9316)(w' + 832.4271)}{(w' + 0.0335)(w' + 0.4301 \pm j1.7408)(w' + 3.2013)(w' + 9.0106 \pm j6.2026)(w' + 46.2117)}$$

$$(K = -1.3581 \times 10^{-06})$$

$p_{16_{32}} =$

$$\frac{K(w' - 1.8208)(w' + 2.4520)(w' + 8.9764)(w' - 100)(w' + 116.7217)(w' - 129.0487)(w' + 820.1487)}{(w' + 0.0326)(w' + 0.3934 \pm j1.6425)(w' + 2.8117)(w' + 9.0106 \pm j6.2026)(w' + 46.2117)}$$

$$(K = -1.2038 \times 10^{-06})$$

$p_{17_{32}} =$

$$\frac{K(w' - 1.8299)(w' + 2.4395)(w' + 8.9778)(w' - 100)(w' + 116.7217)(w' - 129.0487)(w' + 820.1488)}{(w' + 0.0328)(w' + 0.3836 \pm j1.6415)(w' + 2.8113)(w' + 9.0106 \pm j6.2026)(w' + 46.2117)}$$

$$(K = -1.2038 \times 10^{-06})$$

$p_{18_{32}} =$

$$\frac{K(w' - 1.8306)(w' + 2.4044)(w' + 10.4044)(w' - 100)(w' + 116.7858)(w' - 128.9354)(w' + 832.0572)}{(w' + 0.0327)(w' + 0.4545 \pm j1.7496)(w' + 3.2017)(w' + 9.0106 \pm j6.2026)(w' + 46.2117)}$$

$$(K = -1.3587 \times 10^{-06})$$

$p_{19_{32}} =$

$$\frac{K(\mathrm{w}' - 1.8409)(\mathrm{w}' + 2.3906)(\mathrm{w}' + 10.4055)(\mathrm{w}' - 100)(\mathrm{w}' + 116.7858)(\mathrm{w}' - 128.9354)(\mathrm{w}' + 832.0573)}{(\mathrm{w}' + 0.0329)(\mathrm{w}' + 0.4433 \pm j1.7484)(\mathrm{w}' + 3.2014)(\mathrm{w}' + 9.0106 \pm j6.2026)(\mathrm{w}' + 46.2117)}$$

$(K = -1.3587 \times 10^{-06})$

## Nominal w′–Domain Transfer Function $p_{o_{33}} = \left(\frac{r(w')}{\delta_{rudder}(w')}\right)$

$$p_{o_{33}} = p_{1_{33}} = \frac{K(w' + 0.0658 \pm j0.3201)(w' - 100)(w' + 149.0423)(w' - 208.1660)}{(w' + 0.0141)(w' + 0.9748 \pm j3.9197)(w' + 6.1917)(w' + 46.2117)}$$

$(K = 0.0016)$

## Off–Nominal w′–Domain Transfer Functions $\left(\frac{r(w')}{\delta_{rudder}(w')}\right)$

$$p_{2_{33}} = \frac{K(w' + 0.0542 \pm j0.3222)(w' - 100)(w' + 149.0496)(w' - 208.1436)}{(w' + 0.0142)(w' + 0.9505 \pm j3.9175)(w' + 6.1917)(w' + 46.2117)}$$

$(K = 0.0016)$

$$p_{3_{33}} = \frac{K(w' + 0.0774 \pm j0.3175)(w' - 100)(w' + 148.9724)(w' - 208.3999)}{(w' + 0.0141)(w' + 1.1198 \pm j4.1808)(w' + 6.1917)(w' + 46.2117)}$$

$(K = 0.0019)$

$$p_{4_{33}} = \frac{K(w' + 0.0641 \pm j0.3205)(w' - 100)(w' + 148.9807)(w' - 208.3742)}{(w' + 0.0141)(w' + 1.0919 \pm j4.1780)(w' + 6.1917)(w' + 46.2117)}$$

$(K = 0.0019)$

$$p_{5_{33}} = \frac{K(w' + 0.0637 \pm j0.3156)(w' - 100)(w' + 149.0583)(w' - 208.1158)}{(w' + 0.0144)(w' + 0.9462 \pm j3.9014)(w' + 6.1917)(w' + 46.2117)}$$

$(K = 0.0016)$

$$p_{6_{33}} = \frac{K(w' + 0.0524 \pm j0.3176)(w' - 100)(w' + 149.0658)(w' - 208.0927)}{(w' + 0.0144)(w' + 0.9219 \pm j3.8992)(w' + 6.1917)(w' + 46.2117)}$$

$(K = 0.0016)$

$$p_{7_{33}} = \frac{K(w' + 0.0749 \pm j0.3132)(w' - 100)(w' + 148.9906)(w' - 208.3423)}{(w' + 0.0144)(w' + 1.0870 \pm j4.1620)(w' + 6.1917)(w' + 46.2117)}$$

$(K = 0.0018)$

$$p_{8_{33}} = \frac{K(w' + 0.0620 \pm j0.3160)(w' - 100)(w' + 148.9992)(w' - 208.3159)}{(w' + 0.0144)(w' + 1.0592 \pm j4.1593)(w' + 6.1917)(w' + 46.2117)}$$

$(K = 0.0018)$

$$p18_{33} = \frac{K(w' + 0.0179 \pm j0.3249)(w' - 100)(w' + 149.2950)(w' - 207.2924)}{(w' + 0.0327)(w' + 0.4545 \pm j1.7496)(w' + 6.1917)(w' + 46.2117)}$$

$(K = 3.1530 \times 10^{-4})$

$$p19_{33} = \frac{K(w' + 0.0124 \pm j0.3252)(w' - 100)(w' + 149.2985)(w' - 207.2820)}{(w' + 0.0329)(w' + 0.4433 \pm j1.7484)(w' + 6.1917)(w' + 46.2117)}$$

$(K = 3.1531 \times 10^{-4})$

$$p_{9_{33}} = \frac{K(w' + 0.0303 \pm j0.3224)(w' - 100)(w' + 149.2166)(w' - 207.5518)}{(w' + 0.0251)(w' + 0.6110 \pm j2.3577)(w' + 6.1917)(w' + 46.2117)}$$

$(K = 5.7543 \times 10^{-4})$

$$p_{10_{33}} = \frac{K(w' + 0.0440 \pm j0.3212)(w' - 100)(w' + 149.1370)(w' - 207.8213)}{(w' + 0.0201)(w' + 0.7729 \pm j2.9617)(w' + 6.1917)(w' + 46.2117)}$$

$(K = 9.1579 \times 10^{-4})$

$$p_{11_{33}} = \frac{K(w' + 0.0583 \pm j0.3191)(w' - 100)(w' + 149.0488)(w' - 208.1273)}{(w' + 0.0167)(w' + 0.9552 \pm j3.6039)(w' + 6.1917)(w' + 46.2117)}$$

$(K = 0.0014)$

$$p_{12_{33}} = \frac{K(w' + 0.0108 \pm j0.3200)(w' - 100)(w' + 149.3314)(w' - 207.1789)}{(w' + 0.0333)(w' + 0.3820 \pm j1.6352)(w' + 6.1917)(w' + 46.2117)}$$

$(K = 2.6453 \times 10^{-4})$

$$p_{13_{33}} = \frac{K(w' + 0.0062 \pm j0.3201)(w' - 100)(w' + 149.3345)(w' - 207.1695)}{(w' + 0.0334)(w' + 0.3721 \pm j1.6342)(w' + 6.1917)(w' + 46.2117)}$$

$(K = 2.6454 \times 10^{-4})$

$$p_{14_{33}} = \frac{K(w' + 0.0172 \pm j0.3202)(w' - 100)(w' + 149.3026)(w' - 207.2692)}{(w' + 0.0334)(w' + 0.4414 \pm j1.7420)(w' + 6.1917)(w' + 46.2117)}$$

$(K = 3.0248 \times 10^{-4})$

$$p_{15_{33}} = \frac{K(w' + 0.0120 \pm j0.3204)(w' - 100)(w' + 149.3062)(w' - 207.2584)}{(w' + 0.0335)(w' + 0.4301 \pm j1.7408)(w' + 6.1917)(w' + 46.2117)}$$

$(K = 3.0249 \times 10^{-4})$

$$p_{16_{33}} = \frac{K(w' + 0.0112 \pm j0.3247)(w' - 100)(w' + 149.3248)(w' - 207.1992)}{(w' + 0.0326)(w' + 0.3934 \pm j1.6425)(w' + 6.1917)(w' + 46.2117)}$$

$(K = 2.7574 \times 10^{-4})$

$$p_{17_{33}} = \frac{K(w' + 0.0065 \pm j0.3249)(w' - 100)(w' + 149.3278)(w' - 207.1901)}{(w' + 0.0328)(w' + 0.3836 \pm j1.6415)(w' + 6.1917)(w' + 46.2117)}$$

$(K = 2.7575 \times 10^{-4})$

# Appendix C. MISO Equivalent Transfer Functions

This appendix includes the MISO equivalent transfer functions, $q_{i_{22e}}$ and $q_{i33}$, used in the MIMO part of the rate controller design.

## C.1 $q_{i_{22e}}$ MISO Equivalent Transfer Functions

The flight conditions produce nineteen separate plants. The w′–domain MISO equivalent transfer functions used in the roll channel of the lateral-directional MIMO design are included below:

**Nominal w′–Domain MISO Equivalent Transfer Function $\left(\frac{p(w')}{\delta_{ail}(w')}\right)$:**

$q_{o_{22e}} = p_{1_{22e}} =$

$$\frac{K(w' + 0.0500)(w' + 0.1523)(w' - 100.)(w' + 115.8656)(w' - 130.9069)(w' + 678.3976)}{(w' + 0.0649 \pm j0.3224)(w' + 6.7663)(w' + 9.0107 \pm j6.2026)(w' + 46.3698)}$$

$(K = 3.1345 \times 10^{-4})$

**Off–Nominal MISO Equivalent Transfer Functions $\left(\frac{p(w')}{\delta_{ail}(w')}\right)$**

$p_{2_{11}} =$

$$\frac{K(w' + 0.0500)(w' + 0.1280)(w' - 100.)(w' + 115.8644)(w' - 130.9069)(w' + 678.3922)}{(w' + 0.0529 \pm j0.3245)(w' + 6.7272)(w' + 9.0106 \pm j6.2027)(w' + 46.3866)}$$

$(K = 3.1345 \times 10^{-4})$

$p_{3_{11}} =$

$$\frac{K(w' + 0.0500)(w' + 0.1737)(w' - 100.)(w' + 115.8012)(w' - 131.0527)(w' + 669.6585)}{(w' + 0.0769 \pm j0.3198)(w' + 7.7278)(w' + 9.0107 \pm j6.2024)(w' + 46.3038)}$$

$(K = 3.6273 \times 10^{-4})$

$p_{4_{11}} =$

$$\frac{K(w' + 0.0500)(w' + 0.1519)(w' - 100.)(w' + 115.8012)(w' - 131.0527)(w' + 669.6710)}{(w' + 0.0632 \pm j0.3227)(w' + 7.7272)(w' + 9.0106 \pm j6.2026)(w' + 46.2943)}$$

$(K = 3.6273 \times 10^{-4})$

$p_{5_{11}} =$

$$\frac{K(w' + 0.0500)(w' + 0.1519)(w' - 100.)(w' + 115.8645)(w' - 130.9077)(w' + 678.3620)}{(w' + 0.0626 \pm j0.3181)(w' + 6.7270)(w' + 9.0106 \pm j6.2027)(w' + 46.2802)}$$

$(K = 3.1344 \times 10^{-4})$

$p_{6_{11}} =$

$$\frac{K(w' + 0.0500)(w' + 0.1239)(w' - 100.)(w' + 115.8646)(w' - 130.9077)(w' + 678.3434)}{(w' + 0.0510 \pm j0.3200)(w' + 6.7857)(w' + 9.0107 \pm j6.2025)(w' + 46.2752)}$$

$(K = 3.1344 \times 10^{-4})$

$p_{7_{11}} =$

$$\frac{K(w' + 0.0500)(w' + 0.1684)(w' - 100.)(w' + 115.8008)(w' - 131.0536)(w' + 669.6284)}{(w' + 0.0742 \pm j0.3156)(w' + 7.7316)(w' + 9\ 0107 \pm j6.2025)(w' + 46.2864)}$$

$(K = 3.6272 \times 10^{-4})$

$p_{8_{11}} =$

$$\frac{K(w' + 0.0500)(w' + 0.1519)(w' - 100.)(w' + 115.8008)(w' - 131.0536)(w' + 669.6118)}{(w' + 0.0610 \pm j0.3183)(w' + 7.7310)(w' + 9.0107 \pm j6.2024)(w' + 46.3587)}$$

$(K = 3.6272 \times 10^{-4})$

$p_{9_{11}} =$

$$\frac{K(w' + 0.0500)(w' + 0.0875)(w' - 100.)(w' + 116.0212)(w' - 130.5482)(w' + 700.9376)}{(w' + 0.0237 \pm j0.3244)(w' + 4.3902)(w' + 9.0106 \pm j6.2026)(w' + 46.2751)}$$

$(K = 1.0940 \times 10^{-4})$

$p_{10_{11}} =$

$$\frac{K(w' + 0.0500)(w' + 0.1104)(w' - 100.)(w' + 115.9461)(w' - 130.7197)(w' + 689.9580)}{(w' + 0.0426 \pm j0.3233)(w' + 5.5255)(w' + 9.0107 \pm j6.2025)(w' + 46.2613)}$$

$(K = 1.7678 \times 10^{-4})$

$p_{11_{11}} =$

$$\frac{K(w' + 0.0500)(w' + 0.1361)(w' - 100.)(w' + 115.8625)(w' - 130.9126)(w' + 678.0630)}{(w' + 0.0570 \pm j0.3217)(w' + 6.7545)(w' + 9.0107 \pm j6.2027)(w' + 46.2947)}$$

$(K = 2.6751 \times 10^{-4})$

$p_{12_{11}} =$

$$\frac{K(w' + 0.0500)(w' + 0.0605)(w' - 100.)(w' + 116.1249)(w' - 130.3100)(w' + 716.7692)}{(w' + 0.0089 \pm j0.3216)(w' + 2.8146)(w' + 9.0106 \pm j6.2025)(w' + 46.3636)}$$

$(K = 5.0247 \times 10^{-5})$

$p_{13_{11}} =$

$$\frac{K(w' + 0.0500)(w' + 0.0509)(w' - 100.)(w' + 116.1235)(w' - 130.3100)(w' + 716.7925)}{(w' + 0.0042 \pm j0.3216)(w' + 2.8143)(w' + 9.0106 \pm j6.2026)(w' + 46.2587)}$$

$(K = 5.0247 \times 10^{-5})$

$p_{14_{11}} =$

$$\frac{K(w' + 0.0500)(w' + 0.0691)(w' - 100.)(w' + 116.0976)(w' - 130.3698)(w' + 712.7262)}{(w' + 0.0154 \pm j0.3219)(w' + 3.2090)(w' + 9.0106 \pm j6.2026)(w' + 46.2723)}$$

$(K = 5.7775 \times 10^{-5})$

$p_{15_{11}} =$

$$\frac{K(w' + 0.0500)(w' + 0.0582)(w' - 100.)(w' + 116.0976)(w' - 130.3698)(w' + 712.7281)}{(w' + 0.0101 \pm j0.3221)(w' + 3.2087)(w' + 9.0106 \pm j6.2026)(w' + 46.2707)}$$

$(K = 5.7775 \times 10^{-5})$

$p_{16_{11}} =$

$$\frac{K(w' + 0.0500)(w' + 0.0624)(w' - 100.)(w' + 116.1237)(w' - 130.3097)(w' + 716.7915)}{(w' + 0.0093 \pm j0.3264)(w' + 2.8142)(w' + 9.0106 \pm j6.2025)(w' + 46.2756)}$$

$(K = 5.0247 \times 10^{-5})$

$p_{17_{11}} =$

$$\frac{K(w' + 0.0500)(w' + 0.0525)(w' - 100.)(w' + 116.1237)(w' - 130.3097)(w' + 716.8044)}{(w' + 0.0045 \pm j0.3264)(w' + 2.8139)(w' + 9.0106 \pm j6.2026)(w' + 46.2768)}$$

$(K = 5.0247 \times 10^{-5})$

$p_{18_{11}} =$

$$\frac{K(w' + 0.0500)(w' + 0.0714)(w' - 100.)(w' + 116.0977)(w' - 130.3694)(w' + 712.7576)}{(w' + 0.0160 \pm j0.3267)(w' + 3.2083)(w' + 9.0106 \pm j6.2026)(w' + 46.3536)}$$

$(K = 5.7775 \times 10^{-5})$

$p_{19_{11}} =$

$$\frac{K(w' + 0.0500)(w' + 0.0601)(w' - 100.)(w' + 116.0994)(w' - 130.3694)(w' + 712.7559)}{(w' + 0.0105 \pm j0.3269)(w' + 3.2079)(w' + 9.0106 \pm j6.2026)(w' + 46.2643)}$$

$(K = 5.7775 \times 10^{-5})$

## C.2 $q_{i_{33}}$ MISO Equivalent Transfer Functions

The flight conditions produce nineteen separate plants. The w'-domain MISO equivalent transfer functions used in the yaw channel of the lateral-directional MIMO design are included below:

**Nominal w'-Domain MISO Equivalent Transfer Function $\left(\frac{r(w')}{\delta_{a_{11}}(w')}\right)$:**

$$q_{o_{22e}} = p_{1_{22e}} = \frac{K(w' + 0.1519)(w' - 100.)(w' + 149.0505)(w' - 208.1358)}{(w' + 0.9748 \pm j3.9197)(w' + 6.7389)(w' + 46.2122)}$$

$(K = 0.0016)$

**Off-Nominal MISO Equivalent Transfer Functions $\left(\frac{p(w')}{\delta_{a_{11}}(w')}\right)$**

$$p_{2_{11}} = \frac{K(w' + 0.1279)(w' - 100.)(w' + 149.0577)(w' - 208.1136)}{(w' + 0.9505 \pm j3.9175)(w' + 6.7385)(w' + 46.2120)}$$

$(K = 0.0016)$

$$p_{3_{11}} = \frac{K(w' + 0.1737)(w' - 100.)(w' + 148.9816)(w' - 208.3650)}{(w' + 1.1198 \pm j4.1808)(w' + 6.1917)(w' + 46.2129)}$$

$(K = 0.0019)$

$$p_{4_{11}} = \frac{K(w' + 0.1462)(w' - 100\ )(w' + 148.9898)(w' - 208.3395)}{(w' + 1.0919 \pm j4.1780)(w' + 6.1917)(w' + 46.2120)}$$

$(K = 0.0019)$

$$p_{5_{11}} = \frac{K(w' + 0.1471)(w' - 100.)(w' + 149.0668)(w' - 208.0844)}{(w' + 0.9462 \pm j3.9014)(w' + 6.7390)(w' + 46.2127)}$$

$(K = 0.0016)$

$$p_{6_{11}} = \frac{K(w' + 0.1239)(w' - 100.)(w' + 149.0743)(w' - 208.0615)}{(w' + 0.9219 \pm j3.8992)(w' + 6.7385)(w' + 46.2121)}$$

$(K = 0.0016)$

$$p_{7_{11}} = \frac{K(w' + 0.1682)(w' - 100.)(w' + 149.0003)(w' - 208.3061)}{(w' + 1.0870 \pm j4.1620)(w' + 6.1917)(w' + 46.2120)}$$

$(K = 0.0018)$

$$p_{8_{11}} = \frac{K(w' + 0.1416)(w' - 100.)(w' + 149.0088)(w' - 208.2798)}{(w' + 1.0592 \pm j4.1593)(w' + 6.1917)(w' + 46.2127)}$$

$(K = 0.0018)$

$$p_{9_{11}} = \frac{K(w' + 0.0875)(w' - 100.)(w' + 149.2221)(w' - 207.5327)}{(w' + 0.6110 \pm j2.3577)(w' + 6.1917)(w' + 46.2128)}$$

$(K = 5.7523 \times 10^{-4})$

$$p_{10_{11}} = \frac{K(w' + 0.1103)(w' - 100.)(w' + 149.1439)(w' - 207.7969)}{(w' + 0.7729 \pm j2.9617)(w' + 6.1917)(w' + 46.2126)}$$

$(K = 9.1550 \times 10^{-4})$

$$p_{11_{11}} = \frac{K(w' + 0.1361)(w' - 100.)(w' + 149.0571)(w' - 208.0966)}{(w' + 0.9552 \pm j3.6039)(w' + 6.7669)(w' + 46.2121)}$$

$(K = 0.0014)$

$$p_{12_{11}} = \frac{K(w' + 0.0604)(w' - 100.)(w' + 149.3351)(w' - 207.1668)}{(w' + 0.3820 \pm j1.6352)(w' + 6.1917)(w' + 46.2133)}$$

$(K = 2.6440 \times 10^{-4})$

$$p_{13_{11}} = \frac{K(w' + 0.0509)(w' - 100.)(w' + 149.3382)(w' - 207.1575)}{(w' + 0.3721 \pm j1.6342)(w' + 6.1917)(w' + 46.2120)}$$

$(K = 2.6441 \times 10^{-4})$

$$p_{14_{11}} = \frac{K(w' + 0.0691)(w' - 100.)(w' + 149.3069)(w' - 207.2552)}{(w' + 0.4414 \pm j1.7420)(w' + 6.1917)(w' + 46.2121)}$$

$(K = 3.0234 \times 10^{-4})$

$$p_{15_{11}} = \frac{K(w' + 0.0582)(w' - 100.)(w' + 149.3104)(w' - 207.2446)}{(w' + 0.4301 \pm j1.7408)(w' + 6.1917)(w' + 46.2125)}$$

$(K = 3.0234 \times 10^{-4})$

$$p_{16_{11}} = \frac{K(w' + 0.0624)(w' - 100.)(w' + 149.3283)(w' - 207.1876)}{(w' + 0.3934 \pm j1.6425)(w' + 6.1917)(w' + 46.2123)}$$

$(K = 2.7566 \times 10^{-4})$

$$p_{17_{11}} = \frac{K(w' + 0.0525)(w' - 100.)(w' + 149.3313)(w' - 207.1785)}{(w' + 0.3836 \pm j1.6415)(w' + 6.1917)(w' + 46.2120)}$$

$(K = 2.7567 \times 10^{-4})$

$$p_{18_{11}} = \frac{K(w' + 0.0714)(w' - 100.)(w' + 149.2991)(w' - 207.2790)}{(w' + 0.4545 \pm j1.7496)(w' + 6.1917)(w' + 46.2124)}$$

$(K = 3.1521 \times 10^{-4})$

$$p_{19_{11}} = \frac{K(w' + 0.0601)(w' - 100.)(w' + 149.3025)(w' - 207.2687)}{(w' + 0.4433 \pm j1.7484)(w' + 6.1917)(w' + 46.2120)}$$

$(K = 3.1522 \times 10^{-4})$

# Appendix D. **Template Data**

This appendix includes the phase and magnitude information used to generate the plant templates. Templates are produced for $P_{i_{11}}$, $q_{i_{22e}}$, and $q_{i_{33}}$.

## *D.1 Template Data for Longitudinal SISO System* $P_{i_{11}}$

| Template Data for $v$ =1.0000x10$^{-3}$ [rad/sec] | | | Template Data for $v$ =0.0050 [rad/sec] | | |
|---|---|---|---|---|---|
| Flight Condition | Phase [deg] | Magnitude [dB] | Flight Condition | Phase [deg] | Magnitude [dB] |
| 1 | 451.0064 | -57.3281 | 1 | 455.0611 | -43.2350 |
| 2 | 451.0766 | -59.3048 | 2 | 455.4127 | -45.2076 |
| 3 | 450.9358 | -55.6420 | 3 | 454.7075 | -41.5528 |
| 4 | 451.0241 | -57.7839 | 4 | 455.1499 | -43.6898 |
| 5 | 451.0132 | -52.8514 | 5 | 455.0949 | -38.7571 |
| 6 | 451.0884 | -54.8535 | 6 | 455.4712 | -40.7549 |
| 7 | 450.9388 | -51.1476 | 7 | 454.7224 | -37.0575 |
| 8 | 451.0320 | -53.3126 | 8 | 455.1891 | -39.2172 |
| 9 | 450.5065 | -64.0420 | 9 | 452.5526 | -49.9785 |
| 10 | 450.7775 | -61.6729 | 10 | 453.9150 | -47.5968 |
| 11 | 450.9371 | -58.2826 | 11 | 454.7149 | -44.1957 |
| 12 | 90.2220 | -63.0314 | 12 | 91.1196 | -48.9752 |
| 13 | 90.1883 | -63.2001 | 13 | 90.9497 | -49.1445 |
| 14 | 90.2507 | -62.8565 | 14 | 91.2642 | -48.7998 |
| 15 | 90.2143 | -63.0733 | 15 | 91.0806 | -49.0173 |
| 16 | 90.2163 | -67.2968 | 16 | 91.0909 | -53.2408 |
| 17 | 90.1836 | -67.4597 | 17 | 90.9258 | -53.4042 |
| 18 | 90.2443 | -67.1279 | 18 | 91.2318 | -53.0714 |
| 19 | 90.2088 | -67.3373 | 19 | 91.0530 | -53.2814 |

| Template Data for $v$ =0.0100 [rad/sec] | | | Template Data for $v$ =0.0500 [rad/sec] | | |
|---|---|---|---|---|---|
| Flight Condition | Phase [deg] | Magnitude [dB] | Flight Condition | Phase [deg] | Magnitude [dB] |
| 1 | 460.0183 | -37.1092 | 1 | 490.3924 | -20.2859 |
| 2 | 460.7050 | -39.0696 | 2 | 492.5161 | -22.0410 |
| 3 | 459.3264 | -35.4391 | 3 | 488.2022 | -18.8280 |
| 4 | 460.1918 | -37.5609 | 4 | 490.9300 | -20.6850 |
| 5 | 460.0827 | -32.6279 | 5 | 490.4427 | -15.7258 |
| 6 | 460.8173 | -34.6125 | 6 | 492.7055 | -17.4967 |
| 7 | 459.3539 | -30.9407 | 7 | 488.1333 | -14.2558 |
| 8 | 460.2667 | -33.0847 | 8 | 491.0115 | -16.1285 |
| 9 | 455.0868 | -43.9431 | 9 | 473.9133 | -29.1450 |
| 10 | 457.7794 | -41.5229 | 10 | 484.0482 | -25.7826 |
| 11 | 459.3461 | -38.0890 | 11 | 488.7716 | -21.6523 |
| 12 | 92.2348 | -42.9626 | 12 | 101.0223 | -28.8213 |
| 13 | 91.8959 | -43.1335 | 13 | 99.3893 | -29.0436 |
| 14 | 92.5231 | -42.7856 | 14 | 102.3949 | -28.5955 |
| 15 | 92.1571 | -43.0051 | 15 | 100.6492 | -28.8766 |
| 16 | 92.1777 | -47.2288 | 16 | 100.7510 | -33.1071 |
| 17 | 91.8483 | -47.3938 | 17 | 99.1602 | -33.3195 |
| 18 | 92.4586 | -47.0580 | 18 | 102.0931 | -32.8908 |
| 19 | 92.1021 | -47.2698 | 19 | 100.3872 | -33.1599 |

| Template Data for $v$ =0.1000 [rad/sec] | | | Template Data for $v$ =0.2000 [rad/sec] | | |
|---|---|---|---|---|---|
| Flight Condition | Phase [deg] | Magnitude [dB] | Flight Condition | Phase [deg] | Magnitude [dB] |
| 1 | 506.5487 | -9.1847 | 1 | 496.4792 | 11.1798 |
| 2 | 509.0584 | -10.8101 | 2 | 503.4635 | 9.5797 |
| 3 | 504.0086 | -7.8789 | 3 | 489.7485 | 12.3330 |
| 4 | 507.1652 | -9.5495 | 4 | 497.9968 | 10.8122 |
| 5 | 506.1464 | -4.4537 | 5 | 486.3716 | 17.5230 |
| 6 | 508.8676 | -6.1094 | 6 | 496.7083 | 15.7863 |
| 7 | 503.3913 | -3.1227 | 7 | 476.2673 | 18.6225 |
| 8 | 506.8083 | -4.8260 | 8 | 488.6013 | 17.1076 |
| 9 | 491.6471 | -21.0033 | 9 | 510.9488 | -9.4540 |
| 10 | 502.9172 | -16.1772 | 10 | 516.7388 | -2.0770 |
| 11 | 506.3262 | -11.1374 | 11 | 512.0757 | 5.7209 |
| 12 | 111.4676 | -22.1873 | 12 | 129.4728 | -13.8549 |
| 13 | 108.5054 | -22.5555 | 13 | 125.2952 | -14.6555 |
| 14 | 113.8739 | -21.8282 | 14 | 132.5298 | -13.1423 |
| 15 | 110.7954 | -22.2787 | 15 | 128.5211 | -14.0506 |
| 16 | 110.9964 | -26.5306 | 16 | 128.8913 | -18.3980 |
| 17 | 108.09( 8 | -26.8786 | 17 | 124.7165 | -19.1536 |
| 18 | 113.3714 | -26.1891 | 18 | 131.9918 | -17.7196 |
| 19 | 110.3377 | -26.6164 | 19 | 127.9562 | -18.5803 |

| Template Data for $v$ =0.3000 [rad/sec] | | | Template Data for $v$ =0.4000 [rad/sec] | | |
|---|---|---|---|---|---|
| Flight Condition | Phase [deg] | Magnitude [dB] | Flight Condition | Phase [deg] | Magnitude [dB] |
| 1 | 365.4678 | 9.8066 | 1 | 359.8305 | 5.9965 |
| 2 | 364.9302 | 8.7991 | 2 | 360.3961 | 4.7916 |
| 3 | 366.2341 | 10.5360 | 3 | 359.7401 | 6.9041 |
| 4 | 365.6140 | 9.5837 | 4 | 360.1761 | 5.7313 |
| 5 | 362.7797 | 12.7658 | 5 | 358.2594 | 9.4800 |
| 6 | 362.5770 | 11.9180 | 6 | 358.9374 | 8.4094 |
| 7 | 363.3796 | 13.3692 | 7 | 358.1928 | 10.2750 |
| 8 | 363.1142 | 12.5785 | 8 | 358.7452 | 9.2456 |
| 9 | 519.6604 | 1.9078 | 9 | 488.3650 | 30.9604 |
| 10 | 497.9735 | 18.7854 | 10 | 358.8061 | 10.4306 |
| 11 | 372.3707 | 15.3369 | 11 | 359.2303 | 8.3145 |
| 12 | 144.0963 | -6.4697 | 12 | 156.4607 | 1.3931 |
| 13 | 140.3111 | -7.7293 | 13 | 153.4548 | -0.3208 |
| 14 | 146.4553 | -5.4260 | 14 | 157.6146 | 2.7774 |
| 15 | 143.0991 | -6.7770 | 15 | 155.0899 | 0.9651 |
| 16 | 143.4982 | -11.3478 | 16 | 154.9124 | -4.1379 |
| 17 | 139.6959 | -12.5282 | 17 | 152.1620 | -5.6717 |
| 18 | 145.9830 | -10.3634 | 18 | 156.2506 | -2.9051 |
| 19 | 142.5842 | -11.6284 | 19 | 153.9532 | -4.5049 |

| Template Data for $v$ =0.5000 [rad/sec] | | | Template Data for $v$ =0.6000 [rad/sec] | | |
|---|---|---|---|---|---|
| Flight Condition | Phase [deg] | Magnitude [dB] | Flight Condition | Phase [deg] | Magnitude [dB] |
| 1 | 358.8952 | 4.5442 | 1 | 358.7307 | 3.9158 |
| 2 | 360.0683 | 3.3029 | 2 | 360.3278 | 2.6706 |
| 3 | 358.3759 | 5.4873 | 3 | 357.9373 | 4.8654 |
| 4 | 359.3878 | 4.2699 | 4 | 359.3414 | 3.6391 |
| 5 | 357.2548 | 8.1876 | 5 | 356.8726 | 7.6241 |
| 6 | 358.4982 | 7.0666 | 6 | 358.5305 | 6.4930 |
| 7 | 356.8135 | 9.0284 | 7 | 356.1855 | 8.4762 |
| 8 | 357.8924 | 7.9410 | 8 | 357.6440 | 7.3737 |
| 9 | 352.4083 | 8.3501 | 9 | 353.9721 | 4.7054 |
| 10 | 356.8343 | 6.0066 | 10 | 357.1537 | 4.4550 |
| 11 | 357.9188 | 6.1093 | 11 | 357.7669 | 5.2044 |
| 12 | 193.2719 | 17.1794 | 12 | 327.7772 | 10.9247 |
| 13 | 182.3404 | 13.9689 | 13 | 328.0342 | 10.8510 |
| 14 | 198.9209 | 20.5705 | 14 | 331.1046 | 11.2156 |
| 15 | 184.5266 | 16.6424 | 15 | 331.3082 | 11.1477 |
| 16 | 171.7642 | 8.3267 | 16 | 331.7137 | 10.7428 |
| 17 | 168.7837 | 6.0464 | 17 | 332.0711 | 10.6163 |
| 18 | 171.5080 | 10.2733 | 18 | 335.0268 | 11.0300 |
| 19 | 168.8757 | 7.7809 | 19 | 335.3018 | 10.9143 |

| Template Data for $v$ =0.7000 [rad/sec] | | | Template Data for $v$ =1 [rad/sec] | | |
|---|---|---|---|---|---|
| Flight Condition | Phase [deg] | Magnitude [dB] | Flight Condition | Phase [deg] | Magnitude [dB] |
| 1 | 358.7149 | 3.5790 | 1 | 358.7007 | 3.2357 |
| 2 | 360.6780 | 2.3409 | 2 | 361.6189 | 2.0485 |
| 3 | 357.6967 | 4.5260 | 3 | 357.1218 | 4.1503 |
| 4 | 359.4361 | 3.3023 | 4 | 359.7394 | 2.9635 |
| 5 | 356.5998 | 7.3230 | 5 | 355.7257 | 7.0281 |
| 6 | 358.6230 | 6.1955 | 6 | 358.7207 | 5.9475 |
| 7 | 355.7102 | 8.1749 | 7 | 354.3363 | 7.8500 |
| 8 | 357.5011 | 7.0715 | 8 | 357.0152 | 6.7796 |
| 9 | 355.5162 | 3.1491 | 9 | 358.5813 | 1.6921 |
| 10 | 357.6513 | 3.6815 | 10 | 358.7480 | 2.9070 |
| 11 | 357.7950 | 4.7274 | 11 | 357.8339 | 4.2300 |
| 12 | 338.8857 | 5.8940 | 12 | 348.6898 | 2.3868 |
| 13 | 341.3666 | 5.2139 | 13 | 353.8419 | 1.6816 |
| 14 | 339.6312 | 6.4837 | 14 | 347.4120 | 2.9638 |
| 15 | 341.7837 | 5.8300 | 15 | 352.0904 | 2.2309 |
| 16 | 345.0126 | 3.3999 | 16 | 356.8061 | -1.0428 |
| 17 | 347.4726 | 2.5022 | 17 | 361.8005 | -1.9359 |
| 18 | 345.1903 | 4.1086 | 18 | 354.8338 | -0.3482 |
| 19 | 347.3449 | 3.2410 | 19 | 359.4068 | -1.2697 |

| Template Data for $v$ =2 [rad/sec] | | | Template Data for $v$ =3 [rad/sec] | | |
|---|---|---|---|---|---|
| Flight Condition | Phase [deg] | Magnitude [dB] | Flight Condition | Phase [deg] | Magnitude [dB] |
| 1 | 356.6114 | 3.8486 | 1 | 350.9431 | 5.1130 |
| 2 | 361.6782 | 2.9438 | 2 | 357.0404 | 4.5194 |
| 3 | 353.8613 | 4.5567 | 3 | 347.8792 | 5.5584 |
| 4 | 358.5814 | 3.6039 | 4 | 353.7653 | 4.8869 |
| 5 | 350.5298 | 7.6897 | 5 | 341.1850 | 8.9852 |
| 6 | 355.7939 | 6.9044 | 6 | 347.5668 | 8.5596 |
| 7 | 348.1967 | 8.2946 | 7 | 338.9301 | 9.3051 |
| 8 | 353.0641 | 7.4688 | 8 | 345.0281 | 8.7988 |
| 9 | 356.6500 | 3.0499 | 9 | 340.7239 | 5.7276 |
| 10 | 356.6399 | 3.8931 | 10 | 346.6391 | 5.9107 |
| 11 | 355.0060 | 4.9094 | 11 | 347.4179 | 6.3773 |
| 12 | 336.4446 | 4.3580 | 12 | 293.9965 | 5.2865 |
| 13 | 342.5485 | 4.6169 | 13 | 295.0748 | 5.9115 |
| 14 | 337.3208 | 4.2938 | 14 | 300.7729 | 5.6156 |
| 15 | 343.6051 | 4.4135 | 15 | 303.0118 | 6.2431 |
| 16 | 356.2382 | 0.9276 | 16 | 324.8259 | 4.3467 |
| 17 | 362.9725 | 0.8427 | 17 | 329.4033 | 4.9514 |
| 18 | 354.6237 | 0.9217 | 18 | 329.1126 | 4.0302 |
| 19 | 361.3497 | 0.7309 | 19 | 334.4742 | 4.5015 |

| Template Data for $v$ =4 [rad/sec] | | | Template Data for $v$ =5 [rad/sec] | | |
|---|---|---|---|---|---|
| Flight Condition | Phase [deg] | Magnitude [dB] | Flight Condition | Phase [deg] | Magnitude [dB] |
| 1 | 341.3218 | 6.6151 | 1 | 328.0023 | 8.1153 |
| 2 | 347.8253 | 6.3147 | 2 | 334.5372 | 8.0890 |
| 3 | 338.6963 | 6.7833 | 3 | 326.5393 | 8.0247 |
| 4 | 345.1387 | 6.3916 | 4 | 333.1334 | 7.8958 |
| 5 | 326.6566 | 10.4522 | 5 | 307.1129 | 11.6755 |
| 6 | 333.2715 | 10.4082 | 6 | 312.9838 | 12.0011 |
| 7 | 325.6013 | 10.4863 | 7 | 308.3789 | 11.5254 |
| 8 | 332.1360 | 10.3294 | 8 | 314.5299 | 11.7126 |
| 9 | 310.9286 | 7.7861 | 9 | 275.4928 | 7.6703 |
| 10 | 328.1512 | 8.0279 | 10 | 301.8760 | 9.4559 |
| 11 | 334.5014 | 8.0666 | 11 | 316.4163 | 9.5984 |
| 12 | 258.4558 | 2.6803 | 12 | 236.9638 | -0.1959 |
| 13 | 257.5547 | 2.9603 | 13 | 236.1705 | -0.0828 |
| 14 | 264.4519 | 3.7480 | 14 | 240.9042 | 1.0689 |
| 15 | 263.8149 | 4.1188 | 15 | 240.0510 | 1.2322 |
| 16 | 278.8034 | 4.1017 | 16 | 247.4537 | 1.3216 |
| 17 | 278.6578 | 4.6891 | 17 | 246.3699 | 1.5846 |
| 18 | 287.5658 | 4.6624 | 18 | 253.9762 | 2.5178 |
| 19 | 288.5265 | 5.3299 | 19 | 253.0522 | 2.8817 |

| Template Data for $v$ =6 [rad/sec] | | | Template Data for $v$ =8 [rad/sec] | | |
|---|---|---|---|---|---|
| Flight Condition | Phase [deg] | Magnitude [dB] | Flight Condition | Phase [deg] | Magnitude [dB] |
| 1 | 310.7721 | 9.4589 | 1 | 264.0206 | 10.6302 |
| 2 | 316.9324 | 9.7131 | 2 | 267.0476 | 11.3420 |
| 3 | 311.2977 | 9.1604 | 3 | 270.6100 | 10.4371 |
| 4 | 317.6900 | 9.2930 | 4 | 274.8033 | 11.0557 |
| 5 | 283.3430 | 12.2488 | 5 | 233.8612 | 10.5769 |
| 6 | 287.3358 | 12.8481 | 6 | 233.7984 | 11.1029 |
| 7 | 287.5855 | 12.1381 | 7 | 241.1878 | 11.1825 |
| 8 | 292.4247 | 12.6172 | 8 | 242.0685 | 11.7754 |
| 9 | 246.3988 | 5.8267 | 9 | 208.0563 | 1.2084 |
| 10 | 271.6618 | 9.4795 | 10 | 221.5176 | 6.1004 |
| 11 | 293.3535 | 10.6046 | 11 | 240.9859 | 9.6687 |
| 12 | 221.3371 | -2.6558 | 12 | 196.1251 | -6.8690 |
| 13 | 220.7668 | -2.6043 | 13 | 195.8145 | -6.8563 |
| 14 | 224.0507 | -1.3658 | 14 | 197.6792 | -5.6064 |
| 15 | 223.3839 | -1.2887 | 15 | 197.3012 | -5.5859 |
| 16 | 227.4330 | -1.4247 | 16 | 198.9812 | -6.0486 |
| 17 | 226.5507 | -1.3030 | 17 | 198.4922 | -6.0131 |
| 18 | 231.7414 | -0.0895 | 18 | 201.2170 | -4.7294 |
| 19 | 230.7717 | 0.0876 | 19 | 200.6312 | -4.6765 |

| Template Data for $v$ =10 [rad/sec] | | | Template Data for $v$ =20 [rad/sec] | | |
|---|---|---|---|---|---|
| Flight Condition | Phase [deg] | Magnitude [dB] | Flight Condition | Phase [deg] | Magnitude [dB] |
| 1 | 217.6759 | 8.4873 | 1 | 121.2243 | -8.2085 |
| 2 | 217.2781 | 9.0371 | 2 | 120.7495 | -8.1751 |
| 3 | 226.5072 | 9.1392 | 3 | 123.3980 | -6.8927 |
| 4 | 227.1094 | 9.7840 | 4 | 122.8285 | -6.8429 |
| 5 | 198.3325 | 6.9711 | 5 | 118.4538 | -9.0163 |
| 6 | 197.3999 | 7.2247 | 6 | 118.1523 | -9.0045 |
| 7 | 204.1604 | 8.0790 | 7 | 119.9703 | -7.7565 |
| 8 | 203.4242 | 8.4207 | 8 | 119.6032 | -7.7374 |
| 9 | 183.1024 | -2.8379 | 9 | 115.1689 | -18.1767 |
| 10 | 190.5620 | 1.9648 | 10 | 116.9206 | -13.9070 |
| 11 | 202.1266 | 6.1292 | 11 | 119.2223 | -10.1549 |
| 12 | 175.8515 | -10.4868 | 12 | 112.8788 | -25.1350 |
| 13 | 175.6529 | -10.4841 | 13 | 112.8155 | -25.1390 |
| 14 | 176.9245 | -9.2508 | 14 | 113.3059 | -23.9459 |
| 15 | 176.6820 | -9.2452 | 15 | 113.2303 | -23.9503 |
| 16 | 177.6268 | -9.8671 | 16 | 113.4761 | -24.7848 |
| 17 | 177.3169 | -9.8533 | 17 | 113.3793 | -24.7865 |
| 18 | 179.0818 | -8.5903 | 18 | 114.0025 | -23.5850 |
| 19 | 178.7071 | -8.5693 | 19 | 113.8878 | -23.5864 |

| Template Data for $v$ =50 [rad/sec] | | | Template Data for $v$ =100 [rad/sec] | | |
|---|---|---|---|---|---|
| Flight Condition | Phase [deg] | Magnitude [dB] | Flight Condition | Phase [deg] | Magnitude [dB] |
| 1 | 45.8746 | -33.1618 | 1 | 2.4878 | -50.1788 |
| 2 | 45.7741 | -33.1633 | 2 | 2.4368 | -50.1821 |
| 3 | 46.4182 | -31.9618 | 3 | 2.7825 | -48.9989 |
| 4 | 46.2990 | -31.9630 | 4 | 2.7229 | -49.0026 |
| 5 | 45.2562 | -33.5169 | 5 | 2.1597 | -50.4719 |
| 6 | 45.1906 | -33.5209 | 6 | 2.1262 | -50.4765 |
| 7 | 45.6964 | -32.3283 | 7 | 2.4047 | -49.2956 |
| 8 | 45.6178 | -32.3327 | 8 | 2.3652 | -49.3008 |
| 9 | 44.3382 | -42.3415 | 9 | 1.6524 | -59.2470 |
| 10 | 44.8797 | -38.2592 | 10 | 1.9580 | -55.1912 |
| 11 | 45.5107 | -34.7465 | 11 | 2.3061 | -51.7132 |
| 12 | 43.5168 | -49.0937 | 12 | 1.1767 | -65.9704 |
| 13 | 43.4947 | -49.0984 | 13 | 1.1639 | -65.9751 |
| 14 | 43.6835 | -47.9197 | 14 | 1.2746 | -64.7985 |
| 15 | 43.6576 | -47.9251 | 15 | 1.2597 | -64.8039 |
| 16 | 43.7371 | -48.8183 | 16 | 1.3048 | -65.7053 |
| 17 | 43.7035 | -48.8220 | 17 | 1.2855 | -65.7092 |
| 18 | 43.9363 | -47.6430 | 18 | 1.4212 | -64.5334 |
| 19 | 43.8973 | -47.6471 | 19 | 1.3988 | -64.5379 |

## *D.2 Template Data for Lateral–Directional MIMO System $q_{i_{22e}}$*

| Template Data for $v$ =1.0000x10$^{-3}$ [rad/sec] | | | Template Data for $v$ =0.0050 [rad/sec] | | |
|---|---|---|---|---|---|
| Flight Condition | Phase [deg] | Magnitude [dB] | Flight Condition | Phase [deg] | Magnitude [dB] |
| 1 | -183.6963 | -16.2144 | 1 | -197.8654 | -15.7056 |
| 2 | -183.5840 | -17.6546 | 2 | -197.3086 | -17.1470 |
| 3 | -183.7780 | -15.2906 | 3 | -198.2714 | -14.7812 |
| 4 | -183.6729 | -16.7719 | 4 | -197.7523 | -16.2648 |
| 5 | -183.6000 | -16.1040 | 5 | -197.4227 | -15.6130 |
| 6 | -183.4840 | -17.5659 | 6 | -196.8474 | -17.0760 |
| 7 | -183.6827 | -15.8949 | 7 | -197.8344 | -15.4035 |
| 8 | -183.5759 | -17.3111 | 8 | -197.3056 | -16.8217 |
| 9 | -181.5717 | -21.4814 | 9 | -187.7862 | -21.2950 |
| 10 | -182.3100 | -19.3960 | 10 | -191.3732 | -19.1272 |
| 11 | -183.0014 | -18.1925 | 11 | -194.6621 | -17.8203 |
| 12 | -180.6445 | -25.1780 | 12 | -183.2049 | -25.0411 |
| 13 | -180.4235 | -26.6121 | 13 | -182.1025 | -26.4596 |
| 14 | -180.7842 | -24.1569 | 14 | -183.9043 | -24.0299 |
| 15 | -180.5879 | -25.5838 | 15 | -182.9229 | -25.4451 |
| 16 | -180.7180 | -25.3050 | 16 | -183.5700 | -25.1673 |
| 17 | -180.5042 | -26.7476 | 17 | -182.5031 | -26.5954 |
| 18 | -180.8530 | -24.2779 | 18 | -184.2460 | -24.1495 |
| 19 | -180.6628 | -25.7200 | 19 | -183.2948 | -25.5808 |

| Template Data for $v$ =0.0100 [rad/sec] | | | Template Data for $v$ =0.0500 [rad/sec] | | |
|---|---|---|---|---|---|
| Flight Condition | Phase [deg] | Magnitude [dB] | Flight Condition | Phase [deg] | Magnitude [dB] |
| 1 | -211.9206 | -14.4141 | 1 | -237.4629 | -4.0932 |
| 2 | -210.8502 | -15.8550 | 2 | -233.2268 | -5.3313 |
| 3 | -212.7059 | -13.4901 | 3 | -240.7390 | -3.3048 |
| 4 | -211.7145 | -14.9763 | 4 | -236.7608 | -4.6376 |
| 5 | -211.2159 | -14.3580 | 5 | -236.4382 | -4.0912 |
| 6 | -210.1092 | -15.8202 | 6 | -232.1125 | -5.3386 |
| 7 | -212.0139 | -14.1496 | 7 | -239.7550 | -4.0280 |
| 8 | -211.0010 | -15.5696 | 8 | -235.6969 | -5.2834 |
| 9 | -194.7545 | -20.7528 | 9 | -212.3705 | -12.6818 |
| 10 | -201.2093 | -18.3758 | 10 | -223.6120 | -9.5362 |
| 11 | -206.8336 | -16.8243 | 11 | -232.0372 | -7.2664 |
| 12 | -186.1339 | -24.6302 | 12 | -194.1450 | -16.9202 |
| 13 | -184.0060 | -26.0023 | 13 | -188.8801 | -17.5870 |
| 14 | -187.4991 | -23.6490 | 14 | -198.1251 | -16.4477 |
| 15 | -185.5910 | -25.0290 | 15 | -192.8136 | -17.2093 |
| 16 | -186.8311 | -24.7546 | 16 | -195.6982 | -17.0889 |
| 17 | -184.7673 | -26.1396 | 17 | -190.4239 | -17.7912 |
| 18 | -188.1530 | -23.7649 | 18 | -199.6693 | -16.5884 |
| 19 | -186.3008 | -25.1635 | 19 | -194.3699 | -17.3930 |

| Template Data for $v$ =0.1000 [rad/sec] | | | Template Data for $v$ =0.2000 [rad/sec] | | |
|---|---|---|---|---|---|
| Flight Condition | Phase [deg] | Magnitude [dB] | Flight Condition | Phase [deg] | Magnitude [dB] |
| 1 | -233.6027 | 3.7009 | 1 | -233.8232 | 15.5879 |
| 2 | -227.3772 | 2.8763 | 2 | -225.9895 | 15.4074 |
| 3 | -238.7709 | 4.1769 | 3 | -240.7399 | 15.4551 |
| 4 | -232.5140 | 3.2122 | 4 | -232.2900 | 15.1950 |
| 5 | -232.4350 | 3.7947 | 5 | -233.1271 | 15.8983 |
| 6 | -226.1861 | 2.9722 | 6 | -225.3309 | 15.7182 |
| 7 | -237.5786 | 3.5341 | 7 | -239.8901 | 15.0255 |
| 8 | -231.2864 | 2.6598 | 8 | -231.4838 | 14.8597 |
| 9 | -208.6173 | -3.8827 | 9 | -208.5504 | 9.7262 |
| 10 | -219.2547 | -1.1762 | 10 | -218.7133 | 11.8289 |
| 11 | -228.1300 | 0.7124 | 11 | -228.2552 | 13.0486 |
| 12 | -193.0056 | -7.4680 | 12 | -194.7414 | 6.8247 |
| 13 | -188.5884 | -7.7129 | 13 | -190.8458 | 6.7806 |
| 14 | -196.7192 | -7.3699 | 14 | -198.4580 | 6.6956 |
| 15 | -191.9003 | -7.6745 | 15 | -194.0588 | 6.6449 |
| 16 | -194.1949 | -7.7205 | 16 | -195.3866 | 6.4049 |
| 17 | -189.6905 | -7.9902 | 17 | -191.4437 | 6.3468 |
| 18 | -197.9737 | -7.5996 | 18 | -199.1298 | 6.2904 |
| 19 | -193.0725 | -7.9396 | 19 | -194.6796 | 6.2158 |

| Template Data for $v$ =0.3000 [rad/sec] | | | Template Data for $v$ =0.4000 [rad/sec] | | |
|---|---|---|---|---|---|
| Flight Condition | Phase [deg] | Magnitude [dB] | Flight Condition | Phase [deg] | Magnitude [dB] |
| 1 | -274.8380 | 26.5272 | 1 | -338.0638 | 26.2476 |
| 2 | -267.4827 | 27.7744 | 2 | -340.9402 | 26.9106 |
| 3 | -280.3593 | 25.1738 | 3 | -335.3087 | 25.3054 |
| 4 | -273.1934 | 26.3378 | 4 | -337.6750 | 25.9980 |
| 5 | -277.6025 | 26.9561 | 5 | -340.1445 | 26.0936 |
| 6 | -270.8736 | 28.2655 | 6 | -343.0338 | 26.6631 |
| 7 | -282.4118 | 24.8301 | 7 | -337.0283 | 24.4972 |
| 8 | -275.8648 | 26.1303 | 8 | -339.5341 | 25.1889 |
| 9 | -249.8870 | 25.8330 | 9 | -352.2171 | 22.2017 |
| 10 | -262.5350 | 25.6124 | 10 | -345.6565 | 23.5912 |
| 11 | -271.6581 | 24.8462 | 11 | -340.0357 | 23.9366 |
| 12 | -222.6590 | 27.5537 | 12 | -365.6071 | 19.3073 |
| 13 | -209.3516 | 28.3509 | 13 | -368.1115 | 19.3764 |
| 14 | -235.1797 | 25.8709 | 14 | -360.4935 | 19.1019 |
| 15 | -223.4363 | 27.0086 | 15 | -363.2823 | 19.2300 |
| 16 | -218.2281 | 25.8120 | 16 | -365.1232 | 19.7573 |
| 17 | -206.5229 | 26.3559 | 17 | -367.9133 | 19.8302 |
| 18 | -229.9543 | 24.5052 | 18 | -359.6124 | 19.5390 |
| 19 | -218.8768 | 25.3427 | 19 | -362.7001 | 19.6735 |

| Template Data for $v$ =0.5000 [rad/sec] | | | Template Data for $v$ =0.6000 [rad/sec] | | |
|---|---|---|---|---|---|
| Flight Condition | Phase [deg] | Magnitude [dB] | Flight Condition | Phase [deg] | Magnitude [dB] |
| 1 | -357.8584 | 23.3670 | 1 | -364.7886 | 21.9617 |
| 2 | -359.5887 | 23.5452 | 2 | -365.8425 | 22.0430 |
| 3 | -355.4504 | 22.8737 | 3 | -362.7691 | 21.5748 |
| 4 | -357.1914 | 23.0483 | 4 | -363.8645 | 21.6304 |
| 5 | -358.6015 | 23.2409 | 5 | -365.2103 | 21.8753 |
| 6 | -360.2487 | 23.3771 | 6 | -366.2104 | 21.9248 |
| 7 | -355.9108 | 22.0585 | 7 | -362.8300 | 20.7934 |
| 8 | -357.6311 | 22.2773 | 8 | -363.9316 | 20.9046 |
| 9 | -365.8028 | 17.9792 | 9 | -370.7559 | 16.3427 |
| 10 | -362.2805 | 19.8778 | 10 | -367.9978 | 18.3260 |
| 11 | -358.6000 | 20.8115 | 11 | -365.0099 | 19.3743 |
| 12 | -372.7130 | 14.7859 | 12 | -376.4998 | 13.1119 |
| 13 | -373.5425 | 14.8098 | 13 | -376.9522 | 13.1316 |
| 14 | -369.7785 | 14.6723 | 14 | -373.9396 | 13.0177 |
| 15 | -370.7272 | 14.7094 | 15 | -374.4599 | 13.0442 |
| 16 | -372.7451 | 14.9433 | 16 | -376.5842 | 13.1953 |
| 17 | -373.6357 | 14.9600 | 17 | -377.0636 | 13.2069 |
| 18 | -369.7105 | 14.8369 | 18 | -373.9731 | 13.1096 |
| 19 | -370.7279 | 14.8601 | 19 | -374.5240 | 13.1205 |

| Template Data for $v$ =0.7000 [rad/sec] | | | Template Data for $v$ =1 [rad/sec] | | |
|---|---|---|---|---|---|
| Flight Condition | Phase [deg] | Magnitude [dB] | Flight Condition | Phase [deg] | Magnitude [dB] |
| 1 | -368.8826 | 21.1533 | 1 | -376.9396 | 20.0182 |
| 2 | -369.5967 | 21.2012 | 2 | -377.2650 | 20.0396 |
| 3 | -366.9995 | 20.8072 | 3 | -374.9118 | 19.7176 |
| 4 | -367.7426 | 20.8201 | 4 | -375.2288 | 19.6958 |
| 5 | -369.1945 | 21.0908 | 5 | -377.2083 | 19.9873 |
| 6 | -369.8714 | 21.1102 | 6 | -377.5126 | 19.9826 |
| 7 | -366.8775 | 20.0510 | 7 | -374.5656 | 19.0092 |
| 8 | -367.6504 | 20.1233 | 8 | -374.9557 | 19.0485 |
| 9 | -374.1885 | 15.4492 | 9 | -382.3962 | 14.1989 |
| 10 | -371.6350 | 17.4671 | 10 | -379.6040 | 16.2749 |
| 11 | -368.8538 | 18.5614 | 11 | -376.6073 | 17.4362 |
| 12 | -379.7292 | 12.1920 | 12 | -388.6724 | 10.8372 |
| 13 | -380.0258 | 12.2108 | 13 | -388.8145 | 10.8558 |
| 14 | -377.2187 | 12.1135 | 14 | -385.8491 | 10.8144 |
| 15 | -377.5607 | 12.1372 | 15 | -386.0132 | 10.8363 |
| 16 | -379.8195 | 12.2414 | 16 | -388.7429 | 10.8477 |
| 17 | -380.1312 | 12.2521 | 17 | -388.8896 | 10.8581 |
| 18 | -377.2763 | 12.1717 | 18 | -385.9038 | 10.8337 |
| 19 | -377.6352 | 12.1794 | 19 | -386.0728 | 10.8394 |

| Template Data for $v$ =2 [rad/sec] | | | Template Data for $v$ =3 [rad/sec] | | |
|---|---|---|---|---|---|
| Flight Condition | Phase [deg] | Magnitude [dB] | Flight Condition | Phase [deg] | Magnitude [dB] |
| 1 | -396.6341 | 18.9464 | 1 | -414.5258 | 18.2577 |
| 2 | -396.7455 | 18.9596 | 2 | -414.5983 | 18.2702 |
| 3 | -393.2318 | 18.7413 | 3 | -409.8118 | 18.1824 |
| 4 | -393.2808 | 18.7097 | 4 | -409.7851 | 18.1517 |
| 5 | -397.1074 | 18.9318 | 5 | -415.2386 | 18.2402 |
| 6 | -397.1964 | 18.9198 | 6 | -415.2806 | 18.2278 |
| 7 | -392.8044 | 18.1346 | 7 | -409.7507 | 17.6569 |
| 8 | -393.0016 | 18.1588 | 8 | -409.9176 | 17.6745 |
| 9 | -405.2385 | 12.7686 | 9 | -425.5009 | 11.6307 |
| 10 | -400.7818 | 15.0486 | 10 | -419.9527 | 14.1542 |
| 11 | -396.0515 | 16.4095 | 11 | -413.9597 | 15.7560 |
| 12 | -414.6143 | 8.8804 | 12 | -436.1799 | 7.1873 |
| 13 | -414.6900 | 8.8970 | 13 | -436.2434 | 7.2016 |
| 14 | -410.6573 | 9.1044 | 14 | -431.9008 | 7.6473 |
| 15 | -410.7461 | 9.1235 | 15 | -431.9771 | 7.6635 |
| 16 | -414.6380 | 8.8697 | 16 | -436.1875 | 7.1741 |
| 17 | -414.7145 | 8.8781 | 17 | -436.2508 | 7.1801 |
| 18 | -410.6723 | 9.1028 | 18 | -431.9010 | 7.6435 |
| 19 | -410.7610 | 9.1056 | 19 | -431.9759 | 7.6434 |

| Template Data for $v$ =4 [rad/sec] | | | Template Data for $v$ =5 [rad/sec] | | |
|---|---|---|---|---|---|
| Flight Condition | Phase [deg] | Magnitude [dB] | Flight Condition | Phase [deg] | Magnitude [dB] |
| 1 | -431.8906 | 17.4577 | 1 | -448.0866 | 16.5443 |
| 2 | -431.9484 | 17.4700 | 2 | -448.1383 | 16.5567 |
| 3 | -426.0793 | 17.5449 | 3 | -441.4598 | 16.8093 |
| 4 | -426.0045 | 17.5168 | 4 | -441.3499 | 16.7847 |
| 5 | -432.8644 | 17.4310 | 5 | -449.3300 | 16.5020 |
| 6 | -432.8819 | 17.4187 | 6 | -449.3311 | 16.4901 |
| 7 | -426.6750 | 17.0635 | 7 | -442.8022 | 16.3244 |
| 8 | -426.8221 | 17.0760 | 8 | -442.9304 | 16.3333 |
| 9 | -444.1831 | 10.3602 | 9 | -460.8354 | 9.0247 |
| 10 | -438.1392 | 13.1212 | 10 | -454.7059 | 11.9826 |
| 11 | -431.4525 | 14.9678 | 11 | -447.7625 | 14.0410 |
| 12 | -454.9211 | 5.4559 | 12 | -471.0619 | 3.7875 |
| 13 | -454.9757 | 5.4686 | 13 | -471.1097 | 3.7992 |
| 14 | -450.7908 | 6.0960 | 14 | -467.2436 | 4.5497 |
| 15 | -450.8579 | 6.1102 | 15 | -467.3028 | 4.5625 |
| 16 | -454.9220 | 5.4422 | 16 | -471.0593 | 3.7735 |
| 17 | -454.9757 | 5.4465 | 17 | -471.1054 | 3.7769 |
| 18 | -450.7860 | 6.0920 | 18 | -467.2370 | 4.5457 |
| 19 | -450.8503 | 6.0898 | 19 | -467.2922 | 4.5421 |

| Template Data for $v$ =6 [rad/sec] | | | Template Data for $v$ =8 [rad/sec] | | |
|---|---|---|---|---|---|
| Flight Condition | Phase [deg] | Magnitude [dB] | Flight Condition | Phase [deg] | Magnitude [dB] |
| 1 | -463.2829 | 15.5226 | 1 | -491.5934 | 13.1379 |
| 2 | -463.3329 | 15.5350 | 2 | -491.6464 | 13.1499 |
| 3 | -456.1017 | 15.9723 | 3 | -484.0139 | 13.9596 |
| 4 | -455.9660 | 15.9519 | 4 | -483.8521 | 13.9490 |
| 5 | -464.7974 | 15.4566 | 5 | -493.5896 | 12.9934 |
| 6 | -464.7855 | 15.4452 | 6 | -493.5579 | 12.9839 |
| 7 | -458.1478 | 15.4411 | 7 | -487.0237 | 13.2385 |
| 8 | -458.2581 | 15.4475 | 8 | -487.1030 | 13.2427 |
| 9 | -475.9358 | 7.6434 | 9 | -503.1593 | 4.7064 |
| 10 | -469.9314 | 10.7567 | 10 | -497.6221 | 8.0404 |
| 11 | -462.9806 | 12.9889 | 11 | -490.9570 | 10.5311 |
| 12 | -485.4773 | 2.1697 | 12 | -511.3595 | -1.0669 |
| 13 | -485.5198 | 2.1808 | 13 | -511.3954 | -1.0564 |
| 14 | -481.9930 | 3.0149 | 14 | -508.4647 | -0.1209 |
| 15 | -482.0460 | 3.0269 | 15 | -508.5092 | -0.1098 |
| 16 | -485.4722 | 2.1557 | 16 | -511.3493 | -1.0811 |
| 17 | -485.5124 | 2.1584 | 17 | -511 3816 | -1.0789 |
| 18 | -481.9855 | 3.0109 | 18 | -508.4548 | 0.1250 |
| 19 | -482.0331 | 3.0064 | 19 | -508.4916 | -0.1303 |

| Template Data for $v$ =10 [rad/sec] | | | Template Data for $v$ =20 [rad/sec] | | |
|---|---|---|---|---|---|
| Flight Condition | Phase [deg] | Magnitude [dB] | Flight Condition | Phase [deg] | Magnitude [dB] |
| 1 | -515.6506 | 10.5329 | 1 | -591.2190 | -2.4737 |
| 2 | -515.7091 | 10.5438 | 2 | -591.2716 | -2.4691 |
| 3 | -508.4783 | 11.6678 | 3 | -588.3983 | -0.8430 |
| 4 | -508.3227 | 11.6663 | 4 | -588.3692 | -0.8344 |
| 5 | -517.8735 | 10.2829 | 5 | -591.9451 | -3.0081 |
| 6 | -517.8308 | 10.2757 | 6 | -591.9151 | -3.0086 |
| 7 | -511.5738 | 10.7179 | 7 | -587.4635 | -2.1040 |
| 8 | -511.6328 | 10.7217 | 8 | -587.5024 | -2.0996 |
| 9 | -525.7421 | 1.7527 | 9 | -595.8472 | -11.7578 |
| 10 | -520.6630 | 5.2257 | 10 | -592.3827 | -7.9715 |
| 11 | -514.3395 | 7.8898 | 11 | -587.6225 | -4.8535 |
| 12 | -532.9274 | -4.1881 | 12 | -600.4073 | -18.0284 |
| 13 | -532.9603 | -4.1780 | 13 | -600.4366 | -18.0195 |
| 14 | -530.4586 | -3.1886 | 14 | -598.9674 | -16.9358 |
| 15 | -530.4989 | -3.1780 | 15 | -599.0017 | -16.9268 |
| 16 | -532.9122 | -4.2022 | 16 | -600.3787 | -18.0405 |
| 17 | -532.9403 | -4.2004 | 17 | -600.3978 | -18.0399 |
| 18 | -530.4455 | -3.1926 | 18 | -598.9488 | -16.9378 |
| 19 | -530.4758 | -3.1983 | 19 | -598.9624 | -16.9448 |

| Template Data for $v$ =50 [rad/sec] | | | Template Data for $v$ =100 [rad/sec] | | |
|---|---|---|---|---|---|
| Flight Condition | Phase [deg] | Magnitude [dB] | Flight Condition | Phase [deg] | Magnitude [dB] |
| 1 | -670.9220 | -26.0958 | 1 | -716.0840 | -43.1133 |
| 2 | -670.9450 | -26.0938 | 2 | -716.0995 | -43.1119 |
| 3 | -671.0455 | -24.6027 | 3 | -716.8083 | -41.7557 |
| 4 | -671.0525 | -24.6018 | 4 | -716.8100 | -41.7558 |
| 5 | -669.5680 | -26.4823 | 5 | -714.5870 | -43.2967 |
| 6 | -669.5598 | -26.4822 | 6 | -714.5832 | -43.2966 |
| 7 | -667.5264 | -25.3656 | 7 | -713.4400 | -42.1471 |
| 8 | -667.5517 | -25.3637 | 8 | -713.4567 | -42.1462 |
| 9 | -671.4317 | -35.3039 | 9 | -715.8592 | -52.1446 |
| 10 | -669.6975 | -31.3613 | 10 | -714.7103 | -48.1538 |
| 11 | -667.3224 | -27.9808 | 11 | -713.3036 | -44.7217 |
| 12 | -673.8975 | -41.7418 | 12 | -717.6348 | -58.6434 |
| 13 | -673.9292 | -41.7350 | 13 | -717.6704 | -58.6394 |
| 14 | -673.1953 | -40.6071 | 14 | -717.1755 | -57.4930 |
| 15 | -673.2289 | -40.6004 | 15 | -717.2116 | -57.4890 |
| 16 | -673.8574 | -41.7505 | 16 | -717.5932 | -58.6482 |
| 17 | -673.8659 | -41.7506 | 17 | -717.5973 | -58.6483 |
| 18 | -673.1839 | -40.6072 | 18 | -717.1719 | -57.4926 |
| 19 | -673.1718 | -40.6140 | 19 | -717.1466 | -57.4968 |

## D.3 Template Data for Lateral-Directional MIMO System $q_{i_{33}}$

| Template Data for $v$ =1.0000x10$^{-3}$ [rad/sec] | | | Template Data for $v$ =0.0050 [rad/sec] | | |
|---|---|---|---|---|---|
| Flight Condition | Phase [deg] | Magnitude [dB] | Flight Condition | Phase [deg] | Magnitude [dB] |
| 1 | 0.3593 | -15.3414 | 1 | 1.8114 | -15.3368 |
| 2 | 0.4303 | -16.8028 | 2 | 2.1690 | -16.7963 |
| 3 | 0.3120 | -14.2072 | 3 | 1.5730 | -14.2036 |
| 4 | 0.3741 | -15.6638 | 4 | 1.8859 | -15.6589 |
| 5 | 0.3717 | -15.8706 | 5 | 1.8736 | -15.8657 |
| 6 | 0.4450 | -17.3327 | 6 | 2.2428 | -17.3258 |
| 7 | 0.3228 | -14.7357 | 7 | 1.6275 | -14.7320 |
| 8 | 0.3869 | -16.1932 | 8 | 1.9505 | -16.1879 |
| 9 | 0.6320 | -20.2703 | 9 | 3.1835 | -20.2565 |
| 10 | 0.4986 | -18.2516 | 10 | 2.5129 | -18.2429 |
| 11 | 0.4022 | -16.4373 | 11 | 2.0274 | -16.4316 |
| 12 | 0.9204 | -23.5971 | 12 | 4.6309 | -23.5681 |
| 13 | 1.0988 | -25.0588 | 13 | 5.5235 | -25.0180 |
| 14 | 0.8013 | -22.4610 | 14 | 4.0342 | -22.4388 |
| 15 | 0.9574 | -23.9182 | 15 | 4.8163 | -23.8869 |
| 16 | 0.8903 | -23.0680 | 16 | 4.4804 | -23.0407 |
| 17 | 1.0631 | -24.5290 | 17 | 5.3454 | -24.4906 |
| 18 | 0.7750 | -21.9325 | 18 | 3.9021 | -21.9117 |
| 19 | 0.9262 | -23.3889 | 19 | 4.6600 | -23.3595 |

| Template Data for $v$ =0.0100 [rad/sec] | | | Template Data for $v$ =0.0500 [rad/sec] | | |
|---|---|---|---|---|---|
| Flight Condition | Phase [deg] | Magnitude [dB] | Flight Condition | Phase [deg] | Magnitude [dB] |
| 1 | 3.6125 | -15.3225 | 1 | 17.3525 | -14.8924 |
| 2 | 4.3238 | -16.7762 | 2 | 20.5000 | -16.1822 |
| 3 | 3.1379 | -14.1927 | 3 | 15.1896 | -13.8597 |
| 4 | 3.7609 | -15.6435 | 4 | 18.0193 | -15.1815 |
| 5 | 3.7353 | -15.8505 | 5 | 17.9091 | -15.3936 |
| 6 | 4.4704 | -17.3043 | 6 | 21.1342 | -16.6743 |
| 7 | 3.2464 | -14.7203 | 7 | 15.6888 | -14.3663 |
| 8 | 3.8894 | -16.1715 | 8 | 18.5929 | -15.6809 |
| 9 | 6.3348 | -20.2136 | 9 | 28.6393 | -19.0360 |
| 10 | 5.0066 | -18.2159 | 10 | 23.3809 | -17.4366 |
| 11 | 4.0422 | -16.4138 | 11 | 19.2615 | -15.8845 |
| 12 | 9.1615 | -23.4791 | 12 | 38.2667 | -21.3206 |
| 13 | 10.9208 | -24.8933 | 13 | 43.1859 | -22.1108 |
| 14 | 8.0112 | -22.3705 | 14 | 34.5473 | -20.6231 |
| 15 | 9.5439 | -23.7911 | 15 | 39 3578 | -21 5059 |
| 16 | 8.8867 | -22.9571 | 16 | 37 3568 | -20.9022 |
| 17 | 10.5748 | -24.3735 | 17 | 42.2573 | -21.7151 |
| 18 | 7.7515 | -21.8475 | 18 | 33 6687 | -20.1881 |
| 19 | 9.2384 | -23.2695 | 19 | 38.4413 | -21.0923 |

| Template Data for $v$ =0.1000 [rad/sec] | | | Template Data for $v$ =0.2000 [rad/sec] | | |
|---|---|---|---|---|---|
| Flight Condition | Phase [deg] | Magnitude [dB] | Flight Condition | Phase [deg] | Magnitude [dB] |
| 1 | 31.5686 | -13.7740 | 1 | 49.1602 | -10.9681 |
| 2 | 36.2511 | -14.7266 | 2 | 53.8154 | -11.4245 |
| 3 | 28.1424 | -12.9609 | 3 | 45.4068 | -10.5375 |
| 4 | 32.5944 | -13.9945 | 4 | 50.2399 | -11.0810 |
| 5 | 32.4254 | -14.2175 | 5 | 50.0614 | -11.3195 |
| 6 | 37.1538 | -15.1493 | 6 | 54.6649 | -11.7559 |
| 7 | 28.9510 | -13.4187 | 7 | 46.3338 | -10.9058 |
| 8 | 33.4632 | -14.4336 | 8 | 51.1317 | -11.4278 |
| 9 | 46.5126 | -16.6274 | 9 | 61.7122 | -12.2894 |
| 10 | 40.1237 | -15.6408 | 10 | 56.9525 | -11.9142 |
| 11 | 34.4223 | -14.5571 | 11 | 51.9446 | -11.4312 |
| 12 | 56.0888 | -17.8437 | 12 | 67.6055 | -12.7236 |
| 13 | 60.3077 | -18.1627 | 13 | 70.2268 | -12.7969 |
| 14 | 52.5899 | -17.5339 | 14 | 65.3690 | -12.6598 |
| 15 | 57 0844 | -17.9255 | 15 | 68.2905 | -12.7585 |
| 16 | 55.2440 | -17.5162 | 16 | 67.0323 | -12.4497 |
| 17 | 59.5315 | -17.8519 | 17 | 69.7219 | -12.5288 |
| 18 | 51.7008 | -17.1913 | 18 | 64.7378 | -12.3798 |
| 19 | 56.2533 | -17.6018 | 19 | 67.7320 | -12.4858 |

| Template Data for $v$ =0.3000 [rad/sec] | | | Template Data for $v$ =0.4000 [rad/sec] | | |
|---|---|---|---|---|---|
| Flight Condition | Phase [deg] | Magnitude [dB] | Flight Condition | Phase [deg] | Magnitude [dB] |
| 1 | 57.9010 | -8.3507 | 1 | 61.9815 | -6.3116 |
| 2 | 61.6964 | -8.5792 | 2 | 65.1162 | -6.4404 |
| 3 | 54.7076 | -8.1265 | 3 | 59.3102 | -6.1873 |
| 4 | 58.8194 | -8.4134 | 4 | 62.7694 | -6.3547 |
| 5 | 58.6642 | -8.6565 | 5 | 62.6313 | -6.5964 |
| 6 | 62.3829 | -8.8722 | 6 | 65.6911 | -6.7169 |
| 7 | 55.5274 | -8.4443 | 7 | 60.0206 | -6.4305 |
| 8 | 59.5665 | -8.7162 | 8 | 63.4031 | -6.6376 |
| 9 | 66.8205 | -9.0348 | 9 | 68.2831 | -6.6926 |
| 10 | 63.6957 | -8.8870 | 10 | 66.2579 | -6.6571 |
| 11 | 60.0334 | -8.6596 | 11 | 63.5770 | -6.5488 |
| 12 | 70.1911 | -9.1816 | 12 | 69.9954 | -6.6524 |
| 13 | 72.0605 | -9.1946 | 13 | 71.5003 | -6.6428 |
| 14 | 68.6591 | -9.2002 | 14 | 68.8605 | -6.7228 |
| 15 | 70.7566 | -9.2231 | 15 | 70.5446 | -6.7174 |
| 16 | 69.7441 | -8.9236 | 16 | 69.6012 | -6.4031 |
| 17 | 71.6637 | -8.9391 | 17 | 71.1444 | -6.3947 |
| 18 | 68.1667 | -8.9392 | 18 | 68.4301 | -6.4713 |
| 19 | 70.3200 | -8.9652 | 19 | 70.1575 | -6.4674 |

| Template Data for $v$ =0.5000 [rad/sec] | | | Template Data for $v$ =0.6000 [rad/sec] | | |
|---|---|---|---|---|---|
| Flight Condition | Phase [deg] | Magnitude [dB] | Flight Condition | Phase [deg] | Magnitude [dB] |
| 1 | 64.1628 | -4.4449 | 1 | 64.9900 | -2.9518 |
| 2 | 66.7744 | -4.5164 | 2 | 67.2472 | -2.9922 |
| 3 | 61.9402 | -4.3839 | 3 | 63.0894 | -2.9297 |
| 4 | 64.8507 | -4.4804 | 4 | 65.6160 | -2.9872 |
| 5 | 64.7228 | -4.7171 | 5 | 65.4907 | -3.2165 |
| 6 | 67.2675 | -4.7831 | 6 | 67.6887 | -3.2532 |
| 7 | 62.5573 | -4.6618 | 7 | 63.6421 | -3.1987 |
| 8 | 65.3962 | -4.7515 | 8 | 66.1040 | -3.2514 |
| 9 | 68.2446 | -4.6052 | 9 | 67.3527 | -2.9411 |
| 10 | 67.1501 | -4.6614 | 10 | 66.9990 | -3.0774 |
| 11 | 65.2909 | -4.6364 | 11 | 65.7616 | -3.1140 |
| 12 | 68.4434 | -4.3610 | 12 | 66.1827 | -2.4794 |
| 13 | 69.7199 | -4.3374 | 13 | 67.3321 | -2.4459 |
| 14 | 67.6272 | -4.4878 | 14 | 65.6342 | -2.6670 |
| 15 | 69.0454 | -4.4654 | 15 | 66.8992 | -2.6334 |
| 16 | 68.0739 | -4.1203 | 16 | 65.8207 | -2.2476 |
| 17 | 69.3793 | -4.0972 | 17 | 66.9923 | -2.2143 |
| 18 | 67.2288 | -4.2449 | 18 | 65.2479 | -2.4324 |
| 19 | 68.6802 | -4.2231 | 19 | 66.5389 | -2.3991 |

| Template Data for $v$ =0.7000 [rad/sec] | | | Template Data for $v$ =1 [rad/sec] | | |
|---|---|---|---|---|---|
| Flight Condition | Phase [deg] | Magnitude [dB] | Flight Condition | Phase [deg] | Magnitude [dB] |
| 1 | 65.0984 | -1.6491 | 1 | 63.0257 | 1.5773 |
| 2 | 67.0914 | -1.6696 | 2 | 64.5267 | 1.5883 |
| 3 | 63.4503 | -1.6561 | 3 | 61.9074 | 1.5014 |
| 4 | 65.6851 | -1.6886 | 4 | 63.5862 | 1.5084 |
| 5 | 65.5567 | -1.9085 | 5 | 63.4149 | 1.3292 |
| 6 | 67.4974 | -1.9264 | 6 | 64.8791 | 1.3412 |
| 7 | 63.9556 | -1.9188 | 7 | 62.3314 | 1.2511 |
| 8 | 66.1325 | -1.9478 | 8 | 63.9685 | 1.2596 |
| 9 | 65.9385 | -1.4749 | 9 | 59.4577 | 2.3140 |
| 10 | 66.2682 | -1.6947 | 10 | 61.9741 | 1.7793 |
| 11 | 65.5662 | -1.7878 | 11 | 62.7214 | 1.5005 |
| 12 | 63.2987 | -0.7588 | 12 | 50.1004 | 4.1082 |
| 13 | 64.3720 | -0.7161 | 13 | 51.1018 | 4.1906 |
| 14 | 63.0369 | -1.0189 | 14 | 51.3827 | 3.5258 |
| 15 | 64.2047 | -0.9756 | 15 | 52.4304 | 3.6050 |
| 16 | 62.9372 | -0.5379 | 16 | 49.7695 | 4.2760 |
| 17 | 64.0269 | -0.4952 | 17 | 50.7711 | 4.3579 |
| 18 | 62.6541 | -0.7939 | 18 | 51.0169 | 3.7063 |
| 19 | 63.8417 | -0.7507 | 19 | 52.0684 | 3.7853 |

| Template Data for $v$ =2 [rad/sec] | | | Template Data for $v$ =3 [rad/sec] | | |
|---|---|---|---|---|---|
| Flight Condition | Phase [deg] | Magnitude [dB] | Flight Condition | Phase [deg] | Magnitude [dB] |
| 1 | 46.0750 | 8.8178 | 1 | 15.5719 | 14.6874 |
| 2 | 47.1086 | 8.8735 | 2 | 16.5100 | 14.8254 |
| 3 | 46.2437 | 8.4541 | 3 | 19.7053 | 13.8156 |
| 4 | 47.3530 | 8.5099 | 4 | 20.6973 | 13.9397 |
| 5 | 46.4361 | 8.6140 | 5 | 15.6734 | 14.5875 |
| 6 | 47.4599 | 8.6696 | 6 | 16.6215 | 14.7285 |
| 7 | 46.6258 | 8.2438 | 7 | 19.9383 | 13.6904 |
| 8 | 47.7219 | 8.2996 | 8 | 20.9376 | 13.8164 |
| 9 | 9.3879 | 12.3616 | 9 | -76.1418 | 10.6386 |
| 10 | 33.7625 | 10.3514 | 10 | -33.9544 | 15.4484 |
| 11 | 42.8217 | 9.0212 | 11 | 4.1770 | 15.0503 |
| 12 | -66.2528 | 8.3539 | 12 | -102.5524 | 1.1037 |
| 13 | -66.9506 | 8.4471 | 13 | -102.8806 | 1.1169 |
| 14 | -54.2326 | 9.7639 | 14 | -98.8873 | 2.5823 |
| 15 | -54.9231 | 9.9042 | 15 | -99.2815 | 2.6019 |
| 16 | -64.7579 | 8.6657 | 16 | -101.9320 | 1.4763 |
| 17 | -65.4313 | 8.7612 | 17 | -102.2548 | 1.4900 |
| 18 | -52.5977 | 10.0101 | 18 | -98.1460 | 2.9490 |
| 19 | -53.2480 | 10.1519 | 19 | -98.5334 | 2.9693 |

| Template Data for $v$ =4 [rad/sec] | | | Template Data for $v$ =5 [rad/sec] | | |
|---|---|---|---|---|---|
| Flight Condition | Phase [deg] | Magnitude [dB] | Flight Condition | Phase [deg] | Magnitude [dB] |
| 1 | -45.0268 | 17.7938 | 1 | -93.7143 | 14.1949 |
| 2 | -45.2322 | 18.0143 | 2 | -94.3744 | 14.2794 |
| 3 | -29.9615 | 17.6060 | 3 | -82.3571 | 15.6128 |
| 4 | -29.7652 | 17.8372 | 4 | -83.0270 | 15.7402 |
| 5 | -46.5840 | 17.6795 | 5 | -95.1381 | 13.8715 |
| 6 | -46.8431 | 17.9043 | 6 | -95.8191 | 13.9538 |
| 7 | -30.9992 | 17.5434 | 7 | -83.9517 | 15.3476 |
| 8 | -30.8354 | 17.7819 | 8 | -84.6571 | 15.4732 |
| 9 | -106.5135 | 5.1702 | 9 | -121.4210 | 1.4830 |
| 10 | -91.2245 | 11.0165 | 10 | -113.6981 | 6.6889 |
| 11 | -62.1915 | 15.9040 | 11 | -100.6753 | 11.6505 |
| 12 | -117.9428 | -3.1706 | 12 | -128.5814 | -6.2552 |
| 13 | -118.1430 | -3.1659 | 13 | -128.7271 | -6.2527 |
| 14 | -115.9040 | -1.8323 | 14 | -127.1452 | -4.9806 |
| 15 | -116.1407 | -1.8257 | 15 | -127.3156 | -4.9772 |
| 16 | -117.5578 | -2.8003 | 16 | -128.2969 | -5.8872 |
| 17 | -117.7539 | -2.7955 | 17 | -128.4392 | -5.8847 |
| 18 | -115.4520 | -1.4634 | 18 | -126.8143 | -4.6131 |
| 19 | -115.6841 | -1.4565 | 19 | -126.9809 | -4.6097 |

| Template Data for $v$ =6 [rad/sec] | | | Template Data for $v$ =8 [rad/sec] | | |
|---|---|---|---|---|---|
| Flight Condition | Phase [deg] | Magnitude [dB] | Flight Condition | Phase [deg] | Magnitude [dB] |
| 1 | -116.2427 | 10.2631 | 1 | -139.4774 | 4.5390 |
| 2 | -116 7233 | 10.2961 | 2 | -139.7508 | 4.5486 |
| 3 | -109.7925 | 11.8361 | 3 | -136.3917 | 5.9606 |
| 4 | -110.3608 | 11.8870 | 4 | -136.7186 | 5.9746 |
| 5 | -117.1780 | 9.8971 | 5 | -140.0053 | 4.1667 |
| 6 | -117.6668 | 9.9290 | 6 | -140.2835 | 4.1760 |
| 7 | -110.9153 | 11.4893 | 7 | -137.0185 | 5.5919 |
| 8 | -111.4962 | 11.5386 | 8 | -137.3513 | 5.6054 |
| 9 | -131.8159 | -1.3488 | 9 | -147.2348 | -5.8699 |
| 10 | -126.8138 | 3.4794 | 10 | -144.3466 | -1.4071 |
| 11 | -119.3266 | 7.9980 | 11 | -140.5390 | 2.6173 |
| 12 | -137.0630 | -8.7746 | 12 | -150.6770 | -12.9921 |
| 13 | -137.1784 | -8.7731 | 13 | -150.7587 | -12.9914 |
| 14 | -135.9424 | -7.5336 | 14 | -149.8939 | -11.7846 |
| 15 | -136.0765 | -7.5316 | 15 | -149.9882 | -11.7836 |
| 16 | -136.8353 | -8.4080 | 16 | -150.5137 | -12.6271 |
| 17 | -136.9478 | -8.4065 | 17 | -150.5933 | -12.6263 |
| 18 | -135.6789 | -7.1673 | 18 | -149.7059 | -11.4197 |
| 19 | -135.8098 | -7.1652 | 19 | -149.7978 | -11.4187 |

| Template Data for $v$ =10 [rad/sec] | | | Template Data for $v$ =20 [rad/sec] | | |
|---|---|---|---|---|---|
| Flight Condition | Phase [deg] | Magnitude [dB] | Flight Condition | Phase [deg] | Magnitude [dB] |
| 1 | -153.1981 | 0.5164 | 1 | -190.0402 | -11.7771 |
| 2 | -153.3882 | 0.5209 | 2 | -190.1186 | -11.7763 |
| 3 | -151.1674 | 1.8446 | 3 | -189.2448 | -10.5722 |
| 4 | -151.3920 | 1.8510 | 4 | -189.3354 | -10.5712 |
| 5 | -153.5720 | 0.1464 | 5 | -190.2013 | -12.1420 |
| 6 | -153.7661 | 0.1508 | 6 | -190.2819 | -12.1413 |
| 7 | -151.6057 | 1.4758 | 7 | -189.4302 | -10.9370 |
| 8 | -151.8349 | 1.4820 | 8 | -189.5233 | -10.9361 |
| 9 | -158.3788 | -9.3824 | 9 | -192.0872 | -21.0404 |
| 10 | -156.3193 | -5.0759 | 10 | -191.1991 | -16.9337 |
| 11 | -153.7554 | -1.2643 | 11 | -190.1750 | -13.3893 |
| 12 | -160.9816 | -16.3721 | 12 | -193.3030 | -27.8571 |
| 13 | -161.0456 | -16.3716 | 13 | -193.3343 | -27.8570 |
| 14 | -160.3723 | -15.1794 | 14 | -193.0073 | -26.6841 |
| 15 | -160.4459 | -15.1788 | 15 | -193.0431 | -26.6840 |
| 16 | -160.8531 | -16.0078 | 16 | -193.2397 | -27.4938 |
| 17 | -160.9153 | -16.0073 | 17 | -193.2700 | -27.4937 |
| 18 | -160.2247 | -14.8152 | 18 | -192.9348 | -26.3208 |
| 19 | -160.2963 | -14.8146 | 19 | -192.9696 | -26.3207 |

| Template Data for $v$ =50 [rad/sec] | | | Template Data for $v$ =100 [rad/sec] | | |
|---|---|---|---|---|---|
| Flight Condition | Phase [deg] | Magnitude [dB] | Flight Condition | Phase [deg] | Magnitude [dB] |
| 1 | -240.1843 | -29.0456 | 1 | -277.8020 | -41.3495 |
| 2 | -240.2155 | -29.0455 | 2 | -277.8200 | -41.3494 |
| 3 | -239.8716 | -27.8739 | 3 | -277.6208 | -40.1827 |
| 4 | -239.9073 | -27.8737 | 4 | -277.6415 | -40.1826 |
| 5 | -240.2493 | -29.4089 | 5 | -277.8397 | -41.7125 |
| 6 | -240.2814 | -29.4088 | 6 | -277.8583 | -41.7124 |
| 7 | -239.9460 | -28.2372 | 7 | -277.6640 | -40.5457 |
| 8 | -239.9828 | -28.2370 | 8 | -277.6853 | -40.5456 |
| 9 | -240.9892 | -38.1403 | 9 | -278.2683 | -50.4198 |
| 10 | -240.6313 | -34.0878 | 10 | -278.0603 | -46.3753 |
| 11 | -240.2273 | -30.6146 | 11 | -277.8262 | -42.9125 |
| 12 | -241.4905 | -44.9090 | 12 | -278.5605 | -57.1812 |
| 13 | -241.5035 | -44.9090 | 13 | -278.5681 | -57.1812 |
| 14 | -241.3672 | -43.7416 | 14 | -278.4886 | -56.0147 |
| 15 | -241.3822 | -43.7415 | 15 | -278.4973 | -56.0147 |
| 16 | -241.4640 | -44.5460 | 16 | -278.5450 | -56.8183 |
| 17 | -241.4766 | -44.5460 | 17 | -278.5524 | -56.8183 |
| 18 | -241.3369 | -43.3786 | 18 | -278.4709 | -55.6518 |
| 19 | -241.3514 | -43.3785 | 19 | -278.4793 | -55.6518 |

# Appendix E. A Problem With MATRIX$_X$ and QFT Template Generation

A problem with MATRIX$_X$ arose during the longitudinal SISO QFT design. Eight of the nineteen plants used in the design contain unstable poles, while the others are completely stable. Having both stable and unstable plants uncovered a problem with the way MATRIX$_X$ handles phase.

An apparent problem with the MATRIX$_X$ Bode plotting routine exists if used to generate data for plant templates necessary for a QFT design. If the phase of the plant at the lowest plotted frequency exceeds 180° or is less than -180° , the program removes phase information from the Bode data so that the initial phase data will be between $\pm$ 180° . When Bode plots of stable and unstable plants are used together, as in forming QFT templates, the Bode data indicates a minimum phase difference for low input frequencies, and 360° difference at higher frequencies. Note, in general, w′–domain transfer functions are equal order over equal order. Thus, analysis of the plants at very low frequencies, that is by taking the limit as the frequency approaches 0, predicts a wide variation in phase. Further, by taking the limit as the frequency approaches infinity, minimum phase difference should exist for the higher frequencies (for positive gain, an angle of 0° must result, for negative gain, an angle of 180° must result).

An experiment using simple plants illustrates the problem. Plants $p_1(s) = \frac{1}{(s+1)}$ and $p_2(s) = \frac{1}{(s-1)}$ are entered and plotted. MATRIX$_X$ produces the expected results. See Figure E.1. The Bode data for $p_1(s)$ produces 0° phase at very low frequencies and $-90°$ phase at very high frequencies. The unstable plant $p_2$ produces a -180° phase at very low frequencies and -90° phase at very high frequencies, also as expected. When the number of poles in the plants are increased, the results are not consistent with predictions. $p_3(s) = \frac{1}{(s+1)^2}$ and $p_4(s) = \frac{1}{(s-1)^2}$ are entered

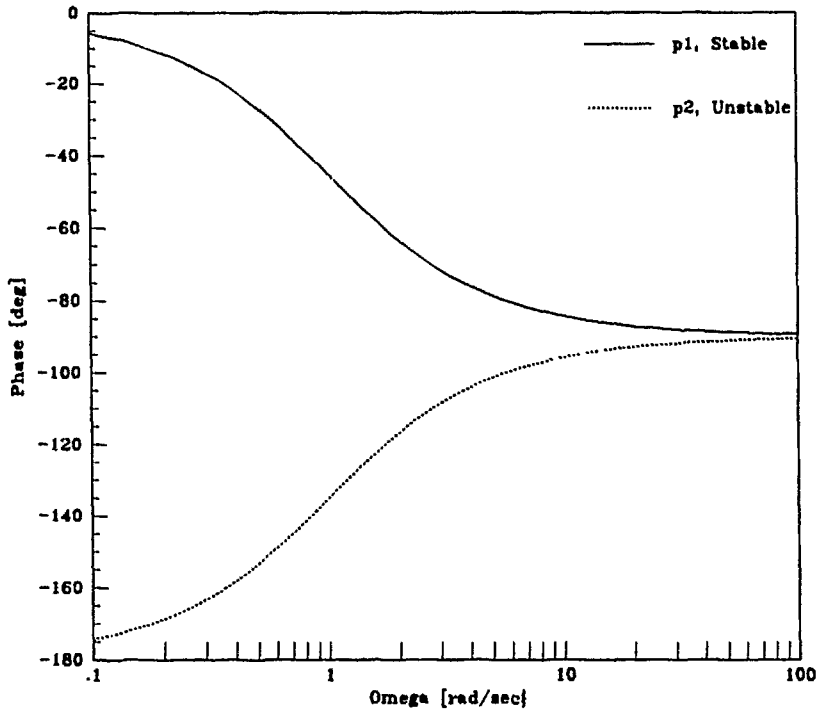


Figure E.1. Comparison of a Single Stable Pole and a Single Unstable Pole

and plotted. MATRIX$_X$ produces Bode phase data for the stable plant, $p_3$ exactly as predicted by mathematical analysis. However, MATRIX$_X$ produces Bode phase data for the unstable plant $p_4$ with 360° subtracted from the predicted values (see Figure E.2). For example, $\lim_{w\to 0} \angle p_4(j\omega) = -360°$, and $\lim_{w\to\infty} \angle p_4(j\omega) = -180°$. Normally, the fact that MATRIX$_X$ starts the Bode phase data between 180 and -180° phase is not a problem but for QFT template generation, the lost phase can greatly change the results. For the above examples, the templates formed from the Bode data of the single pole case, $p_1$ and $p_2$ can be used for QFT synthesis. However, in the double pole case, the MATRIX$_X$ Bode phase data will produce very narrow templates for low frequencies and wide templates for the higher frequencies. The phase data calculated analytically, without MATRIX$_X$ , produces narrow templates at the high frequencies.

One solution is to calculate the initial phase of the plants by taking the $\lim_{\omega\to 0}$. The Bode data taken from MATRIX$_X$ is then adjusted by the proper amount before

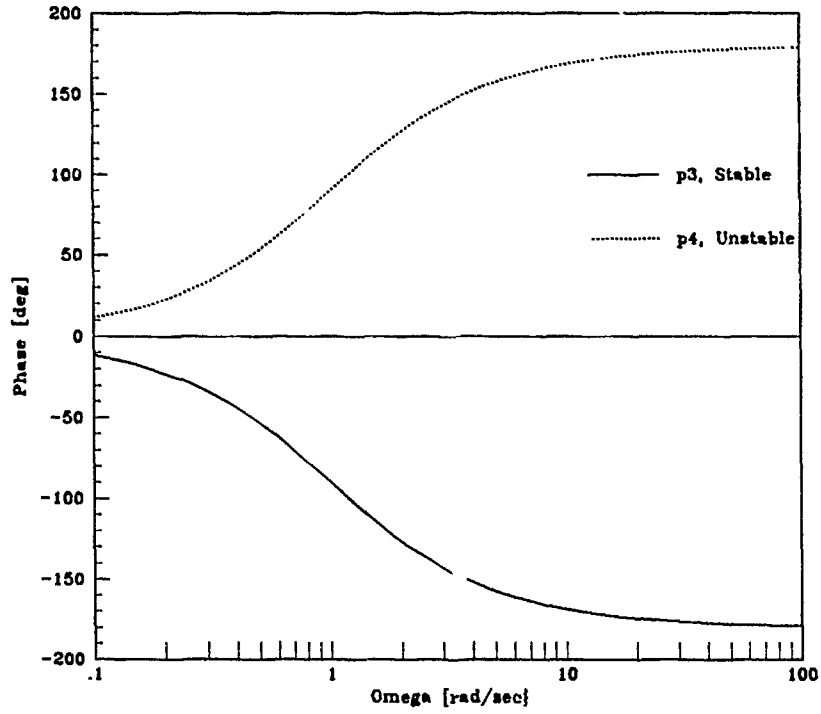


Figure E.2. Comparison of Two Stable Poles and Two Unstable Poles

the data is used to generate the templates. Another solution, which is applicable for transfer fuctions of equal numerator and denominator order like those obtained from bilinear transformations, is to obtain the frequency response data by plotting the Bode plots "backward" in frequency. For example, plotting $p_4(s)$ from 100 (rad/sec)to .1 (rad/sec)results in the correct phase information and may be used in forming templates without adjusting the data (see Figure E.3).

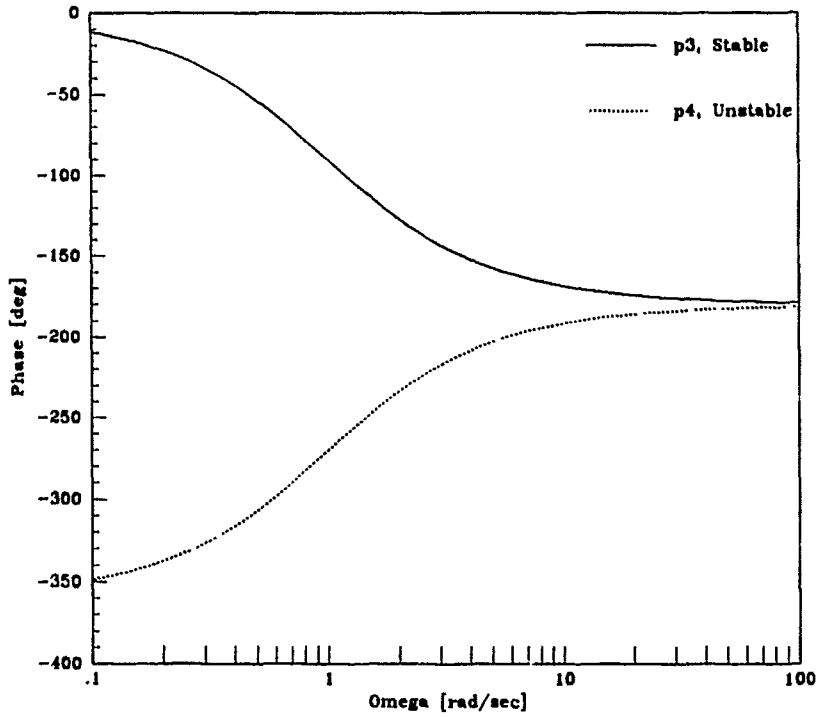


Figure E.3. Comparison of Two Stable Poles and Two Unstable Poles After Plotting "Backward" in Frequency

# Appendix F. **Difference Equations**

This appendix includes the difference equations needed for digital implementation of the QFT rate controller on Lambda assuming a sample rate of 50 Hz.

Equations (3.42) and (3.43) are z–plane representations of the QFT prefilter and compensator for the Longitudinal SISO digital QFT design and Equations (4.23), (4.24), (4.21), and (4.22) are the z–plane representations for the lateral-directional MIMO digital design. The z–plane representations are converted to difference equations for implementation on the Lambda flight control computer and are included in Tables F.1 and F.2.

The z–plane transfer functions are of the form:

$$G(z) = \frac{Y(z)}{U(z)} = \frac{c_m z^m + c_{m-1} z^{m-1} + \cdots + c_1 z + c_0}{d_n z^n + d_{n-1} z^{n-1} + \cdots + d_1 z + d_0} \tag{F.1}$$

where: $n \geq m$ and $d_n = 1$. The difference equation is formed by dividing the equation by $z^n$, cross multiplying, and replacing the negative powers of z with the appropiate delay to obtain:

$$\begin{aligned} y(kT) \;=\; & -d_{n-1} y[(k-1)T] - \cdots - d_1 y[(k+1-n)T] - d_0 y[(k-n)T] \\ & + c_m u[(k+m-n)T] + c_{m-1} u[(k+m-n-1)T] + \cdots \\ & + c_1 u[(k+1-n)T] + c_0 u[(k-n)T] \end{aligned} \tag{F.2}$$

$$\begin{aligned} f_{11}(kT) \;=\; & 1.617064707083078 f_{11}[(k-1)T] \\ & - 0.648907940395999 f_{11}[(k-2)T] \\ & + 0.017911818738518 \delta_{e_{cmd}}[(k)T] \\ & + 0.011941212492345 \delta_{e_{cmd}}[(k-1)T] \\ & + 0.001990202082058 \delta_{e_{cmd}}[(k-2)T] \end{aligned} \tag{F.3}$$

$$
\begin{aligned}
f_{22}(kT) \;=\;& 0.960784313725490 f_{22}[(k-1)T] \\
&+0.084967320261430 \delta_{a_{cmd}}[(k)T] \\
&-0.045751633986928 \delta_{a_{cmd}}
\end{aligned} \tag{F.4}
$$

$$
\begin{aligned}
f_{33}(kT) \;=\;& 1.986073568578539 f_{33}[(k-1)T] \\
&-0.98609740160436 f_{33}[(k-2)] \\
&+0.0149075576510960 \delta_{r_{cmd}}[(k)T] \\
&-0.0148837246252750 \delta_{r_{cmd}}[(k-1)T] \\
&-0.00 \delta_{r_{cmd}}[(k-2)T]
\end{aligned} \tag{F.5}
$$

$$
\begin{aligned}
g_{11}(kT) \;=\;& 0.768292682926834 g_{11}[(k-1)T] \\
&+0.878048780487800 g_{11}[(k-2)T] \\
&-0.170731707317077 g_{11}[(k-3)T] \\
&-0.365853658536584 g_{11}[(k-4)T] \\
&-0.109756097560974 g_{11}[(k-5)T] \\
&+96.0079664634145 \mathrm{u}_1[(k)T] \\
&-371.4464908536588 \mathrm{u}_1[(k-1)T] \\
&+562.6357134146366 \mathrm{u}_1[(k-2)T] \\
&-414.0391280487847 \mathrm{u}_1[(k-3)T] \\
&+146.2375884146371 \mathrm{u}_1[(k-4)T] \\
&-19.3892103658544 \mathrm{u}_1[(k-5)T]
\end{aligned} \tag{F.6}
$$

$$
\begin{aligned}
g_{22}(kT) \;=\;& 2.473684210526316 g_{22}[(k-1)T] \\
&-1.789473684210527 g_{22}[(k-2)T]
\end{aligned}
$$

$$
\begin{aligned}
&+0.526315789473684 g_{22}[(k-3)T] \\
&-0.578947368421052 g_{22}[(k-4)T] \\
&+0.368421052631579 g_{22}[(k-5)T] \\
&+021.7235319457573 \mathrm{u}_2[(k)T] \\
&-100.4706471025779 \mathrm{u}_2[(k-1)T] \\
&+186.6047527121375 \mathrm{u}_2[(k-2)T] \\
&-174.1142948925886 \mathrm{u}_2[(k-3)T] \\
&+81.6824678490870 \mathrm{u}_2[(k-4)T] \\
&-15.4257877749731 \mathrm{u}_2[(k-5)T] \qquad \text{(F.7)}
\end{aligned}
$$

$$
\begin{aligned}
g_{33}(kT) \;=\;& 1.883235004916421 g_{33}[(k-1)T] \\
&-0.719354310062275 g_{33}[(k-2)T] \\
&-0.244428056374959 g_{33}[(k-3)T] \\
&+0.080547361520813 g_{33}[(k-4)T] \\
&+0.00 g_{33}[(k-5)T] \\
&+37.4838623948432 \mathrm{u}_3[(k)T] \\
&-142.5540064277651 \mathrm{u}_3[(k-1)T] \\
&+214.1271236206708 \mathrm{u}_3[(k-2)T] \\
&-158.6615822681088 \mathrm{u}_3[(k-3)T] \\
&+57.9432763392695 \mathrm{u}_3[(k-4)T] \\
&-8.3349961761171 \mathrm{u}_3[(k-5)T] \qquad \text{(F.8)}
\end{aligned}
$$

Table F.1. QFT Prefilter Difference Equations

| Coefficients of Equation (F.2) | $f_{11}$ y(kT)= | $f_{22}$ y(kT)= | $f_{33}$ y(kT)= |
|---|---|---|---|
| $c_m$ | +0.013975 | +0.084967 | +0.014908 |
| $c_{m-1}$ | +0.0093168 | -0.045752 | -0.014884 |
| $c_{m-2}$ | +0.0015578 | | |
| $d_{n-1}$ | -1.6439 | -0.96078 | -1.9861 |
| $d_{n-2}$ | +0.66874 | | +0.98610 |

Table F.2. QFT Compensator Difference Equations

| Coefficients of Equation (F.2) | $g_{11}$ y(kT)= | $g_{22}$ y(kT)= | $g_{33}$ y(kT)= |
|---|---|---|---|
| $c_m$ | +96.749 | +21.724 | +37.484 |
| $c_{m-1}$ | -374.31 | -100.47 | -142.55 |
| $c_{m-2}$ | +566.96 | +186.60 | +214.13 |
| $c_{m-3}$ | -417.22 | -174.11 | -158.66 |
| $c_{m-4}$ | +147.36 | +81.682 | +57.943 |
| $c_{m-5}$ | -19.538 | -15.426 | -8.3350 |
| $d_{n-1}$ | -0.78629 | -2.4737 | -1.8832 |
| $d_{n-2}$ | -0.37805 | +1.7895 | +0.71935 |
| $d_{n-3}$ | +0.17073 | -0.52632 | +0.24443 |
| $d_{n-4}$ | +0.36585 | +0.57895 | -0.080547 |
| $d_{n-5}$ | +0.10976 | -0.36842 | 0 |

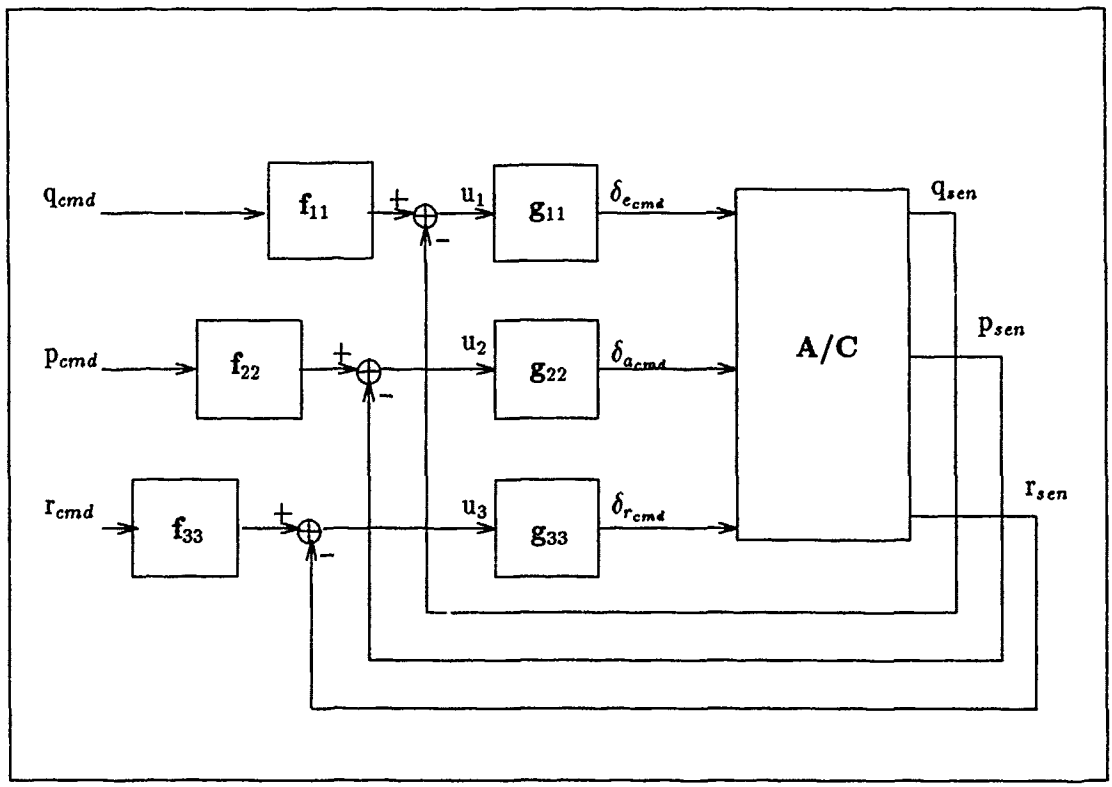


Figure F.1. Block Diagram of Rate Controller QFT Design for Lambda

# *Bibliography*


1. Adams, James M. *QFT Design Of A Robust Longitudinal Digital Controller For The AFTI/F-16 Using Matrix$_x$*. MS thesis, Air Force Institute of Technology , Wright-Patterson AFB, OH , March 1988.
2. Arnold, Phillip B. *Flight Control System Reconfiguration Design Using Quantitative Feedback Theory*. MS thesis, Air Force Institute of Technology , Wright-Patterson AFB, OH , December 1984.
3. Blakelock, John H. *Automatic Control of Aircraft and Missiles* (Second Edition).
4. Clough, Bruce T. *Reconfigurable Flight Control System For A STOL Aircraft Using Quantitative Feedback Theory*. MS thesis, Air Force Institute of Technology , Wright-Patterson AFB, OH , December 1985.
5. Coucoules, John S. *Study of the Effects of Discretizing Quantitative Feedback Theory Analog Control System Designs*. MS thesis, Air Force Institute of Technology , Wright-Patterson AFB, OH , December 1985.
6. Hamilton, Steven W. *QFT Digital Controller For An Unmanned Research Vehicle With An Improved Method For Choosing The Control Weightings*. MS thesis, Air Force Institute of Technology , Wright-Patterson AFB, OH , December 1987.
7. Hofmann, L. G. and R. E. Michael. "Technique for Analysis of Digital Control Systems." General Electric Company, Avionic and Electronic Systems Division. Binghamton, New York.
8. Horowitz, Issac and Adrian Ioinovici. "Quantitative Feedback Theory for Multiple-Input Multiple-Output Feedback Systems with Control Input Failures," *International Journal of Control, 43*:1803-1821 (June 1986).
9. Horowitz, Isaac. "Improved Design Technique For Uncertain Multiple-Input-Multiple-Output Feedback Systems," *International Journal of Control, Vol. 36*(No. 6):pp 977-988 (1982).
10. Horowitz, Isaac M., "Personal Conversation and Correspondance." Professor of Electrical Engineering, University of California Davis, May 1991.
11. Houpis, Constantine H., "Personal Conversation, Correspondance and Class Notes." Professor of Electrical Engineering, Air Force Institute of Technology , Wright-Patterson AFB, OH , May 1990 through December 1991.
12. Houpis, Constantine H. *Quantitative Feedback Theory (QFT)—Technique for Designing Multivariable Control Systems*. Technical Report AFWAL-TR-86-3107, Wright-Patterson AFB, OH : Flight Dynamics Laboratory, January 1987.

13. Houpis Constantine H. and Gary B. Lamont. *Digital Control Systems—Theory, Hardware, Software*. McGraw-Hill, 1985.

14. $MATRIX_X$ CAD/CAE Program, Integrated Systems Inc., Santa Clara, CA, 95054-1215.

15. Migyanko, Barry S. *Design of Integrated Flight/Propulsion Control Laws of a STOL Aircraft During Approach and Landing Using Quantitative Feedback Theory*. MS thesis, Air Force Institute of Technology , Wright-Patterson AFB, OH , December 1986.

16. Military Specification—Flying Qualities of Piloted Aircraft. MIL-STD-1797A. 30 January 1990.

17. Military Specification—Control and Stabilization Systems: Automatic, Piloted Aircraft, General Specification For. MIL-C-18244A. 1 December 1962.

18. Miller, James, "Personal Conversation and Interviews." Contract Test Pilot for Lambda, Jun and Sep 1991 .

19. Neumann, Kurt N. *The Control Reconfigurable Combat Aircraft Designed Using Quantitative Feedback Theory*. MS thesis, Air Force Institute of Technology , Wright-Patterson AFB, OH , December 1988.

20. Nwokah, Osita D. I. and David F. Thompson. "Algebra and Topological Aspects of Quantitative Feedback Theory," *International Journal of Control, 50* (September 1989).

21. Ott, Paul T. *QFT Digital Design For Inherent Reconfiguration of the Flight Control System of An Unmanned Research Vehicle*. MS thesis, Air Force Institute of Technology , Wright-Patterson AFB, OH , June 1988.

22. Russell, Harvey H. *Design of Robust Controllers For a Multiple Input-Multiple Output Control System With Uncertain Parameters Application to the Lateral and Longitudinal Modes of the KC-135 Transport Aircraft*. MS thesis, Air Force Institute of Technology , Wright-Patterson AFB, OH , December 1984.

23. Schneider, Dean L. *QFT Digital Flight Control Design As Applied to the AFTI/F16*. MS thesis, Air Force Institute of Technology , Wright-Patterson AFB, OH , December 1986.

24. Swift, First Lieutenant Gerald A. *Model Identificaion and Control System Design for the Lambda Unmanned Research Vehicle*. MS thesis, Air Force Institute of Technology, Wright Patterson AFB, OH, September 1991.

25. Thompson, Daniel B and Lt Scott D Robertson "Common Core Avionics for Unmanned Aerial Vehicles." *AIAA/AHS/ASEE Aircraft Design, Systems and Operations Conference*. September 1990.

26. Wheaton, Captain David G. *Automatic Flight Control System Design for an Unmanned Research Vehicle Using Discrete Quantitative Feedback Theory*. MS thesis, Air Force Institute of Technology, Wright Patterson AFB,OH, December 1990.

27. Yaniv, Oded and Isaac Horowitz. "Algebra and Topological Aspects of Quantitative Feedback Theory," *International Journal of Control*, *50*:1057–1069 (September 1989).